HIGH AFFINITY PEPTIDE NEUROTOXIN QUANTUM DOT CONJUGATES FOR DETECTING ENDOGENOUS TARGETS IN LIVE CELLS AND EX VIVO TISSUE

By

Rebecca Lee Orndorff

Dissertation

Submitted to the Faculty of the

Graduate School of Vanderbilt University

in partial fulfillment of the requirements

for the degree of

DOCTOR OF PHILOSOPHY

in

Chemistry

August, 2009

Nashville, Tennessee

Approved:

Professor Sandra J. Rosenthal

Professor Michael P. Stone

Professor David W. Wright

Professor Eva M. Harth

To my parents, my brother, and our dogs—past and present

ACKNOWLEDGEMENTS

I wish to express gratitude to a number of people that have aided me in some way as I have pursued my education. My thankfulness for the opportunity to pursue this degree is directed at my advisor, Dr. Sandra J. Rosenthal. She provided me with the opportunity to lead my own studies and develop my independence as a scientist through the freedom afforded me toward the design and the execution of experiments and project development. I would also like to acknowledge Dr. Rosenthal's research group, past and present, who have provided insight and support. Additionally, I would like to express my gratitude to my doctoral committee, Dr. Eva Harth, Dr. Michael Stone, and Dr. David Wright, for guiding me and fostering my development as a researcher over the past years. With that I would like to extend thanks to the Department of Chemistry at Vanderbilt University for providing the opportunity to pursue my education, as well as the funding necessary to perform the research. The National Institutes of Health are also acknowledged for their contribution toward funding this work. I must also express my gratitude to Dr. David Hercules and Dr. Anthony Gies for providing me the opportunity to support their work in mass spectrometry experimentation of various polymers. A thank you is extended to anyone that I have been remiss in mentioning.

Lastly, but most importantly, I wish to express my gratitude to my family—my parents, my brother, and our dogs. Without their unconditional support and love, I could not have made it this far.

TABLE OF CONTENTS

LIST OF TABLES

LIST OF FIGURES

LIST OF SCHEMES

CHAPTER I

INTRODUCTION

1.1: Quantum Dot Nanocrystals

Quantum dots are nanocrystals composed of semiconductors arranged in a core/shell structure. Typical composition consists of a CdSe core, although CdTe may also be used to produce the nanocrystals.[1-3] To enhance the photoemission properties of the material, a shell of ZnS is commonly added to the outer surface of the nanocrystal core.[4] Following shelling, various surface chemistry modifications may be performed to make the nanocrystals suitable for their intended application.[5, 6] Due to their structure and composition, quantum dots exhibit unique photophysical properties that are not seen with organic fluorophores, such as near 100% quantum yield.[7] These unique photophysical properties are potentially advantageous for integration of nanomaterials with bioscience assays.[8] Quantum dots enable the possibility of multiplexing experiments, a methodology wherein a single excitation source excites multiple fluorescent markers and results in separate and unique emission spectra (Figure 1.1). This quantum dot ability is due to their properties of broad excitation spectra, narrow emission spectra, and emission spectra size and composition tunability that spans the visible spectrum.[4, 9-17] Recent evidence has supported the use of alloy nanocrystals to produce composition-based emission spectra tunability, in addition to nanocrystal size-based tunability.[18-20] This affords the capacity to design nanoprobes with emission properties that meet size requirements for specific applications.

The nanomaterials also show marked photostability, which is in contrast to their fluorophore complements.[21] Organic based fluorescent probes exhibit a finite emission capacity, in that they are easily photobleached after a short duration of optical excitation. This prevents long-term tracking potential, and limits overall knowledge on time-lapse dependent tracking. Quantum dots exhibit high resistance to photobleaching. This characteristic of the nanocrystals increases their desirability for use as a biological marker[11, 14-16, 22] within applications ranging from fixed samples to live-cell trafficking.

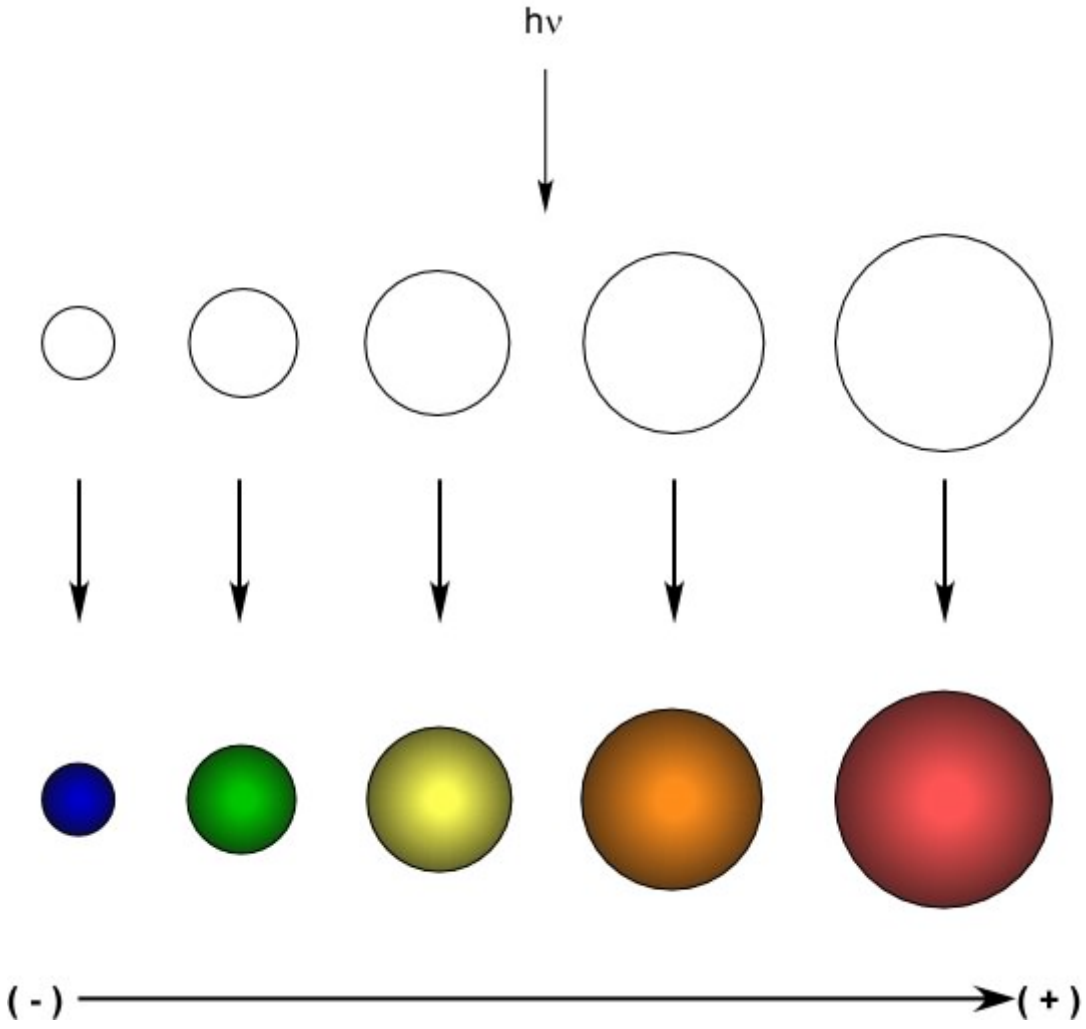

Figure 1.1: Cartoon of quantum dot size-dependent emission resulting from single excitation source.

1.2: Quantum Dot Incorporation with Biology

Incorporation of semiconductor nanocrystals into biological assays is facilitated through both surface modifications and targeting ligand selection (Figure 1.2). Surface modification becomes necessary to not only create an amphiphilic chemistry that is compatible with the water soluble cellular environment, but also to prevent unwanted interactions between surface ligands and cell surface proteins.[23-25] Modifications enable the quantum dots to be used as highly specific targeting fluorescent probes; whereas, their intrinsic, water insoluble, composition would ordinarily prevent suitability within biological assays. These modifications have varied in methodology aimed at altering the surface for the potential application being addressed.[5, 6, 8, 21, 23-26] Each modification has presented with both advantages[16] and disadvantages[27] for the intended usage or for further attachment of targeting ligands. Conjugation chemistry is greatly enhanced by the introduction of functional groups capable of serving as highly reactive branches toward building a high affinity fluorescent probe; however, with each additional molecule added to the nanocrystal, the radial bulk of the material is increased accordingly, and the surface reactivity is altered. The estimated size of quantum dot nanoconjugates is approximately 15-20 nm.[28] This is greater than conventional fluorescent organic dye molecules, but approximately equivalent in size to fluorescent proteins.[28] With their increased size, the probe may potentially lose its capacity to perform its function within the scale of the biological system. Inclusion of a balance between surface modification and nanoconjugate size is necessary to moderate the incorporation of quantum dot nanotechnology into biological experimentation.

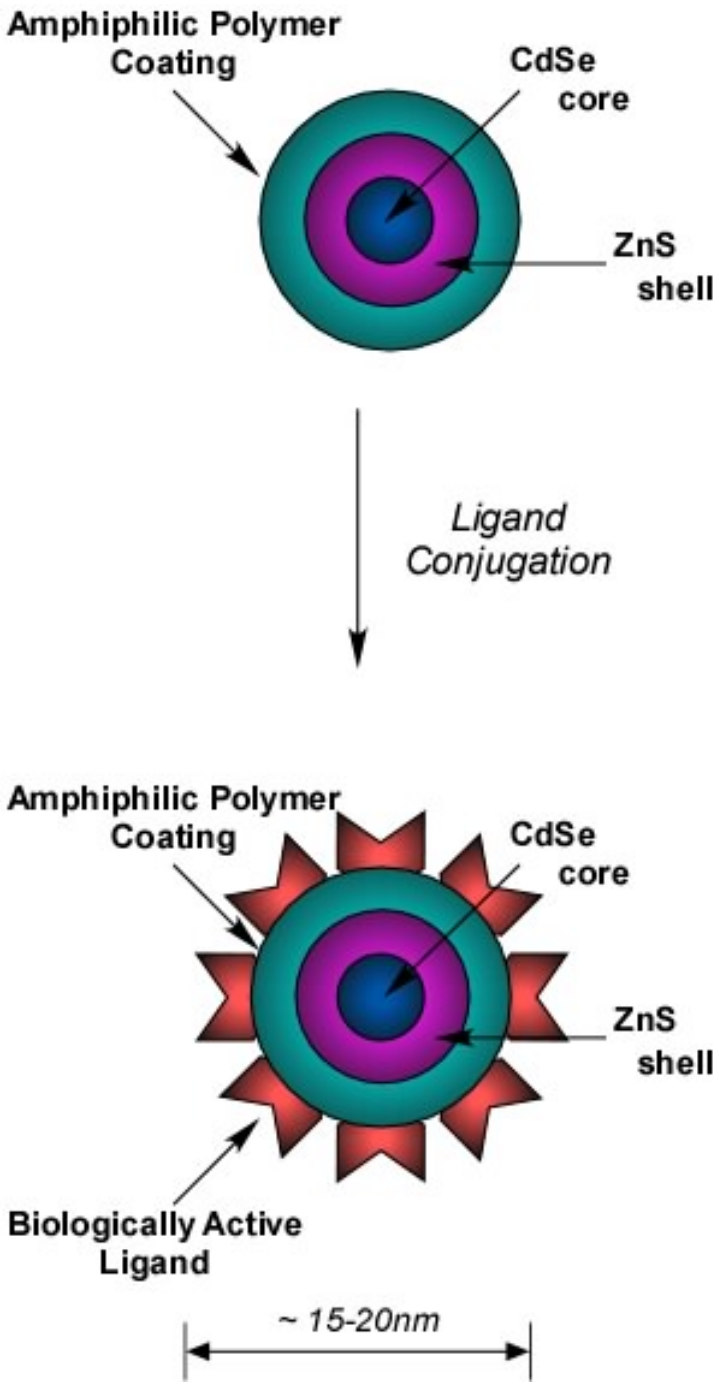

Figure 1.2: Cartoon of general quantum dot structure. Each layer is colored to provide emphasis for the various layers within the structure. The structure consists of a CdSe core surrounded by a ZnS shell. For biocompatibility, an amphiphilic polymer is added to the surface prior to ligand conjugation. The estimated size is approximately 15-20 nm in diameter, although this varies depending upon the probe in question.[28]

1.3: Quantum Dot Surface Modifications

Incorporation into biological experiments necessitates nanocrystal surface modifications for biocompatibility. Without extensive surface modifications, quantum dots will often produce high incidence of non-specific binding interactions within a biological environment. This cumbersome property requires chemical alterations to adapt the semiconductor materials to suit the conditions imposed upon them. A number of modifications have been reported within the literature in an effort to reduce non-specific binding to cell membranes. These have included alterations such as micelle encapsulation,[29] pegilation,[30] selinization,[31] coating in amphiphilic polymers,[32, 33] and the addition of biologically active molecules such as proteins,[22, 34, 35] peptides,[36-38] small molecules,[39-41] and antibodies[42-45] to the surface of the quantum dots. The outcome of these efforts has produced successful results within both cell culture labeling[22, 23, 30, 46-56] and tissue labeling.[57]

Recent advances in probe development have generated streptavidin quantum dot conjugates that may be even more suitable for biological applications given their multiplexing capabilities and resistance to photobleaching.[11, 14-16, 22] By adding streptavidin to the surface of fluorescent nanocrystals, the utility of quantum dots is greatly enhanced. Coupling of biotin and avidin, or streptavidin, yields an interaction with femtomolar affinity and a long half-life in solution. This provides a means for including quantum dot probes in applications that previously were not adaptable. It also enables for quantum dots to detect biotin-tagged proteins[57] and small molecules used as ligands. This provides a platform for quantum dot integration into biological studies. Recently, a study reported success with exploiting the femtomolar relationship between

streptavidin and biotin. The study demonstrated that streptavidin quantum dot conjugates were able to label a series of biotinylated cellular targets through use of biotin ligase biotinylation.[43] Their results demonstrated the utility of biotin-streptavidin quantum dot coupling for targeting cellular targets neuroreceptors and neurons.

Fundamental to quantum dot probe development for biological assays is ligand selection. Ligands selected for use with quantum dots are chosen based upon a few criteria. The first criterion governing the selection is based upon the biological assay being performed. This dictates the target, and thus governs the ligand coupled with quantum dots for detection. The second criterion entails ligand size. Ligand size is an issue particularly directed at polymeric molecules, such as peptides and DNA, coupled to quantum dots. The peptide neurotoxins chosen for these studies were selected based upon these criteria.

1.4: Inhibiting Ion Channels with Peptide Neurotoxins

Ion channels play intricate roles in neuronal activity.[58] Their roles in an array of diseases, ranging from degenerative malformations to cancers, are emerging but remain poorly understood due to lack of adequate high affinity ligands and probes.[58-60] Peptide neurotoxins are of experimental interest for their high target specificity, and are of therapeutic value for their medicinal potential.[61] Their high specificity for their target, often an ion channel, enables accurate labeling without the propensity for cross-talk between targets, as seen with many small molecule probes. They also provide the possibility to be utilized as therapeutic agents ranging from cancer detection[62] and treatments to chronic pain alleviation.[63] This therapeutic potential arises from the

inhibitory interaction between toxin and ion channel. The high affinity of the neurotoxins makes them suitable for use as ligands in quantum dot fluorescence microscopy studies to examine the behavior of their target. Until recently, organic fluorophores provided the best opportunity to visualize a protein in its native environment. Laden with the issue of rapid photobleaching, organic fluorophores provide a narrow window of opportunity to examine the target and thus negate the possibility of sample archiving. Quantum dot conjugate induction into biological research enables extended tracking technology to be applied at the cellular, tissue, and organism levels.

Peptide-mediated quantum dot detection of neural targets has been demonstrated to be an effective methodology for probing biological systems with high specificity. Targeted neurotoxin approaches have been employed to selectively label proteins for monitoring,[39] detection,[56, 57] and destruction.[63, 64] An array of neurotoxins from various sources ranging from animals to plants, bacteria to fungi, have been isolated and characterized with numerous others yet to be studied.[61, 64, 65] Although designed to induce disruption of its targeting system, each toxin provides the possibility to be utilized as a therapeutic vehicle for disease detection and destruction, and as a means to study its target in greater depth. Typically, peptide neurotoxins inhibit ion channels by acting as antagonists, and result in the cessation of neurotransmission propagation and loss of channel functionality.[58, 66] Because of their high specificity, peptide neurotoxins aid in characterization and understanding of the behaviors associated with its target and genetically modified targets without adequate ligands.[56] Quantum dot application to neural studies has the potential to be greatly enhanced by method development, which

harnesses peptide neurotoxins as vehicles to perform in depth examinations of neurologically significant targets (Figure 1.3).

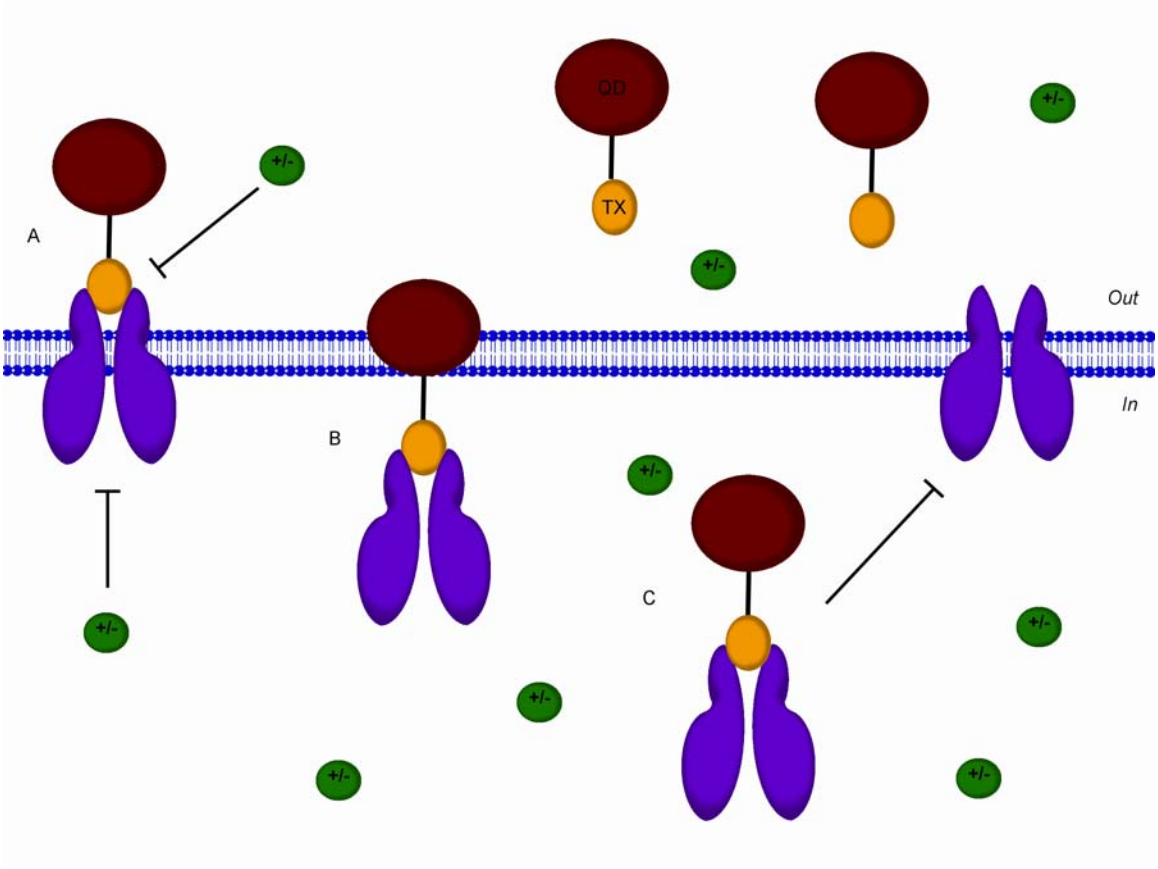

Figure 1.3: Peptide-mediated quantum dot inhibition of ion channels. (A) Neurotoxin binding inhibits or disrupts ion channel function. (B) The neurotoxin-quantum dot binding event induces internalization. (C) The channel is internalized with the complex intact, and channel expression at the membrane is potentially reduced.

Quantum dot cellular targeting may be mediated with use of toxins that inhibit endogenously expressed ion channels. Because neurotoxins typically have very high affinities for their cellular targets, they may serve as an acceptable means of facilitating nanoprobe development for use in biological systems. Of particular neurological interest

is incorporation of quantum dots into biological labeling of tissue.[57, 67-70] Quantum dot detection within tissue entails the need for high specificity to accurately label biological targets among the complexity of a tissue environment. Additionally, quantum dot labeling to identify disease markers in cells, such as the primary brain glial cell cancer, glioma, is of interest for developing techniques for endogenous target detection. Glioma cells are malignant cancer cells that infiltrate healthy brain tissue, and evade complete surgical resection through yet fully understood mechanisms.[71] To study these cells for their mechanisms of motility through the tight brain tissue cavities, peptide toxins may be employed to develop methods to monitor responses with quantum dots. Thorough analysis with quantum dots may yield information that provides detail into cancer mechanisms, and provide information regarding the cooperative nature of the toxin targets.

1.5: Peptide Neurotoxin Conjugation to Quantum Dots

There are generally two possible approaches to peptide detection using quantum dots: (1) direct peptide conjugation to quantum dots, and (2) peptide biotinylation followed with avidin-linked quantum dot detection (Figure 1.4). Both methods present with advantages and disadvantages. Direct peptide conjugation to quantum dots is possible using coupling reagents, and requires separation of unreacted reagents from product. It has been reported that Traut's reagent was used to create a sulfydryl reactive group on the peptide. Following the reaction with Traut's reagent, the peptide was conjugated to amine terminated pegylated iron oxide nanoparticles via a thioether linkage.[72] A similar procedure is amenable for application with quantum dots.

Additionally the semiconductor nanocrystals may also be modified using the more common protocol that utilizes coupling agents, such as N-hydroxysuccinimide and 1-ethyl-3-(3-dimethylaminopropyl) carbodiimine hydrochloride, to attach the neurotoxins to the nanocrystals. The suitability of biotin coupled neurotoxin detection has been demonstrated with an avidin-linked probe techniques in our previous studies.[57]

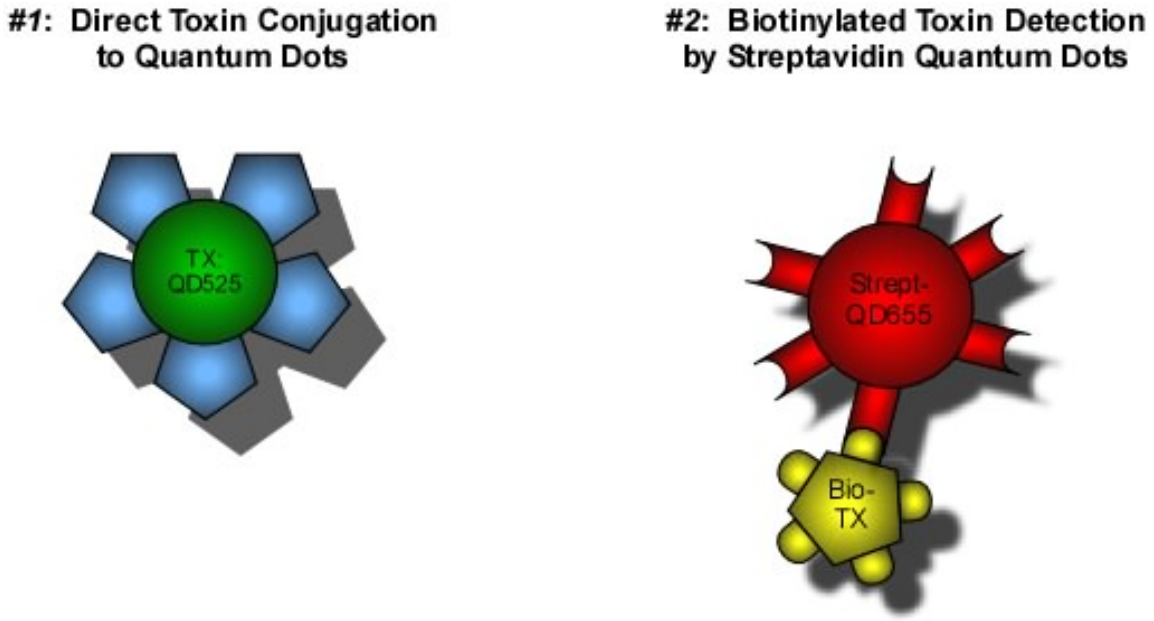

Figure 1.4: Conjugation methods for binding neurotoxin peptides to quantum dot conjugates. The two methods combining high affinity peptide neurotoxins with quantum dots include direct conjugation to the nanocrystals through covalent bonds between the peptide residues and the surface of the quantum dot, and streptavidin-linked quantum dots binding to biotinylated neurotoxin. Both methods are effective means to achieve successful incorporation of high affinity peptide neurotoxin with highly fluorescent nanocrystals.

For cellular labeling of multiple targets, the biotinylated peptides require binding with the desired quantum dot color determined for the protein of interest. This requires separation techniques to be employed following pre-conjugation methods. In addition to centrifugation techniques, dialysis is another type of method that may be employed to

remove unbound small molecules from biotinylated peptide-streptavidin quantum dot complexes.

1.6: α-Bungarotoxin Structure and Properties

α-Bungarotoxin is a high affinity peptide neurotoxin that has been used to extensively classify nicotinic acetylcholine receptors. Isolation of the peptide from banded krait venom resulted in elucidation of ion channel activity, and provided a model template for ion channels.[73] α-Bungarotoxin is a single peptide within a venom cocktail that targets muscle-type nicotinic acetylcholine receptors, and results in cessation of neural impulses at the neuromuscular junction.[74-77] The α-bungarotoxin peptide binds to the post-synaptic cleft of the neuromuscular junction. This prevents acetylcholine from binding to the ion channel, and inhibits ion flux through the channel.[78] Essentially, the toxin binds to a gatekeeper transmembrane protein responsible for furthering neural signal between the neuron and the muscle. The neural signal is stunted when in the presence of α-bungarotoxin because acetylcholine is unable to bind to the receptor and induce a conformation change in the channel that allows for exchange of ions across the cell membrane.[79, 80] The α-bungarotoxin roadblock results in a reduction of functioning muscle-type nicotinic acetylcholine receptors, which eventually results in death, if left untreated.

The α-bungarotoxin peptide consists of 74 amino acids (Table 1.1), which contains five disulfide bonds (Figure 1.5).[81] There are a total of five disulfide bonds throughout the protein, which aid in binding distant portions of the sequence together. The disulfide bonds are located at ^{3}Cys-^{23}Cys, ^{16}Cys-^{44}Cys, ^{29}Cys-^{33}Cys, ^{48}Cys-^{60}Cys, and

^{59}Cys-^{65}Cys residues, and are scattered through the peptide. There are also six lysine residues in peptide sequence.

Table 1.1: α-Bungarotoxin amino acid sequence.[81] Disulfide linkages are individually colored to illustrate bonding sites within the peptide. Each disulfide linkage is labeled with a different color.

1	ILE	*14*	VAL	*27*	MET	*40*	VAL	*53*	PRO	*66*	ASN
2	VAL	*15*	THR	*28*	TRP	*41*	GLU	*54*	TYR	*67*	PRO
3	CYS	*16*	CYS	*29*	CYS	*42*	LEU	*55*	GLU	*68*	HIS
4	HIS	*17*	PRO	*30*	ASP	*43*	GLY	*56*	GLU	*69*	PRO
5	THR	*18*	PRO	*31*	ALA	*44*	CYS	*57*	VAL	*70*	LYS
6	THR	*19*	GLY	*32*	PHE	*45*	ALA	*58*	THR	*71*	GLN
7	ALA	*20*	GLU	*33*	CYS	*46*	ALA	*59*	CYS	*72*	ARG
8	THR	*21*	ASN	*34*	SER	*47*	THR	*60*	CYS	*73*	PRO
9	SER	*22*	LEU	*35*	SER	*48*	CYS	*61*	SER	*74*	GLY
10	PRO	*23*	CYS	*36*	ARG	*49*	PRO	*62*	THR		
11	ILE	*24*	TYR	*37*	GLY	*50*	SER	*63*	ASP		
12	SER	*25*	ARG	*38*	LYS	*51*	LYS	*64*	LYS		
13	ALA	*26*	LYS	*39*	VAL	*52*	LYS	*65*	CYS		

The α-bungarotoxin peptide has elucidated the organization of nicotinic acetylcholine receptors within muscle membrane. Clusters of nicotinic acetylcholine receptors are found at the peaks of highly folded post-synaptic membrane in muscle.[82] These receptors are highly expressed in diaphragm muscle, which further contributes to the potency of exposure to α-bungarotoxin. The toxin was initially isolated by Taiwanese researchers in the first half of the 20th century in an effort to deduce the mechanism governing the venom potency.[73] Further research revealed that α-bungarotoxin harbors a subnanomolar affinity for nicotinic acetylcholine receptors. A 1981 report by Stevenson and coworkers[83] found that in fixed tissue, the affinity the toxin has for receptors is approximated to be 500 picomolar. The supports the use of the neurotoxin as a known high affinity ligand for coupling with nanocrystals to demonstrate nanotechnology utility

for applications requiring increased sensitivity, as well as benefiting from the photophysical properties exhibited by the nanomaterials.

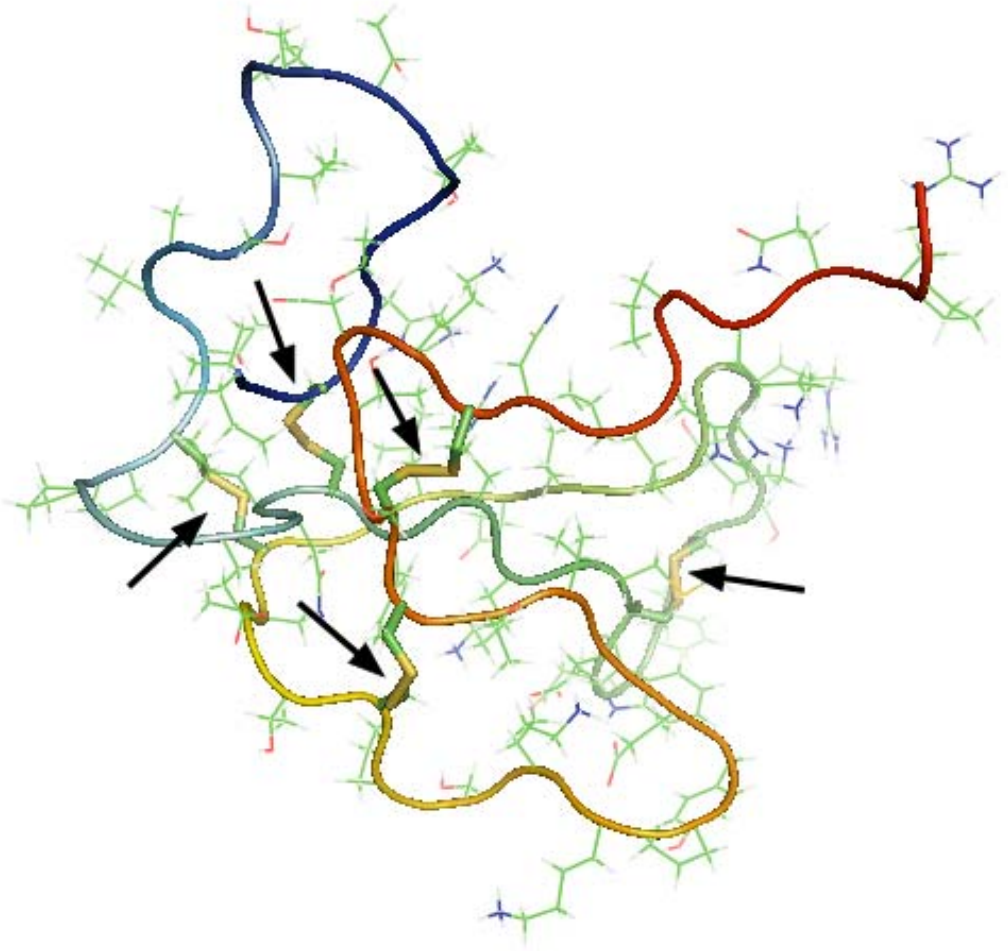

Figure 1.5: Illustration of α-bungarotoxin structure. Atomic coordinates were retrieved from the Protein Data Bank, 1IDI,[81] and imported into Pymol[84] for illustration purposes. Arrows indicate the location of the disulfide linkages within the peptide.

These properties, along with the known subnanomolar affinity for nicotinic acetylcholine receptors, enable α-bungarotoxin to provide a suitable ligand and targeting system for incorporation of nanotechnology. Because the target for α-bungarotoxin is highly

expressed in diaphragm tissue, it provides a platform for furthering quantum dots within endogenous detection within the native environment of tissue.

1.7: Chlorotoxin Structure and Properties

Insect toxins have also been shown to be capable of serving as high affinity ligands toward fluorescent probe development.[72] Recently isolated within the previous two decades, chlorotoxin is a short chain peptide from scorpion venom that consists of 36 amino acids (Table 1.2).[85, 86] Like α-bungarotoxin, chlorotoxin also has multiple disulfide bonds throughout its structure, ^{2}Cys-^{19}Cys, ^{5}Cys-^{28}Cys, ^{16}Cys-^{33}Cys, and ^{20}Cys-^{35}Cys[87] (Figure 1.6).

Table 1.2: Chlorotoxin amino acid sequence.[88] Disulfide linkages are individually colored to illustrate bonding sites within the peptide. Each disulfide linkage is labeled with a different color. There are a total of four disulfide linkages throughout the chlorotoxin peptide.

1	MET	*13*	ALA	*25*	ARG
2	CYS	*14*	ARG	*26*	GLY
3	MET	*15*	LYS	*27*	LYS
4	PRO	*16*	CYS	*28*	CYS
5	CYS	*17*	ASP	*29*	TYR
6	PHE	*18*	ASP	*30*	GLY
7	THR	*19*	CYS	*31*	PRO
8	THR	*20*	CYS	*32*	GLN
9	ASP	*21*	GLY	*33*	CYS
10	HIS	*22*	GLY	*34*	LEU
11	GLN	*23*	LYS	*35*	CYS
12	MET	*24*	GLY	*36*	ARG

Chlorotoxin harbors the interesting property of preferentially binding with cancer cells over non-cancer cells.[62, 89] This property provides the potential to utilize the neurotoxin as a tool to further quantum dot probe development. The toxin offers the opportunity to

develop quantum dot probes designed to be used in trafficking experiments. Because chlorotoxin is much smaller than some peptide antagonists, it is more easily shuttled into the cell.[62, 89, 90]

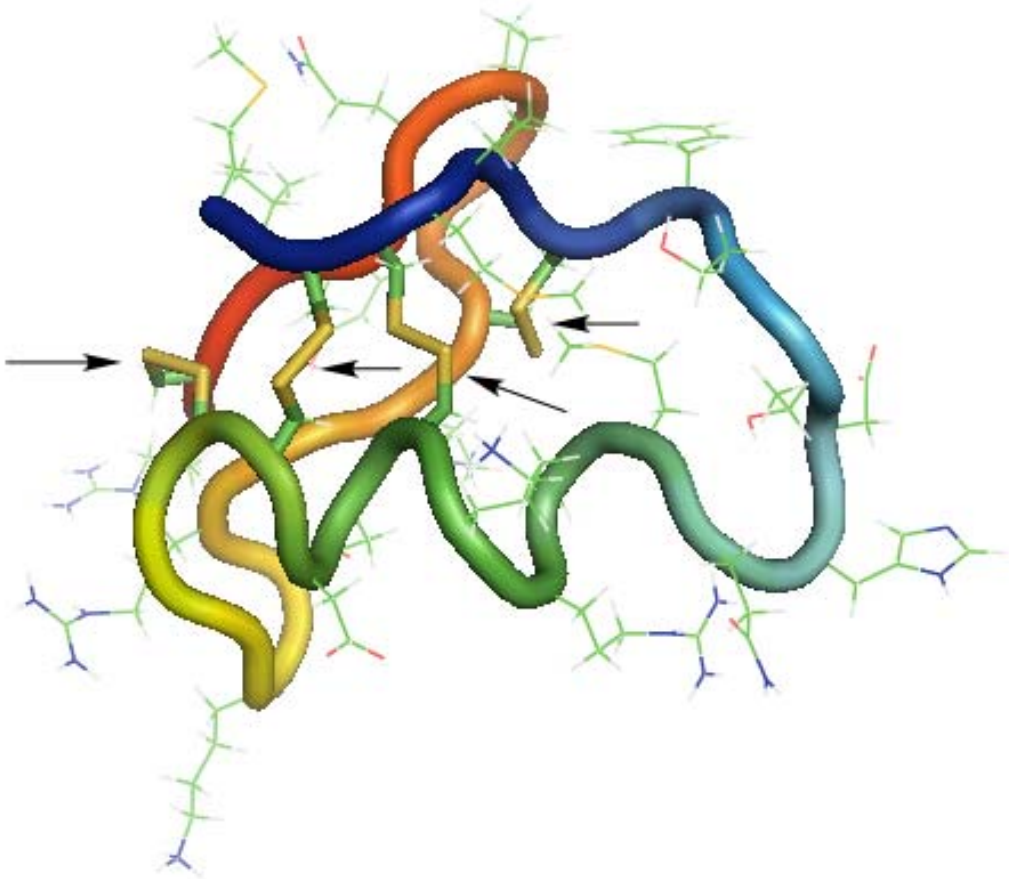

Figure 1.6: Illustration of chlorotoxin structure. Atomic coordinates were retrieved from the Protein Data Bank, 1CHL,[88] and imported into Pymol[84] for illustration purposes. Arrows indicate the location of the disulfide linkages within the peptide.

Initial studies with chlorotoxin indicated that the peptide disrupts chloride channel currents based upon patch-clamp analyses.[85] Sontheimer and colleagues demonstrated that chlorotoxin binds to matrix metalloproteinase-2 through recombinant His tagging

experimentation.[89] This confirmed the chlorotoxin cellular target to be the gelatinase enzyme. When exposed to chlorotoxin there is an observed loss of gelatinase activity, disruption in chloride channel currents, reduction in both matrix metalloproteinase-2 and chloride channel expressions, and internalization of chloride channels.[60, 62, 89-91] Matrix metalloproteinase-2 as the biological target for chlorotoxin was further confirmed a few years later by Olson and co-workers in 2007.[90] Confirmation was achieved using a fluorescent dye, Cy5.5, conjugated to chlorotoxin for use in cell culture and in vivo detection. MCF7 cells were transfected with a plasmid containing matrix metalloproteinase-2 for expression within the host cells. Matrix metalloproteinase-2 antibody colocalization with the chlorotoxin fluorescent organic dye conjugate affirmed that chlorotoxin interacts with matrix metalloproteinase-2.[90] These studies have garnered evidence that matrix metalloproteinase-2 is influential in glioma cell proliferation, and raise questions regarding the nature of the chloride channel interactions with matrix metalloproteinase-2.

An interesting property of chlorotoxin is that it is believed to severely reduce cell motility, if not stop it entirely.[91, 92] When taken in context with a glioma, which undergoes metastasis through motility mechanisms unlike other cancers, reduction in cell motility potential results in loss of metastatic ability.[59, 60, 71, 92] Figure 1.7 illustrates the reduction in cell volume that is believed to account for the glioma motility.[60, 91] Loss of functional ion channels may aid to limit proliferation of the disease, and may also indicate that ion channel expression and functionality are essential to glioma motility.[91]

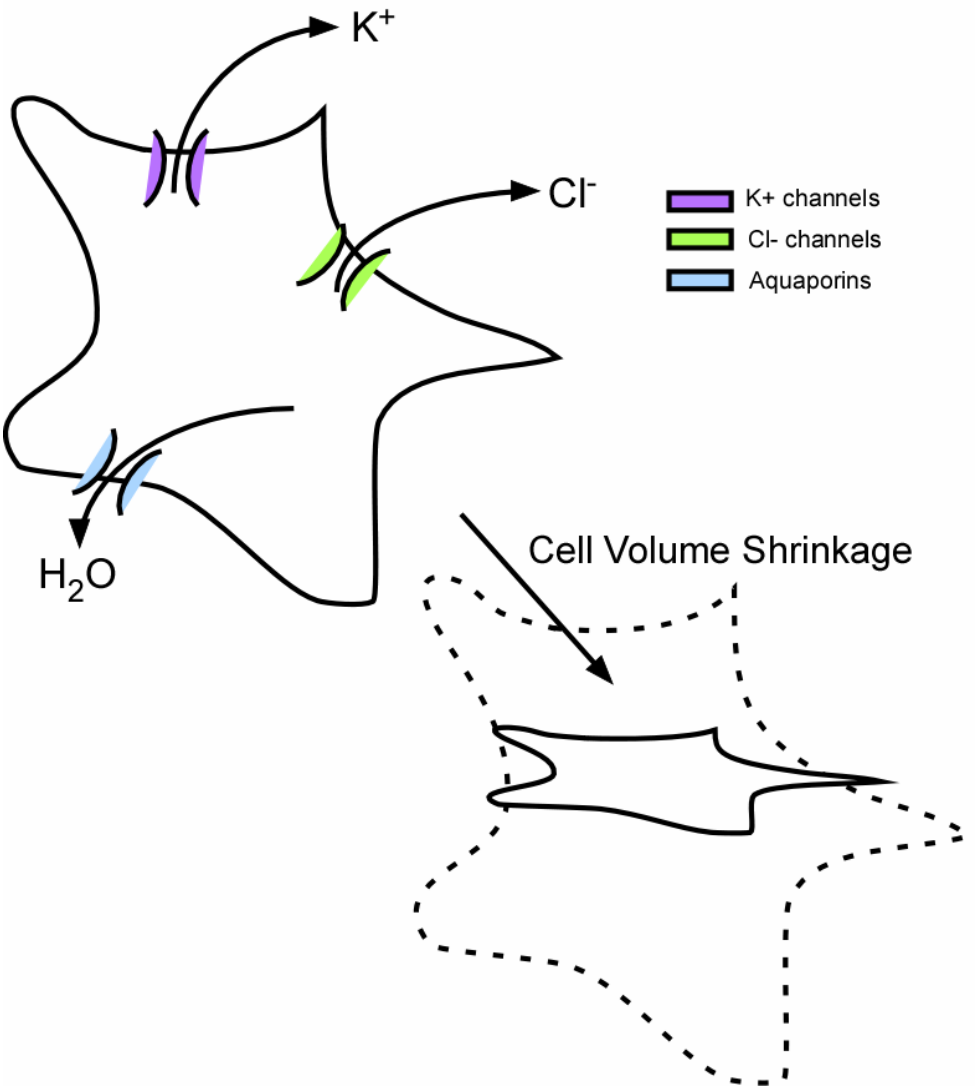

Figure 1.7: Cell volume reduction as a function of electrolytic loss through expressed channels. Illustration represents hypothesis that cell volume reduction may play a role in the capacity for glioma cells, and other similarly diseased cells, to metastasize and proliferate within a living organism.

This property indicates that chlorotoxin has the potential to be used as a therapy for gliomas, and affords insights into the understanding of all cancer metastasis and into the poorly characterized chloride channel superfamily.[93] Chlorotoxin fluorescent dye conjugates are currently in Phase I/II clinical trials for tagging glioma cells for surgical resection.[90]

1.8: Dendrotoxin-1 Structure and Properties

Like α-bungarotoxin, dendrotoxins are high affinity cation channel antagonists.[94] Dendrotoxins are a class of peptides isolated from the venoms of the mamba snake family, and are approximately 7000 Da and range in size from 57-60 amino acids in length.[95] The peptides mechanisms act to block various subtypes of voltage-gated potassium channels. This is accomplished by extending the duration of the action potential, where acetylcholine is then depleted at the neuromuscular junction. Interference with maintenance of cell membrane potential and membrane repolarization functionalities results in dendrotoxins having the effect of hyperexciting muscles. This causes severe muscle contractions, which leads to convulsions and eventual death due to loss of functioning potassium channels.[96] These outcomes to dendrotoxin exposure enable the peptides to be utilized as high affinity ligands with quantum dots in order to study the interplay between potassium channels and other biological targets.

Venom from the Black Mamba contains a dendrotoxin peptide designated as dendrotoxin-1.[94] This isolated peptide has been used as a ligand to target potassium channels expressed by C6 glioma cells.[97] Dendrotoxin-1 contains 60 amino acids within its chain, and has three disulfide linkages (Table 1.3). The three disulfide linkages are located at ^{7}Cys-^{53}Cys, ^{16}Cys-^{40}Cys, and ^{32}Cys-^{57}Cys. Dendrotoxin-1 also contains seven lysine residues within its 60 amino acid structure.[98] The structure (Figure 1.8) is similar to both chlorotoxin and α-bungarotoxin, in that it contains disulfide linkages that link the ends of the peptide together to enhance a pocket-like shape for the peptide.

Table 1.3: Dendrotoxin-1 amino acid sequence.[98] Disulfide linkages are individually colored to illustrate bonding sites within the peptide. Each disulfide linkage is labeled with a different color. There are a total of three disulfide linkages throughout the dendrotoxin-1 peptide.

1	GLN	*13*	PRO	*25*	TYR	*37*	TRP	*49*	THR
2	PRO	*14*	GLY	*26*	ASN	*38*	SER	*50*	ILE
3	LEU	*15*	ARG	*27*	GLN	*39*	GLY	*51*	GLU
4	ARG	*16*	CYS	*28*	LYS	*40*	CYS	*52*	GLU
5	LYS	*17*	TYR	*29*	LYS	*41*	GLY	*53*	CYS
6	LEU	*18*	GLN	*30*	LYS	*42*	GLY	*54*	ARG
7	CYS	*19*	LYS	*31*	GLN	*43*	ASN	*55*	ARG
8	ILE	*20*	ILE	*32*	CYS	*44*	SER	*56*	THR
9	LEU	*21*	PRO	*33*	GLU	*45*	ASN	*57*	CYS
10	HIS	*22*	ALA	*34*	GLY	*46*	ARG	*58*	ILE
11	ARG	*23*	PHE	*35*	PHE	*47*	PHE	*59*	ARG
12	ASN	*24*	TYR	*36*	THR	*48*	LYS	*60*	LYS

Dendrotoxin-1 selectively targets three Shaker family potassium channels, Kv1.1, Kv1.2 and Kv1.6.[94] Allen et al.[97] determined that unstimulated C6 glioma cells express potassium channels of the subtype, Kv1.1, which are targeted by dendrotoxin-1. This study showed that dendrotoxin-1 exposure blocked potassium channels, and thus potassium channel currents were significantly reduced. An additional finding was that not all cells recovered completely from exposure to the toxin.[97] Because dendrotoxin-1 elicits such a strong reaction within cells, to the extent of causing a failure to fully recover from exposure, the peptide exhibits high affinity for its target. Exposure to the peptide may also result in the internalization and complete loss of potassium channel functionality. Based upon these evidences, dendrotoxin-1 is a suitable ligand for furthering nanotechnology initiatives with biological studies.

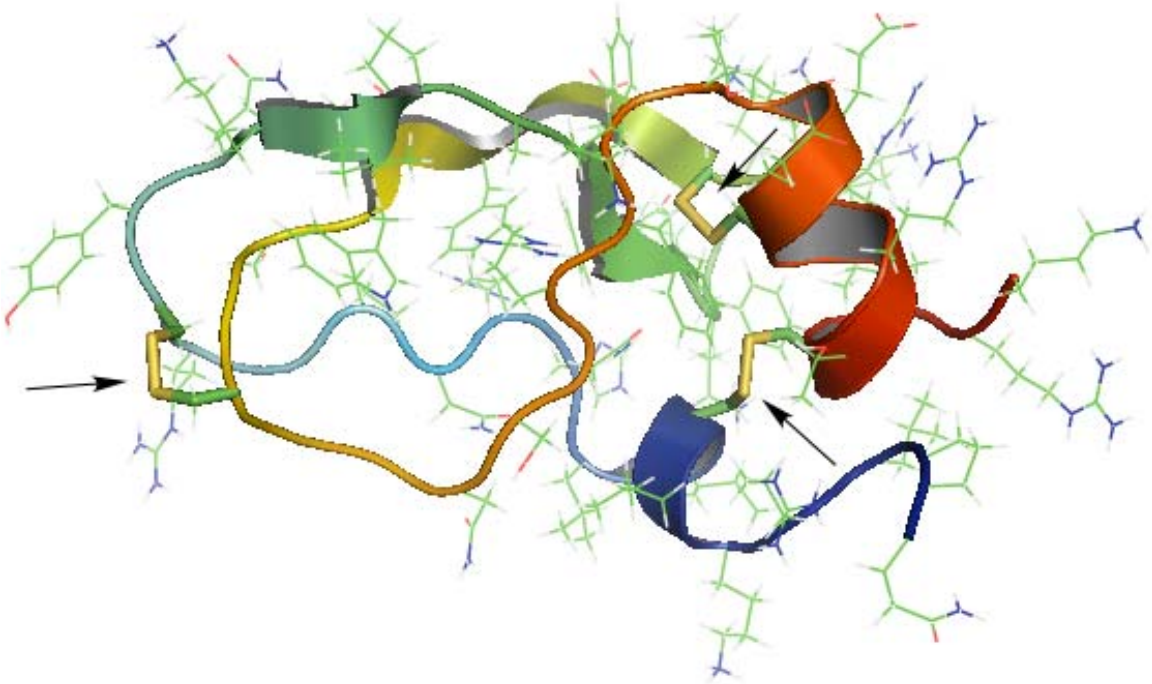

Figure 1.8: Illustration of dendrotoxin-1 structure. Atomic coordinates were retrieved from the Protein Data Bank, 1DEM,[98] and imported into Pymol[84] for illustration purposes. Arrows indicate the location of the disulfide linkages within the peptide.

1.9: Research Overview

This research is focused upon furthering techniques and methodologies toward incorporation of nanotechnology with biological studies. Specifically, the central focus revolves around using high affinity peptide neurotoxins as ligands with fluorescent semiconductor nanocrystals, known as quantum dots, to detect endogenously expressed biological targets in both tissue and living cells. In these studies, three high affinity peptide neurotoxins were used as vehicles toward successful quantum dot integration into detection of targets within complex biological systems. It was demonstrated that two separate methodologies were capable of combining nanotechnology with suitable ligands to navigate sensitive detection in complex biological environments.

The first study[57] focused upon detection of a well classified ligand-gated ion channel, nicotinic acetylcholine receptors, in ex vivo diaphragm tissue. To accomplish this, the neurotoxin, α-bungarotoxin, was employed to facilitate quantum dot labeling in whole mount tissue. Endogenously expressed nicotinic acetylcholine receptors located at the post-synaptic cleft of the neuromuscular junction were labeled with fluorescent probes in a two-step labeling protocol. This revealed that quantum dots, specifically streptavidin quantum dot conjugates, are able to provide specificity in order to identify a cellular protein at the post-synaptic cleft in unfixed native tissue.

The second study[99] centered on the creation of unique quantum dot nanoconjugates. Again, high affinity peptide neurotoxins were employed to operate as targeting ligands. The neurotoxins chosen were more recently isolated than α-bungarotoxin, and may have therapeutic value. One of the toxins, chlorotoxin, is of interest for identifying malignant glioma cells amidst healthy cells in the human brain. The toxin purportedly binds with matrix metalloproteinase-2, and elicits effects on chloride channel currents. The other toxin, dendrotoxin-1, targets a voltage-gated potassium channel which plays critical roles in neural transmission. Incorporating quantum dot technology with these toxins may serve to enable monitoring of these as yet well understood cellular processes. In support of potential applications, the toxins were coupled with fluorescent quantum dots and used to illuminate endogenous expression of their respective targets within living cells. This evinces the versatility of quantum dots for biological systems requiring analyses be performed in dynamic and native environments.

1.10: Summary

Advances in biotechnology enable better disease detection, and potential elimination. A major focus of biotechnological advances has been the development of fluorescent probes to aid in monitoring specific targets in living systems. Use of highly fluorescent quantum dot conjugates relies on ligand suitability for the desired target. High affinity peptide neurotoxins, isolated from a variety of sources, are effective agents for integrating technological advances with biological inquiries. Quantum dot technology enhances biological studies through characteristics, such as enhanced photostability, size-tunable emission, and broad excitation spectra, inherent in the material. Development of protocols that utilize quantum dots for tagging biological, specifically neurologically significant, targets will enable extended monitoring within living systems. This will provide information leading to the development of better therapeutic agents for diseases and conditions that are poorly understood.

CHAPTER II

METHODS AND MATERIALS

2.1: Introduction

Experimental methodology employed high affinity peptide neurotoxins with quantum dots to detect endogenous biological targets in ex vivo tissue and live cells. The methods for handling, executing, and analyzing the assays utilized to assess the efficacy for these peptide ligands as detected by quantum dots to distinguish their targets within ex vivo and living environments are outlined in Table 2.1.

Table 2.1: Outline for high affinity peptide neurotoxin quantum dot experimental methodology.

Study	Analysis	Section
	Neurotoxin Handling Safety Protocols	2.2
	Objective for Detection in Animal Tissue	2.3
	Tissue Preparation	2.4
Ex Vivo	α-Bungarotoxin Detection Time Dependence	2.5
Tissue	α-Bungarotoxin Binding Site Specificity	2.6
	α-Bungarotoxin Affinity	2.7
	Streptavidin-Quantum Dot Photobleaching	2.8
	Objective for Endogenous Detection in Live Cells	2.9
	Biotin-Streptavidin Detection of Endogenous Proteins	2.10
	Cell Culture Maintenance and Conditions	2.11
	Detection of Biotinylated Chlorotoxin in Saline	2.12
	Detection of Biotinylated Chlorotoxin in Buffers at 4^{o}C	2.13
	Peptide Neurotoxin Conjugation to Quantum Dots	2.14
	Confirmation of Toxin and Quantum Dot Confirmation	2.15
Live Cells	Matrix Metalloproteinase-2 Antibody Colocalization in Cell Culture	2.16
	Potassium Channel Kv1.1 Antibody Colocalization in Cell Culture	2.17
	CTX:QD525 Conjugate Blocking	2.18
	DTX-1:QD655 Conjugate Blocking	2.19
	Chlorotoxin Affinity Determined by Saturation Binding Curve	2.20
	Dendrotoxin-1 Affinity Determined by Saturation Binding Curve	2.21
	Multiplexing Experimentation	2.22
	Flow Cytometry	2.23
	Confocal Microscopy	2.24

2.2: Neurotoxin Handling Safety Protocols

High affinity peptide neurotoxins are a class of molecules that require specific handling to be used safely. They are considered to be health hazards, and as such, must be used with caution and careful handling. Although the peptides are isolated from venom, and are possibly absent of the full venom effects, accidental injection or similar mishaps may result in serious consequences. Each peptide neurotoxin is capable of binding to a specific target within a living organism with high affinity. This interaction results in a multitude of effects if accidentally exposed to personnel improperly.

All peptide neurotoxins were used within the guidelines of Biosafety Level-2 (BL-2) research protocols. To use the peptide neurotoxins, all proper personal protective gear must be worn. Each neurotoxin was provided as a lyophilized powder in need of reconstitution prior to use. Lyophilized powders were reconstituted according to manufacturer's instructions within a BL-2 biohood under sterile conditions. Aliquots were stored in low volumes, and in conditions determined by the manufacturer. All waste was collected and disposed as biowaste in compliance with Vanderbilt Environmental Health and Safety guidelines.

2.3: Quantum Dot Objective for Detection within Animal Tissue

The objective of these experiments was to demonstrate that quantum dots are a viable means of detecting an endogenous target within animal tissue. To accomplish this, a ligand with known high affinity for nicotinic acetylcholine receptors was chosen for the task. From there, a protocol for quantum dot detection of the ligand in ex vivo tissue was developed. The protocol was able to demonstrate that the nanocrystals were capable of

binding to the receptor bound peptide ligand within the complex environment of extracted mouse diaphragm. The efficacy of quantum dot detection was determined through examination with colocalized fluorescent antibodies bound to different subunits on the nicotinic acetylcholine receptors, analysis of photostability, and quantitation leading to approximation of neurotoxin ligand specificity for the native receptor.

2.4: Mouse Diaphragm Ex Vivo Tissue Preparation

All experiments were performed using C57BL/6 inbred mice between 8 and 10 weeks of age and sacrificed in accordance to IACUC standards and procedure protocols. Dissected mouse diaphragm was obtained from the Blakely Laboratory and washed in 1x phosphate-buffered saline (PBS) solution for approximately 1 hour on ice. The tissue was then divided into equal portions and incubated in 100mM glycine in 1xPBS (pH 7.3) for 1 hour on ice. Overnight incubation at 4°C followed in blocking solution consisting of 1xPBS (pH 7.3), 5% normal goat serum, 3% bovine serum albumin, 0.2% Triton X-100, and 0.01% thimerasol. The tissue was then briefly washed in 1xPBS solution. The tissue pieces were then exposed to the experimental conditions prescribed for the assay being evaluated.

2.5: Quantum Dot Time Dependent Detection of α-Bungarotoxin

Following tissue preparation, mouse diaphragm sections were exposed to biotinylated α-bungarotoxin for the experimental time intervals of 10, 60, 180, 360, or 720 minutes (Figure 2.1).

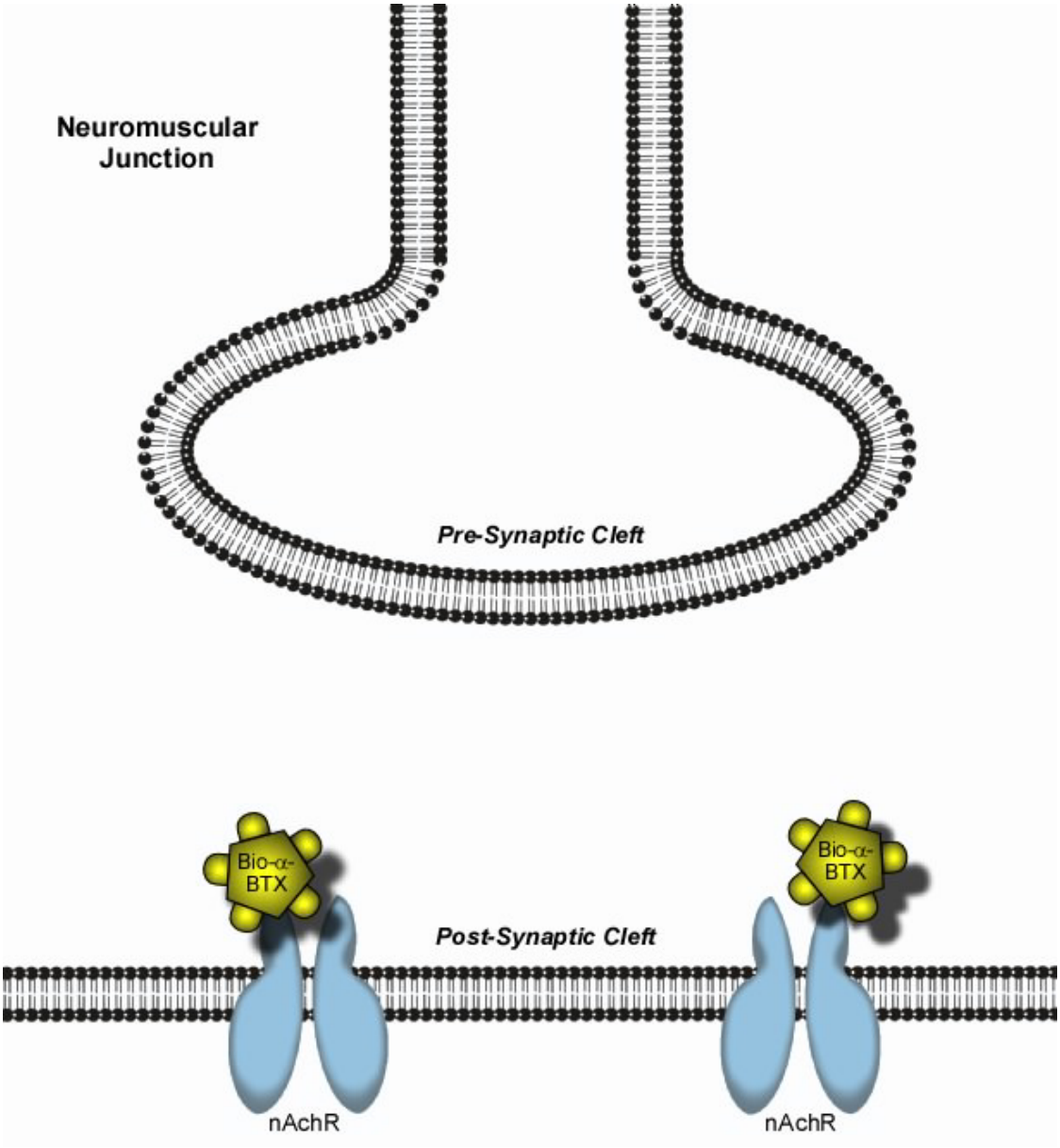

Figure 2.1: Representation of biotinylated α-bungarotoxin (bio-α-BTX) labeling of nicotinic acetylcholine receptors (nAchRs) at the neuromuscular junction. This step represents the first of a two-step quantum dot detection method employing avidin-linked probe affinity for biotinylated ligands.

The tissue was incubated at 4°C in blocking solution consisting of 1xPBS (pH 7.3), 5% normal goat serum, 3% bovine serum albumin, 0.01% thimerasol, nicotinic acetylcholine

receptor β-subunit rat-anti-nicotinic acetylcholine receptor primary antibody (1:5000) (Sigma, Inc.), and 10nM biotinylated α-bungarotoxin (Invitrogen, Inc.) (Figure 2.2).

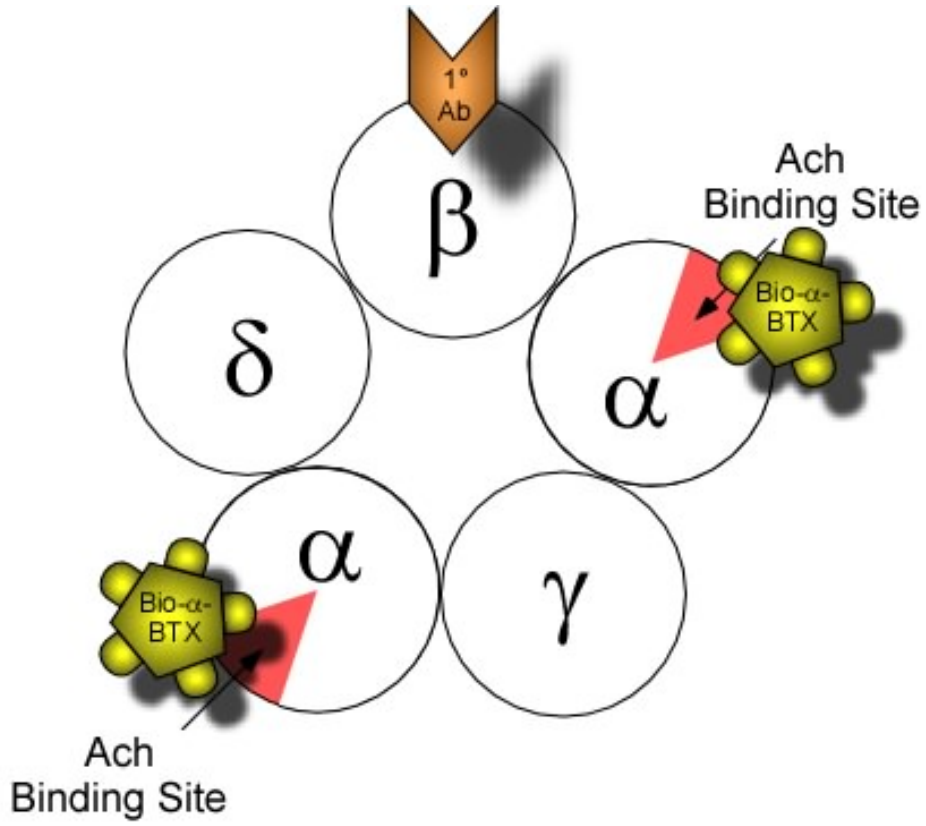

Figure 2.2: Aerial view of labeling with biotinylated α-bungarotoxin and anti-β-subunit antibody on a nicotinic acetylcholine receptor. This was accomplished using ex vivo mouse diaphragm tissue that was first treated with 100mM glycine, followed by blocking solution with Triton X-100. Biotinylated high affinity peptide neurotoxin and primary antibody exposure were achieved within blocking solution at 4°C.

Mouse diaphragm tissue was also treated as a control series by exposing the pieces to the same quantum dot detection conditions without the biotinylated α-bungarotoxin.

The tissue sections were briefly washed in 1x PBS solution. Overnight incubation at 4°C followed with 10nM streptavidin-QD655 conjugates in blocking solution (Figure 2.3).

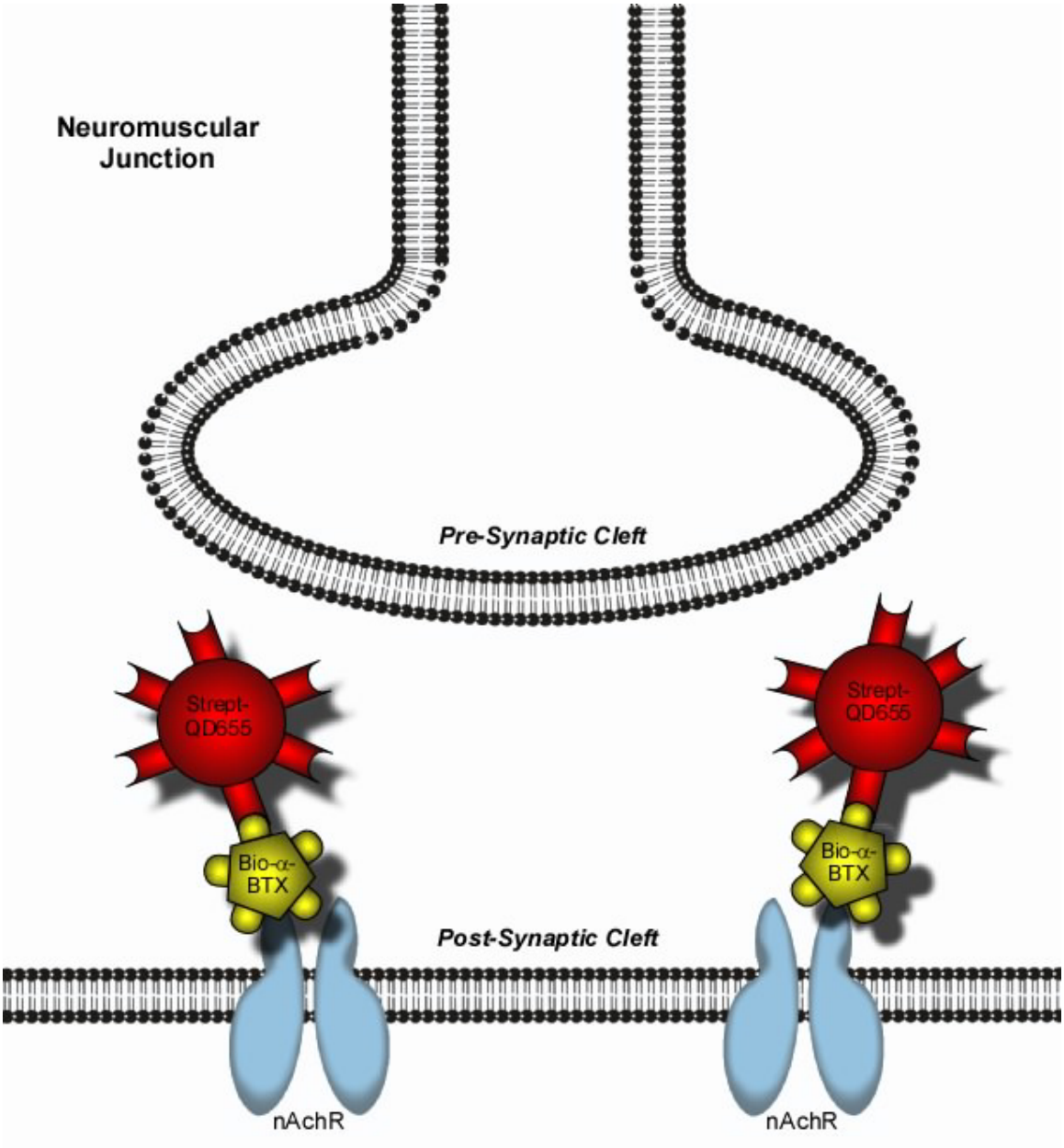

Figure 2.3: Representation of streptavidin-QD655 conjugate detection of biotinylated α-bungarotoxin bound to nicotinic acetylcholine receptors present at the neuromuscular junctions of ex vivo mouse diaphragm tissue. This corresponds to the second step of a two-step quantum dot detection strategy utilizing the femtomolar affinity for biotin exhibited by streptavidin.

The anti-β-subunit primary antibody was detected with Alexafluor488-rabbit-anti-rat secondary antibody conjugate (1:5000) simultaneously with the biotinylated α-bungarotoxin detection with streptavidin-QD655 conjugates (Figure 2.4). The procedure was repeated in parallel with 10nM streptavidin-Alexafluor-555, swapped for streptavidin-QD655, conjugates in blocking solution with the remaining tissue sections. The tissue sections were then washed in 1x PBS three times for 10 minutes on ice and mounted using AquaMount anti-photo-bleaching solution for imaging. The labeling protocol was repeated for 10, 60, 180, and 360 minutes with tissue that was incubated in blocking solution at 4°C for seven days.

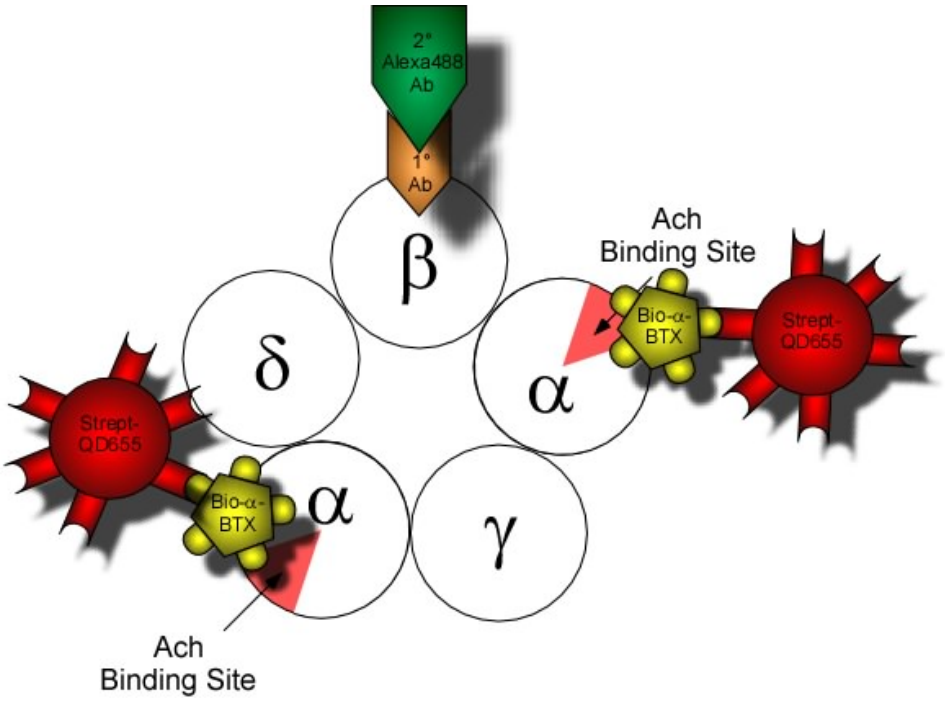

Figure 2.4: Overhead view of two-step detection methodology utilizing the strong binding interaction between streptavidin and biotin. Representation shows biotinylated α-bungarotoxin detected by streptavidin-QD655 conjugates, along with anti-β-subunit primary antibody detected by Alexafluor488 secondary antibody, bound to nicotinic acetylcholine receptor at the neuromuscular junction of ex vivo mouse diaphragm tissue.

2.6: α-Bungarotoxin Binding Site Specificity Assay

Quantum dot detection specificity was analyzed using unconjugated α-bungarotoxin (Figure 2.5). The objective of these experiments was to ascertain that quantum dot detection was ligand dependent and not stemming from non-specific binding.

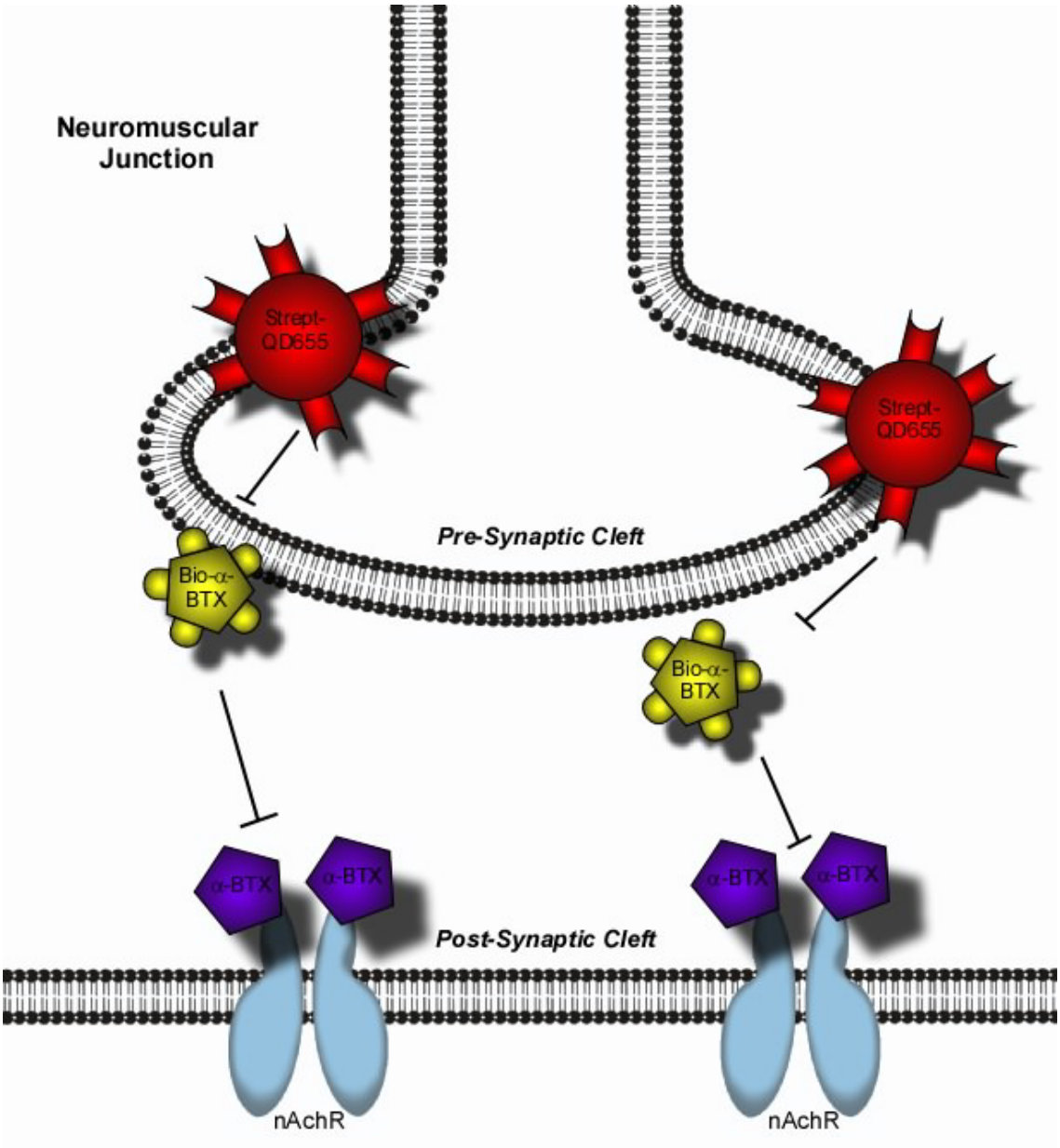

Figure 2.5: Depiction of biotinylated α-bungarotoxin binding inhibited by unconjugated α-bungarotoxin blocking the binding region on nicotinic acetylcholine receptors. Streptavidin-QD655 detection is additionally inhibited due to lack of biotinylation necessary for probe-ligand interaction.

Because these studies are based upon quantum dot detection of endogenous targets within ex vivo tissue, it was of particular importance to perform these experiments. To do this, mouse diaphragm pieces were prepared as before and additionally exposed to 100nM α-bungarotoxin in blocking solution overnight, for approximately 12 hours, at 4°C as pre-treatment to determine specificity. The tissue was treated as before with 10nM biotinylated α-bungarotoxin and primary antibody (1:5000). After 12 hours of ligand exposure, the tissue pieces were incubated with streptavidin-QD655 and streptavidin-Alexafluor555 fluorescent probes. The primary antibody was again illuminated using Alexafluor488 secondary antibodies (Figure 2.6). At the end of the overnight incubation at 4°C, the tissue was washed and mounted as previously described. All tissue was imaged using an inverted confocal microscope (Zeiss, Inc.) and analyzed using Metamorph software (MDS, Inc.). Data was analyzed and saturation binding curves were generated using GraphPad Prism (GraphPad Prism Software, Inc.).

2.7: α-Bungarotoxin Affinity Assay

Ligand affinity was assessed through saturation binding curve analysis. Saturation binding curves were generated using dissected tissue, treated as previously described. The tissue was incubated with a series of dilutions of biotinylated α-bungarotoxin for 10 minutes at 4°C. From there, the tissue pieces were incubated overnight in 10nM streptavidin-QD655s. After overnight incubation, the tissue was washed three times for 10 minutes, and then mounted with AquaMount. Each concentration was imaged at least three times with experiments run in triplicate. The curve was generated using GraphPad Prism software (GraphPad Prism Software, Inc.).

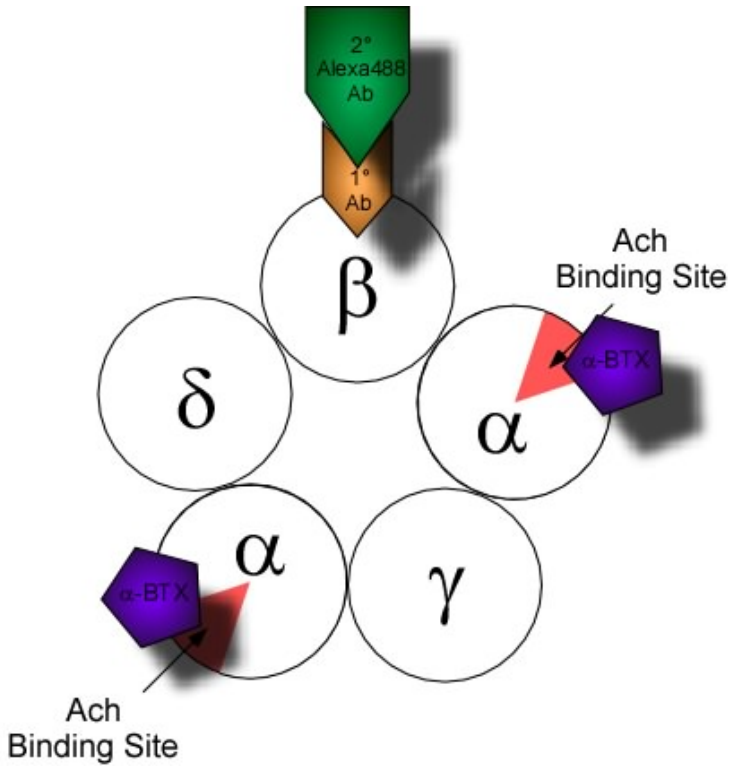

Figure 2.6: View from above of α-bungarotoxin bound to nicotinic acetylcholine receptors. The unconjugated α-bungarotoxin prevents biotinylated α-bungarotoxin from binding to the receptors.

2.8: Streptavidin-Quantum Dot Photobleaching Assays

In order to examine and establish quantum dot photostability within an ex vivo tissue environment, photobleaching experiments were performed. Mouse diaphragm pieces were obtained and prepared as before. The tissue was then exposed to 10nM biotinylated α-bungarotoxin for 10 minutes. Following ligand incubation for 10 minutes, the tissue was incubated with either streptavidin-QD655 or streptavidin-Alexafluor555 conjugates overnight at 4°C. The samples were washed in 1xPBS three times for ten minutes and mounted in MatTek dishes. The β-subunit primary antibody employed for other experiments, and the secondary Alexafluor488 antibody fluorescence label were incorporated with the protocol as previously described. Following sample preparations,

each was imaged as before on a Zeiss inverted confocal microscope. The fluorescent conjugates were exposed to continuous excitation for approximately 30 minutes, and images were collected as a time series. Each conjugate was also spin-cast, dropped onto a spinning surface for solvent evaporation, and imaged using a Zeiss Axiovert 200M widefield microscope with Metamorph. FITC was run as a standard.

2.9: Quantum Dot Objective for Endogenous Detection in Living Cells

Development of labeling methodologies using quantum dots within living cells promotes usage for live trafficking experimentation. Because of their unique photostability, quantum dots bridge a potentially critical step in nanotechnology advancement within fundamental biological research. Capacity to detect ligands bound to target proteins that are native to the cell type being studied invites possibilities for generation of knowledge concerning complex interactions between multiple proteins. Since nanocrystals emit narrow emission spectra based upon size and composition, they may be used within a single system to examine multiple targets. The targets would then be differentiated by emission color when imaged using fluorescence microscopy techniques. This quantum dot characteristic, along with single-source excitation ability, was demonstrated using fluorescence microscopy to perform multiplexing experiments. Multiplexing was accomplished following synthesis of novel conjugates using two separate high affinity peptide neurotoxins, and confirmation of binding accuracy via fluorescence antibodies. Toxin conjugate affinities for endogenously expressed proteins were additionally determined within living cells.

2.10: Biotin-Streptavidin Detection of Endogenous Proteins in Live Cells

Chlorotoxin was biotinylated for detection with streptavidin-quantum dots according to the reaction in Scheme 2.1.

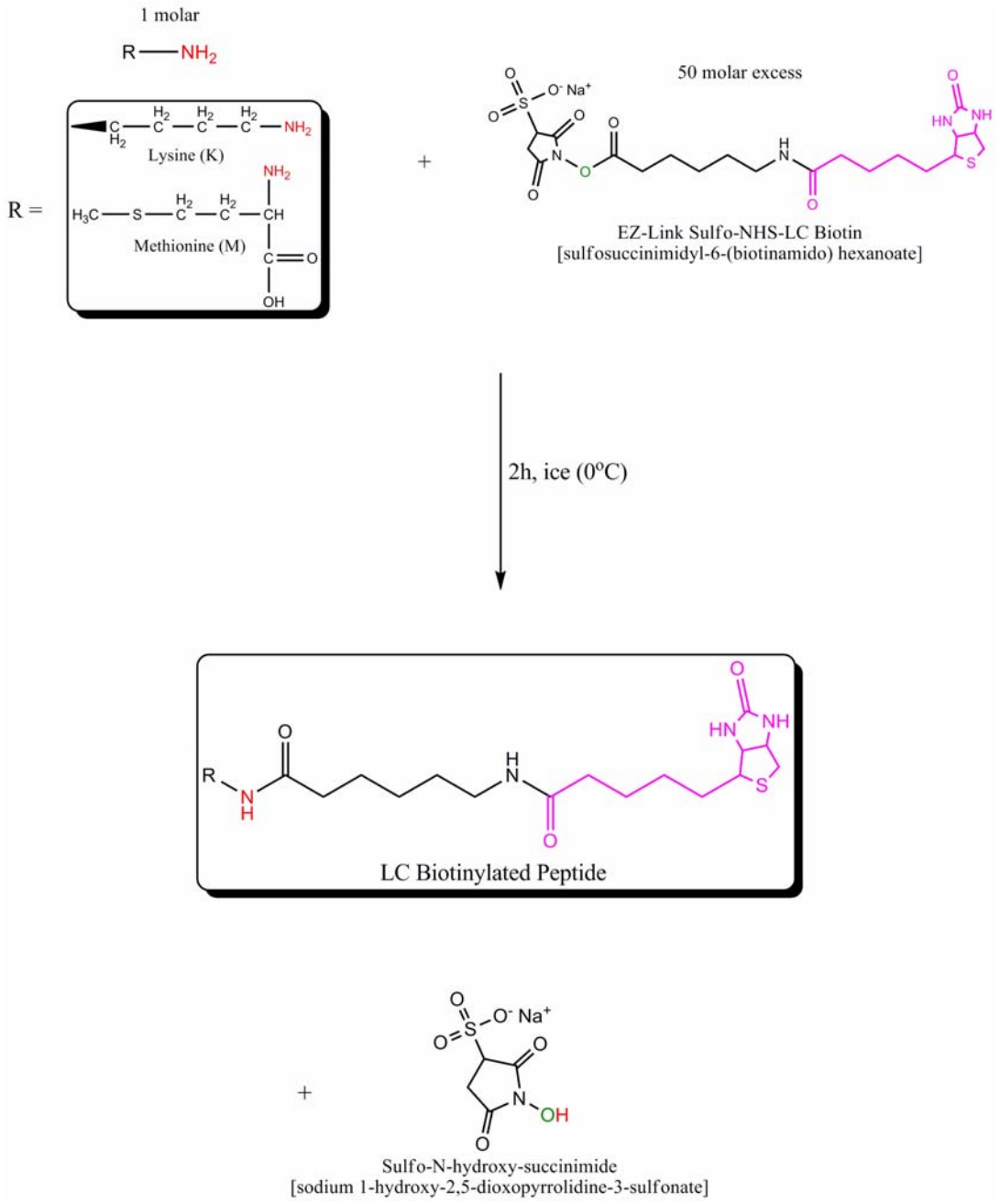

Scheme 2.1: Biotinylation reaction scheme used for biotinylation of chlorotoxin.

Biotinylation was achieved using Pierce EZ-link NHS biotin kit (Pierce, Inc.). The peptide was reconstituted from its lyophilized form in bicarbonate buffer (pH 8.5) per kit recommendations. Reconstitution resulted in a final peptide concentration of 2μM and the solution was subsequently stored in small volume aliquots. Chlorotoxin has an estimated four biotinylation sites where sulfo-succinimidyl-6-(biotinamido) hexanoate may react to alter the amino acid residues for avidin-linked fluorescent probe detection. These residues are ^{1}Met, ^{15}Lys, ^{23}Lys, and ^{27}Lys within the peptide sequence of the neurotoxin. Since the peptide concentration was substantially lower than the recommendations in the biotinylation kit, the biotinylation protocol was modified to compensate for this difference. The reaction was prepared such that the reactant ratios were 1:50; that is, 50 molar excess of sulfo-succinimidyl-6-(biotinamido) hexanoate was reacted with one mole of chlorotoxin. The reactants were mixed and placed on ice for 2 hours. Following incubation on ice, separation and biotinylated chlorotoxin isolation was achieved by use of dialysis methods. The solution was injected into a Pierce Dialysis Cassette (MWCO 3500 Da) according to equipment specifications. Dialysis lasted approximately 12 hours. The dialysis proceeded by suspending the cassette in a 1-L solution of 1xPBS (pH 7.4) with constant stirring at 4°C. After 2 hours, the solution of 1xPBS was replaced and the process was allowed to continue for another 2 hours. Following this, dialysis concluded overnight under the same conditions. The biotinylated chlorotoxin solution was removed from the dialysis cassette and tested for evidence of biotinylation. According to the biotinylation kit, UV/Vis analysis will confirm the presence of biotinylation of the peptide. This was determined by comparison of peptide The biotinylated chlorotoxin solution was compared to a HABA solution using UV/Vis

analysis. We were able to determine that the chlorotoxin was biotinylated approximately 2.38 moles of biotin : 1 mole of chlorotoxin. This indicates that we were successful at biotinylating chlorotoxin for our studies.

2.11: Cell Culture Maintenance and Conditions

C6 glioma cells (courtesy of Dr. Daryl Bornhop via Lynn E. Samuelson, Vanderbilt University Department of Chemistry) were cultured in Dulbecco's Minimum Essential Media (DMEM) with 10% fetal bovine serum (FBS), 1% penicillin/streptomycin, and 1% L-glutamate at 37°C and 5% CO_2. Cells were split every four to six days to allow for optimal growth and reduce overcrowding. Cultures were kept in T-75mm flasks, and split with 0.05% trypsin/EDTA solution. H460 cells (courtesy of Dr. Catherine Prudom, Wright Laboratory, Vanderbilt University, Department of Chemistry) were divided and maintained in the same manner as the C6 glioma cells. Similar conditions to those provided for C6 glioma cells and H460 cells were maintained for HEK-293T cells and 3T3/NIH cells.

2.12: Detection of Biotinylated Chlorotoxin in Saline

C6 glioma cells were cultured for 72 hours in six-well plates at 37°C and 5% CO_2 and allowed to propagate until nearly 100% confluent. The cells were then exposed at 37°C and 5% CO_2 to 10nM biotinylated chlorotoxin in 1x PBS with Ca^{2+} and Mg^{2+} for five minutes. The cultures were rinsed three times with room temperature 1xPBS with Ca^{2+} and Mg^{2+} (Figure 2.7). Following the toxin exposure, the cells were incubated with 1nM streptavidin-QD655s in 1x PBS with Ca^{2+} and Mg^{2+} for five minutes at 37°C and

5% CO_2 (Figure 2.8). Each culture was then washed with room temperature 1x PBS with Ca^{2+} and Mg^{2+} three times, again, and imaged. Initial cell experiments were imaged in 1xPBS with Ca^{2+} and Mg^{2+} solution.

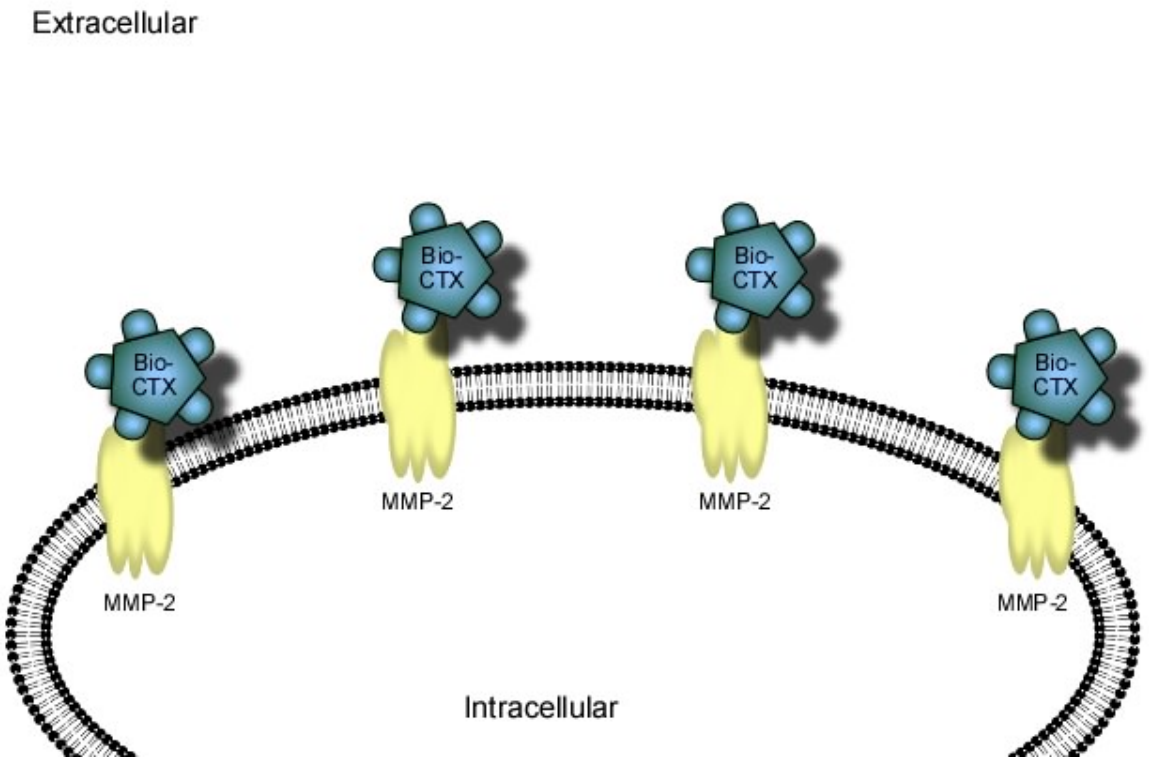

Figure 2.7: Illustration of the first step of a two-step detection protocol for detecting endogenous proteins within cell cultures. A biotinylated high affinity peptide neurotoxin, chlorotoxin (bio-CTX), binds to matrix metalloproteinase-2 (MMP-2) to facilitate avidin-linked probe detection.

The images were captured using a Zeiss Axiovert 200M widefield microscope at 20x. The microscope was equipped with Metamorph imaging software (Metamorph, Inc.). These initial experiments were performed using cells plated in six-well plates with poly-D-lysine coating. The sextet sampling experiment was repeated three times to ascertain chlorotoxin detection was present and not a false positive.

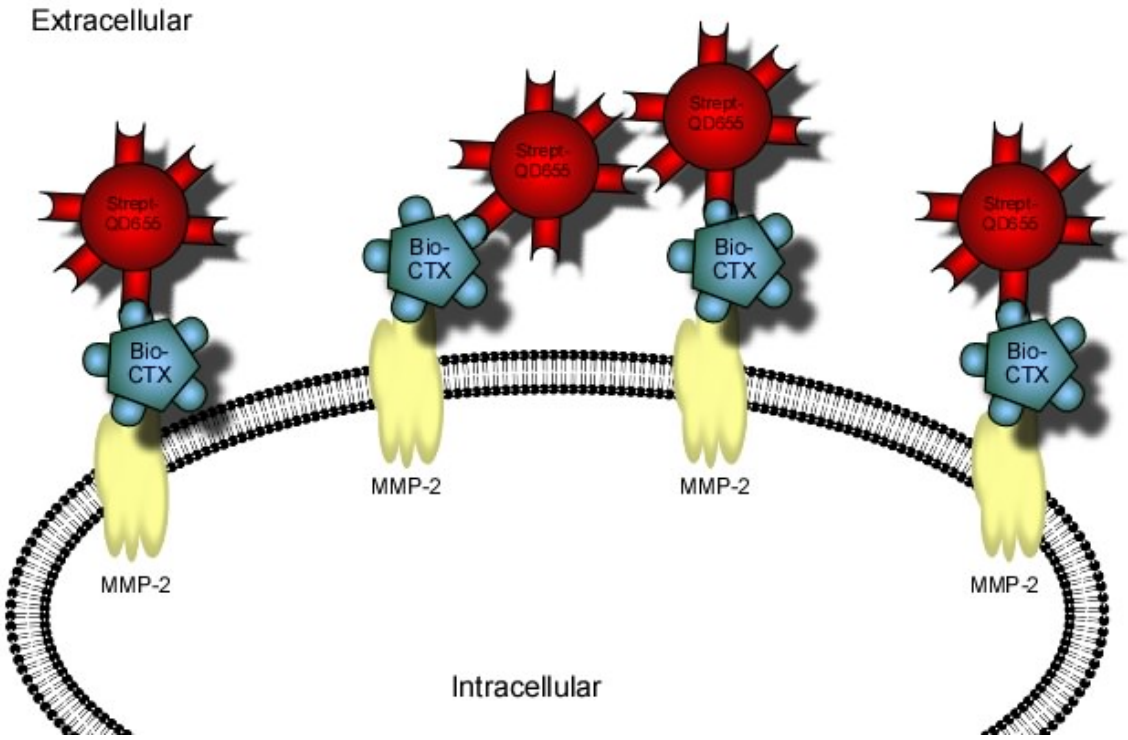

Figure 2.8: The second step of a two-step detection protocol using a biotinylated high affinity peptide neurotoxin, chlorotoxin (bio-CTX), to facilitate avidin-linked probe labeling. Streptavidin-QD655 probes detect biotinylated chlorotoxin bound to endogenous matrix metalloproteinase-2 (MMP-2) within cell culture.

2.13: Detection of Biotinylated Chlorotoxin in Buffers at 4°C

C6 glioma cells were cultured for 24 hours after trypsinizing and plating the cells in poly-D-lysine coated six-well plates. The cells were treated with ice cold Kreb's-Ringer-HEPES (KRH) buffer before exposing the cultures to multiple buffer solutions, including 1x KRH buffer with and without a percent bovine serum albumin (BSA), containing the labeling agents. KRH was chosen because it contains salts and glucose, which may aid in examining shuttling events, and to maintain cell life during the hours of incubation at 4°C. To examine the labeling efficacy within KRH buffers, 10nM bio-CTX and 1nM streptavidin-QD655 conjugates were added to KRH buffer, KRH with 1% BSA,

KRH with 2% BSA, KRH with 3% BSA. Additionally, labeling efficacy was examined within DMEM complete culture medium with 10% FBS, 1x PBS with Ca^{2+} and Mg^{2+}, and tissue buffer with Ca^{2+} and Mg^{2+}. Control experiments were also run in parallel to determine if the methods yielded quantum dot non-specific binding interactions. The solutions were added to the cells for two hours at 4°C with constant agitation. Following the two hour incubation, the cells were washed 4-times in ice cold KRH buffer and imaged. Imaging was performed with a Zeiss 200M Axiovert microscope (Zeiss, Inc.) with Metamorph software (Metamorph, Inc.).

2.14: Peptide Neurotoxin Conjugation to Quantum Dots

Conjugation conditions were adapted from synthesis methods developed by Sun et al.[72] (Scheme 2.2). Briefly, one molar equivalent of ITK Quantum Dot amino(PEG) 525s or 655s (Invitrogen, Inc.) were reacted with 2000 molar equivalents of N-succinimidyl iodoacetate (SIA) (Pierce, Inc.) for two hours at room temperature with constant stirring. The chlorotoxin (Anaspec, Inc.) or dendrotoxin-1 (Sigma, Inc.) was mixed (200 molar equivalents) with 2000 molar equivalents of Traut's reagent (2-iminothiolane HCl) (Pierce, Inc.) for one hour at room temperature. The quantum dot solution was combined with the toxin solution and allowed to react for one hour at room temperature. The conjugates were separated and concentrated using a 7000 MWCO Zeba desalting column at 1000 x *g* for 2 minutes three times (Pierce, Inc.). From there, the solution was centrifuged again in 100,000 MWCO Millipore Ultrafree-0.5 Biomax centrifugation columns at 7500 x *g* for 10 minutes (Millipore, Inc.). Concentration of each conjugate solution was determined using a CaryWin UV/Vis spectrophotometer

with designated extinction coefficients for QD525 (ε=200,000 M-1 cm-1 at 506 nm) and QD655 (ε=800,000 M-1 cm-1 at 638 nm).

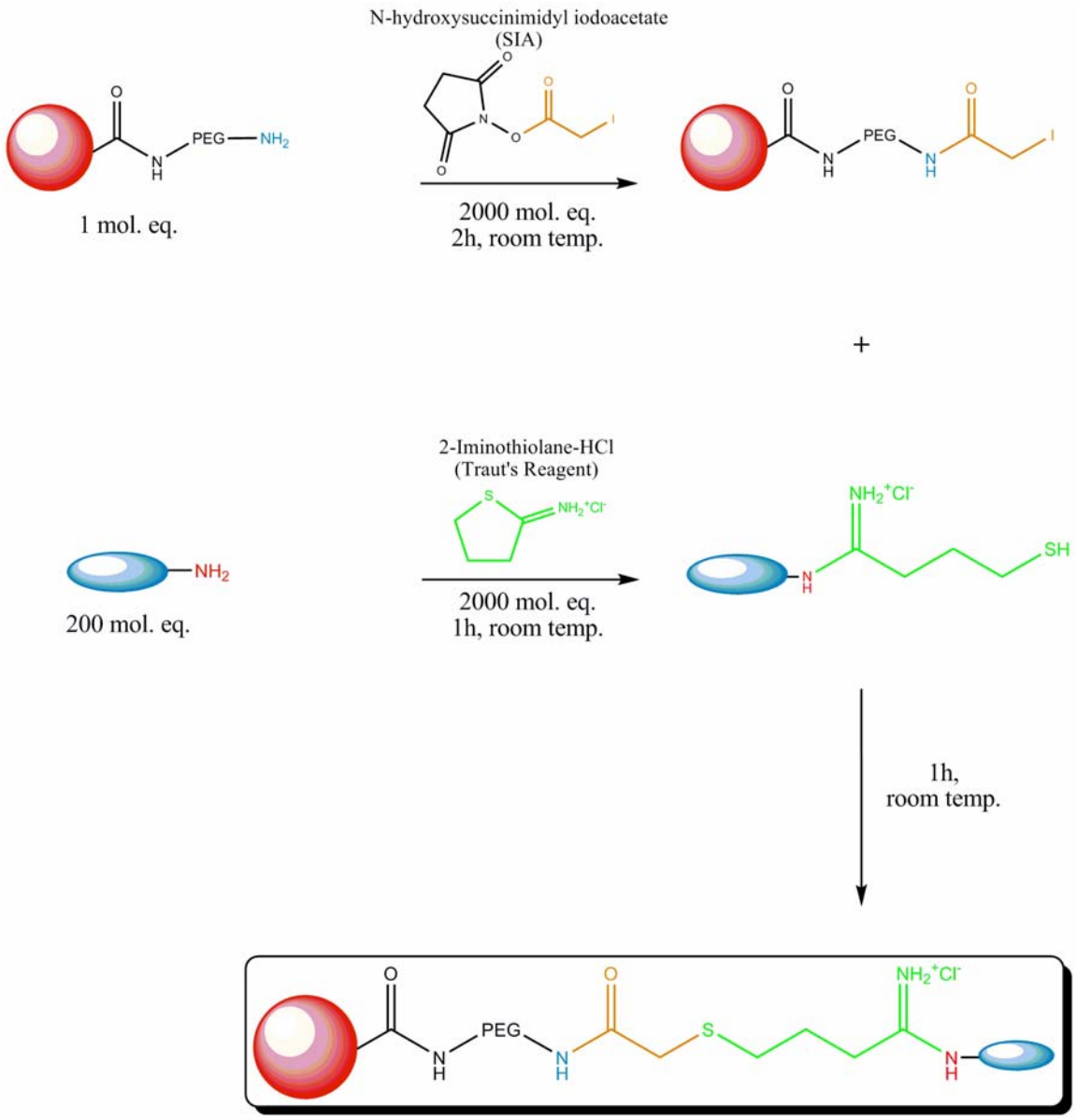

Scheme 2.2: Reaction scheme for high affinity peptide neurotoxin conjugation to ITK Quantum Dot amino(PEG) 525s and 655s.

2.15: Confirmation of Toxin and Quantum Dot Confirmation

To determine whether the high affinity peptide neurotoxins, either chlorotoxin or dendrotoxin-1, had been successfully conjugated to the ITK Quantum Dot amino(PEG) 525s or 655s, respectively, gel electrophoresis techniques were employed. Toxin conjugation to quantum dots was confirmed with a 0.5% agarose gel run at 80V continuously for 120 minutes (Figure 2.9).

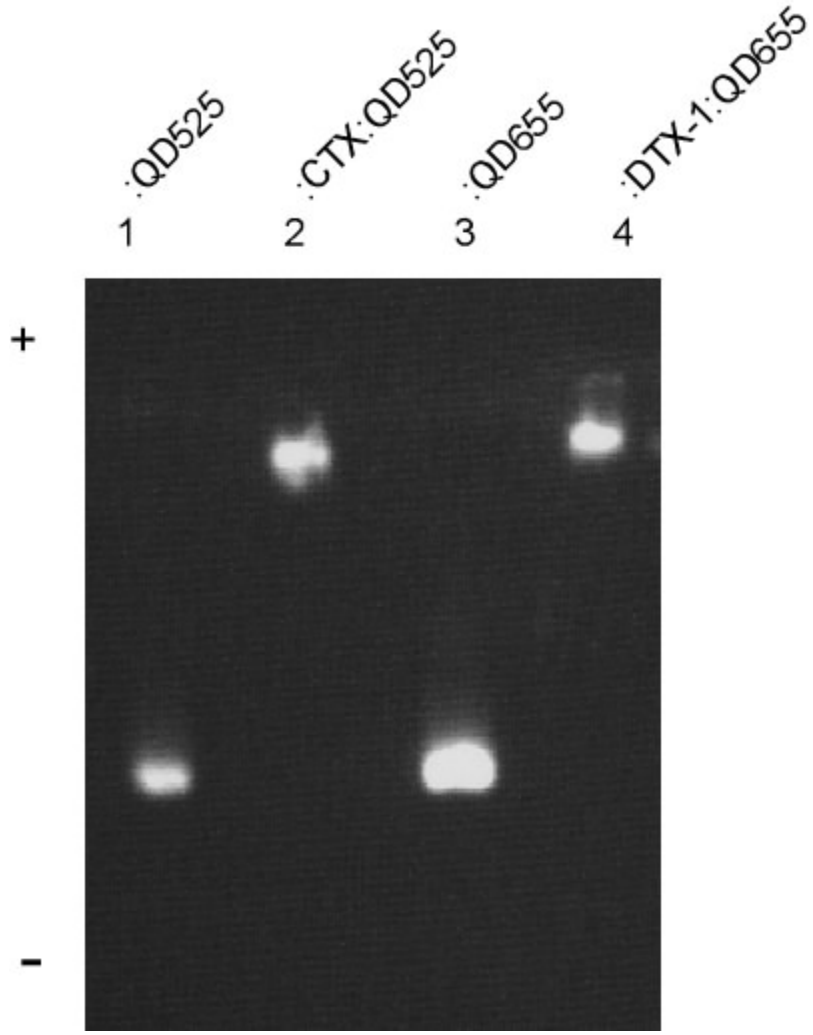

Figure 2.9: Quantum dot fluorescence conjugation analysis via gel electrophoresis techniques. The 0.5% agarose gel was prepared with 1xTBE buffer, and loaded with 12µL of 1nM quantum dot conjugates. The gel electrophoresis proceeded at 80V continuously for approximately 120 minutes with 1xTBE buffer used as vehicle.

The gel was made with and run in 1xTris/Borate/EDTA buffer (TBE). The conjugates and unconjugated quantum dots were diluted 1x borate buffer (pH 8.5) to 1nM concentrations. These aliquots were loaded into the 0.5% agarose gel in 12μL volumes, and allowed to settle for approximately 15 minutes prior to initiating the current for electrophoresis. Imaging utilized a Bio-Rad Chemidox XRS System with Quantity One software (Bio-Rad, Inc.).

2.16: Matrix Metalloproteinase-2 Antibody Colocalization in Cell Culture

Matrix metalloproteinase-2 antibody colocalization with CTX:QD525 was achieved using C6 glioma cells plated on MatTek dishes. The C6 glioma cells were allowed to propagate for 44-48h until approximately 80% confluent. The cell cultures were then exposed to 10nM CTX:QD525 or QD525 in DMEM complete cell culture media for 120 minutes (Figure 2.10). Following exposure to CTX:QD525 or QD525, the cells were washed three times with 1x DPBS and fixed in 4% PFA for 30 minutes at room temperature. The cells were then washed three times in 1x DPBS and incubated for 10 minutes in 0.1% Triton X-100. Each dish was washed three times with 1x DPBS and incubated at 4°C in 1% normal goat serum (NGS) (Jackson BioLabs) with primary polyclonal rabbit anti-MMP-2 antibodies (1:500) (Sigma, Inc.) for approximately 22-24 hours. Following primary antibody exposure, cells were again washed in 1x DPBS three times then treated with secondary goat anti-rabbit Alexafluor594 antibodies (1:500) (Invitrogen, Inc.) in 1% NGS for one hour at room temperature. This portion of the procedure was performed in the dark to prevent photobleaching of the Alexafluor

antibody conjugates. Following this portion of the protocol, the cells were again washed in 1x DPBS three times and mounted using PolyAqua Mount with a coverslip.

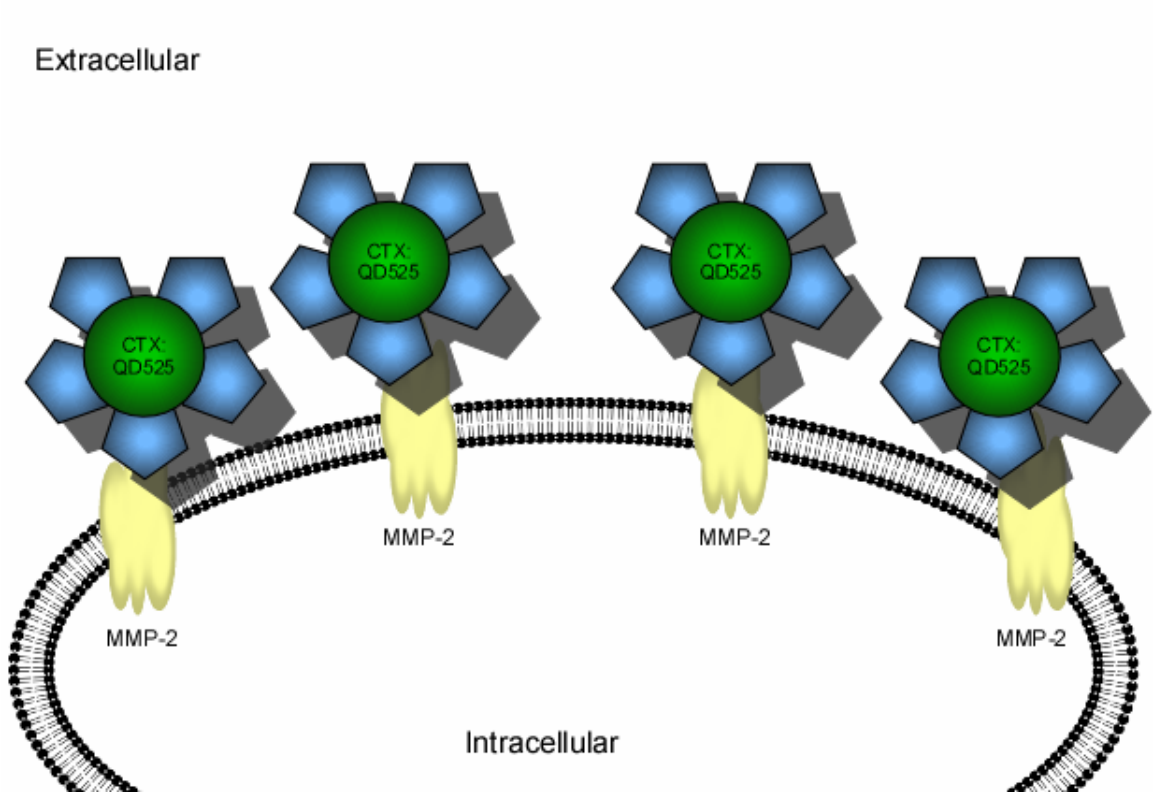

Figure 2.10: Representation of high affinity peptide neurotoxin, chlorotoxin (CTX), quantum dot conjugates (CTX:QD525) labeling endogenous proteins in live cell culture. Conjugates detect endogenous matrix metalloproteinase-2 (MMP-2) present on the cell membrane surface. Detection was accomplished at 37°C and 5%CO_2 in DMEM complete cell culture media.

2.17: Potassium Channel Kv1.1 Antibody Colocalization in Cell Culture

Voltage-gated potassium channel 1.1 antibody colocalization with DTX-1:QD655: was accomplished through similar methodology as colocalization of matrix metalloproteinase-2 antibody colocalization with CTX:QD525 conjugates. C6 glioma cells were plated on MatTek dishes and allowed to propagate for 44-48 hours until

approximately 80% confluent. Cell cultures were exposed to 5nM DTX-1:QD655 or 5nM QD655 in DMEM complete for 180 minutes (Figure 2.11).

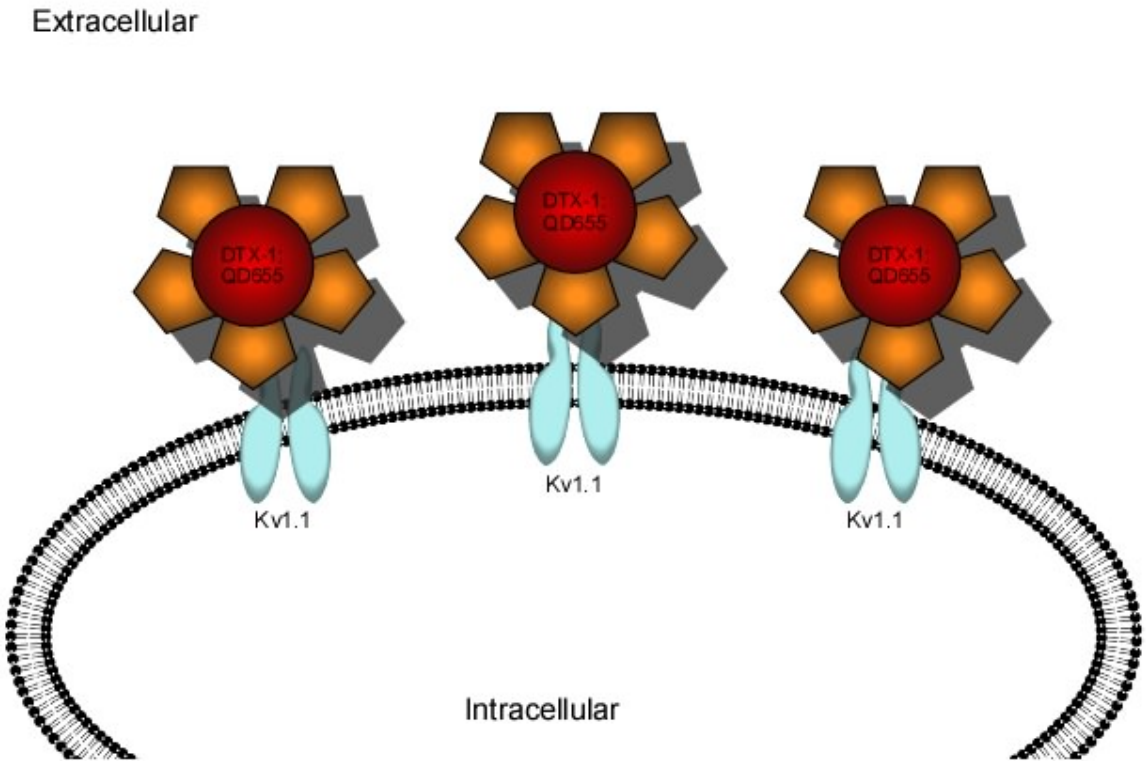

Figure 2.11: Representation of high affinity peptide neurotoxin, dendrotoxin-1 (DTX-1), quantum dot conjugates (DTX-1:QD655) labeling endogenous proteins in live cell culture. Conjugates detect endogenous voltage-gated potassium channel 1.1 (Kv1.1) present on the cell membrane surface. Detection was accomplished at 37°C and 5% CO_2 in DMEM complete cell culture media.

Cells were washed three times with 1x DPBS and fixed in 4% PFA for 30 minutes. The cell cultures were then washed three times in 1x DPBS and incubated for 10 minutes in 0.1% Triton X-100 solution. After incubation in the Triton X-100 solution, each dish was washed three more times with 1x DPBS then incubated at 4°C in 1% NGS (Jackson BioLabs) with primary polyclonal rabbit anti-Kv1.1 antibodies (1:500) (Sigma, Inc.) lasting for 22-24 hours. Following primary antibody exposure, cells were again washed in 1x DPBS three times then treated with secondary goat anti-rabbit Alexafluor488

antibodies (1:500) (Invitrogen, Inc.) in 1% NGS for one hour at room temperature in the dark. The cells were then washed in 1x DPBS three times and mounted using PolyAqua Mount with a coverslip.

2.18: CTX:QD525 Conjugate Blocking Assays

Chlorotoxin binding specificity was examined by using chlorotoxin to bind with matrix metalloproteinase-2 in an effort to prevent the novel conjugates, CTX:QD525s, from labeling the cells (Figure 2.12).

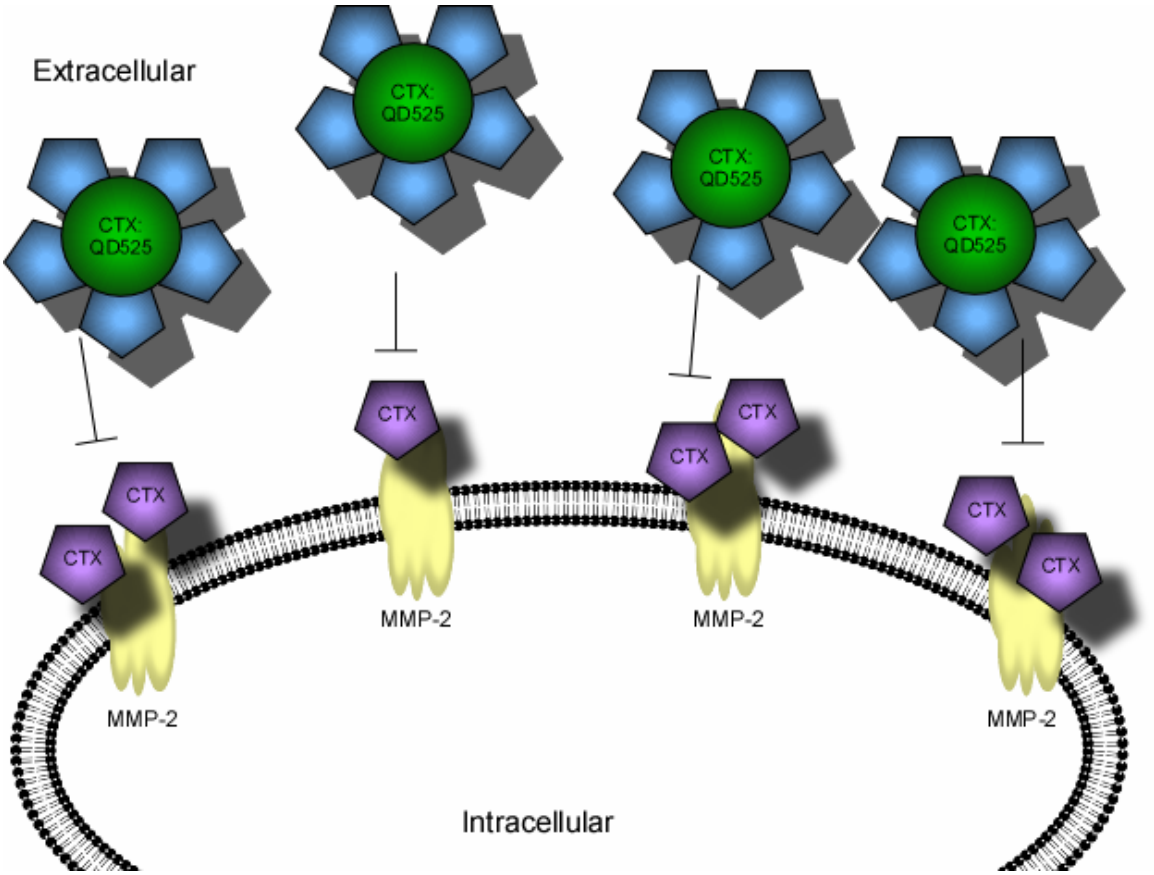

Figure 2.12: Unconjugated chlorotoxin blocks chlorotoxin quantum dot conjugates (CTX:QD488) from binding to matrix metalloproteinase-2 (MMP-2) expression in live cells.

Unconjugated chlorotoxin was used to block matrix metalloproteinase-2 in C6 glioma cells. Glioma cells were plated on MatTek dishes and allowed to propagate for 24-36 hours until estimated 50-60% confluency. The cells were treated with 200nM chlorotoxin in DMEM complete overnight at 37°C and 5% CO_2. Following chlorotoxin incubation, the cultures were exposed to 10nM CTX:QD525 or 10nM QD525 in DMEM complete for time intervals of 30, 60, and 120 minutes. Cells were then washed three times with 1x DPBS and fixed in 4% paraformaldehyde (PFA) for 30 minutes. Afterwards, the cell cultures were washed in 1x DPBS three times, mounted with PolyAqua Mount, and covered with coverslip.

For comparative purposes, the experiment was run in parallel without exposing the C6 glioma cells to unconjugated chlorotoxin before exposure to the quantum dot conjugates. This provided a time based assay of conjugate binding ability within living cells that could be directly compared with the pre-blocked cell detection. First, C6 glioma cells were plated on MatTek dishes (MatTek Corp.) and allowed to propagate for 48 hours until approximately 80% confluent. Following propagation, cells were exposed to 10nM CTX:QD525 or 10nM QD525 in DMEM complete for time increments of 30, 60, and 120 minutes. The cells were then washed three times with 1x DPBS and fixed in 4% paraformaldehyde (PFA) for 30 minutes. After this, the cultures were again washed in 1x DPBS three times, mounted with PolyAqua Mount, and preserved with a coverslip.

2.19: DTX-1:QD655 Conjugate Blocking Assays

Binding to voltage-gated potassium channels, Kv1.1, by dendrotoxin-1 nanocrystal conjugates was assessed in a similar manner as the chlorotoxin conjugates.

Dendrotoxin-1 was used to block voltage-gated potassium channels, Kv1.1, prior to cellular exposure to DTX-1:QD655 conjugates (Figure 2.13). First, C6 glioma cells were plated on MatTek dishes and allowed to propagate for 24-36 hours until approximately 60% confluent. Next, the cells were treated with 100nM dendrotoxin-1 in DMEM complete culture media overnight at 37°C and 5% CO_2. Following dendrotoxin-1 incubation, the cells were exposed to 5nM DTX-1:QD655 or 5nM QD655 in DMEM complete for intervals of 10, 30, 60, 120 and 180 minutes. Finally, the cells were washed in 1x DPBS three times and mounted with PolyAqua Mount with a coverslip.

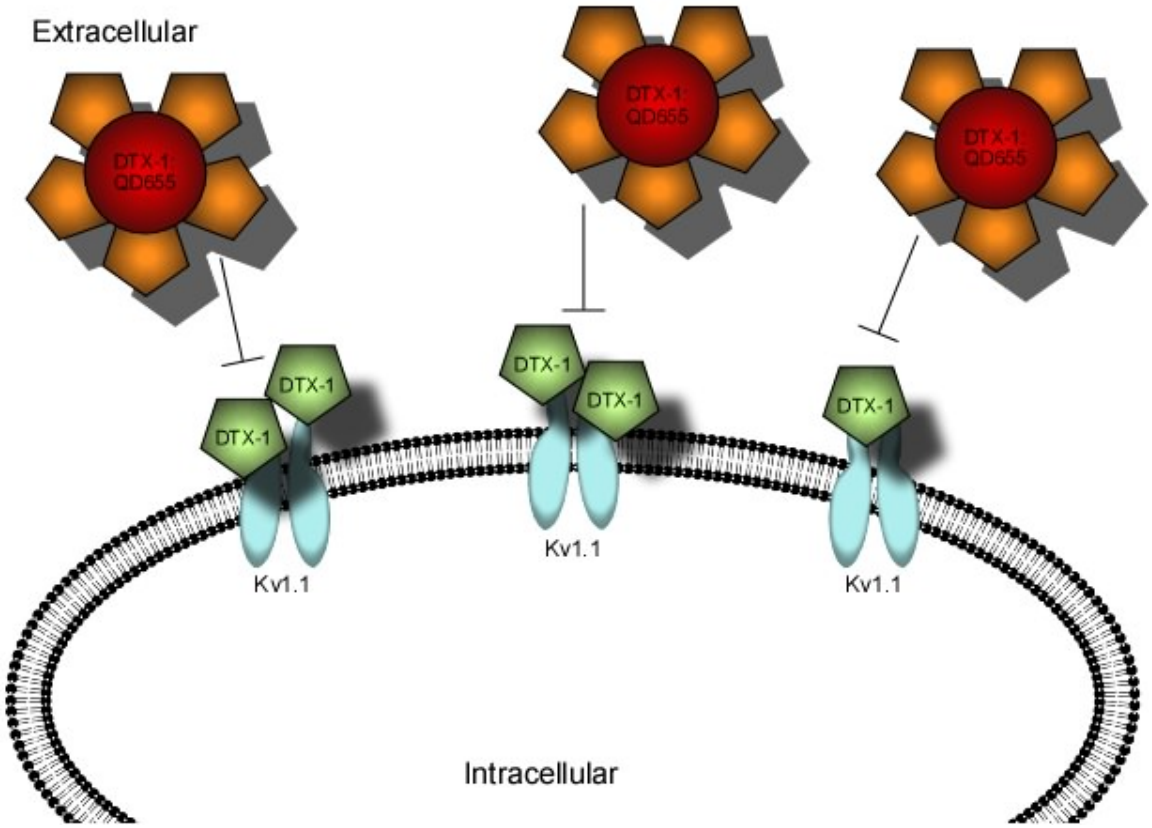

Figure 2.13: Dendrotoxin-1 quantum dot conjugates (DTX-1:QD655) are blocked from binding with voltage-gated potassium channels 1.1 (Kv1.1) in live cells. Unconjugated dendrotoxin-1 prevents high affinity peptide neurotoxin quantum dot conjugates from detecting Kv1.1 by blocking possible binding sites on the ion channel.

Assessment of dendrotoxin-1 conjugate specificity was determined through adequate control experiments. To determine this, C6 glioma cells were plated on MatTek dishes and allowed to propagate for 48 hours until approximately 80% confluent. Following propagation, the cells were exposed to 5nM DTX-1:QD655 or 5nM QD655 in DMEM complete for 10, 30, 60, 120 and 180 minutes. The cell cultures were washed three times with 1x DPBS and fixed in 4% PFA for 30 minutes. Each cell replicate was then washed in 1x DPBS three times, and then mounted with PolyAqua Mount and a coverslip. The replicates of both the pre-blocked and unaffected cells were imaged on a Zeiss inverted confocal microscope. The images were processed using ImageJ (NIH) and GraphPad Prism (GraphPad, Inc.) software.

2.20: Chlorotoxin Affinity Determined By Saturation Binding Curve

Chlorotoxin affinity for endogenous matrix metalloproteinase-2 in living cells was determined through saturation binding curve analysis using quantum dot conjugates. A CTX:QD525 saturation binding curve was generated by plating C6 glioma cells on MatTek dishes and allowing them to propagate for 44-48 hours until approximately 80% confluent. The cells were then treated with increasing concentrations of CTX:QD525 for 120 minutes at 37°C and 5% CO_2. After treatment, the cell cultures were washed three times in 1x DPBS and fixed in 4% PFA for approximately 30 minutes. Following fixing, the cells were washed three times with 1x DPBS, mounted with PolyAqua Mount and covered with a coverslip. All saturation binding curve conjugate concentrations were repeated at least three times with each replicate imaged approximately six times. Each replicate was imaged using inverted confocal microscopy with a Zeiss LSM 510Meta

microscope. The images were processed using ImageJ (NIH) and GraphPad Prism (GraphPad, Inc.).

2.21: Dendrotoxin-1 Affinity Determined By Saturation Binding Curve

Dendrotoxin-1 affinity for endogenous voltage-gated potassium channels, Kv1.1, in living cells was also determined through saturation binding curve analysis using quantum dot conjugates. The DTX-1:QD655 saturation binding curve was accomplished with standard cell culturing technique. Briefly, C6 glioma cells were plated on MatTek dishes and allowed to propagate for 44-48 hours until approximately 80% confluent. The cells were treated with increasing concentrations of DTX-1:QD655 for 180 minutes at 37°C and 5% CO_2. As in previous experiments, the cultures were washed three times in 1x DPBS and fixed in 4% PFA for approximately 30 minutes. Following fixing, cells were washed three times with 1x DPBS, mounted with PolyAqua Mount and covered with a coverslip. All saturation binding curve conjugate concentrations were repeated at least three times with each replicate imaged approximately six times. Each replicate was imaged using inverted confocal microscopy with a Zeiss LSM 510Meta microscope. The images were processed using ImageJ (NIH) and GraphPad Prism (GraphPad, Inc.).

2.22: Multiplexing Experimentation

Since multiplexing is a capability that quantum dots exhibit, initially C6 glioma cells were tested using both toxin quantum dot conjugates for this purpose. The neural cancer cells were treated as previously described for experiments performed prior; briefly, the cells were allowed to propagate for 48 hours until approximately 60-80% confluent at

37°C and 5% CO_2. The cell cultures were then incubated with either 10nM CTX:QD525 and 5nM DTX-1:QD655 in DMEM complete culture media, or 10nM QD525 and 5nM QD655 in DMEM complete culture media (Figure 2.14).

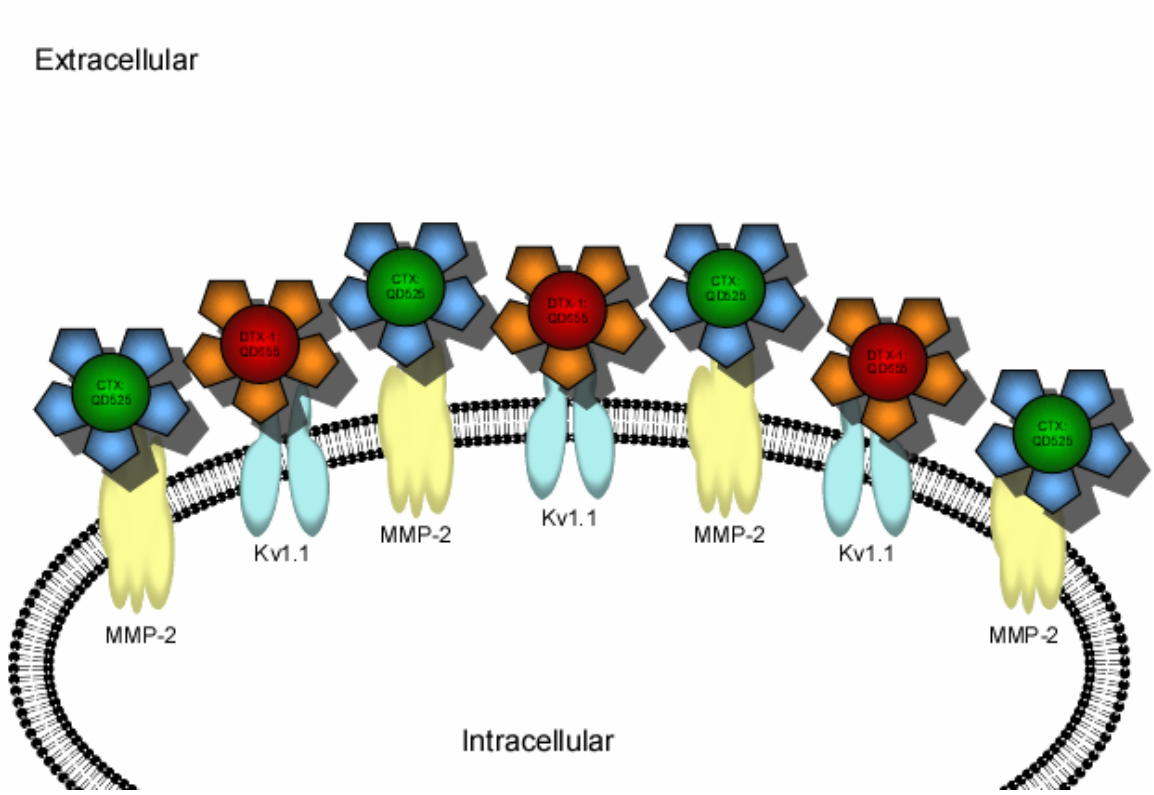

Figure 2.14: Representation of multiplexing experimentation utilizing both chlorotoxin quantum dot conjugates (CTX:QD488) labeling matrix metalloproteinase-2 (MMP-2), and dendrotoxin-1 quantum dot conjugates (DTX-1:QD655) labeling voltage-gated potassium channels 1.1. Quantum dot conjugate detection was of endogenous targets present in live mammalian cells.

Incubation lasted for 120 minutes at 37°C and 5% CO_2. Following incubation with the conjugates, C6 glioma cells were washed three times in 1x DPBS and fixed with 4% PFA for 30 minutes. The cells were then washed in 1x DPBS three more times, mounted with PolyAqua Mount and covered with a coverslip. Imaging was done using a Zeiss inverted confocal microscope, LSM 510Meta, with the excitation source for both quantum dot

conjugates being an Argon 488nm laser. Multiplexing comparison experiments were done which employed three additional cell lines. A comparison was performed using a human Lewis lung carcinoma line, H460, to examine expression levels of the toxins' targets within another cancer cell line. Additional comparisons concerned determination of detectable expression levels within normal cell lines, namely 3T3/NIH and HEK-293T. All cell cultures were treated as described for C6 glioma cells for the multiplexing experimentation protocol. The different cell lines were imaged in an identical manner as the C6 glioma cell line. The results were quantitatively and qualitatively analyzed for overall expression variances between cell types. Results were processed using ImageJ (NIH) and GraphPad Prism (GraphPad, Inc.).

2.23: Flow Cytometry

Cells were seeded at approximately 300,000-350-000 cells per dish, and allowed to propagate for 36-48 h at 37°C and 5% CO_2. Cells were treated as previously described with the toxin:QD conjugates, and allowed to incubate for 120, or 180 min. at approximately 37°C and 5% CO_2. The cells were then washed three times with 1xDPBS without Mg^{2+} and Ca^{2+}, then allowed to sit in 1xDPBS at room temperature for approximately 20-30 min. The cells were then collected for flow cytometry experimentation using a 5-laser BD LSRII flow cytometer. Data were analyzed using GraphPad Prism software.

2.24: Confocal Microscopy

Each culture was imaged approximately five to six times with each experiment run in triplicate. Images were processed and quantified using ImageJ (NIH) and GraphPad Prism (GraphPad, Inc.). For CTX:QD525 antibody colocalization experiments, blocking experiments, and concentration curve determination, CTX:QD525 was excited using an Argon 488nm laser. For antibody colocalization, secondary-Alexafluor594 was excited using a HeNe 543nm laser simultaneously with the Argon 488nm laser used to excite CTX:QD525 conjugates. Similarly, DTX-1:QD655 antibody colocalization experiments, blocking experiments, and concentration curve determination were imaged using a HeNe 633 nm laser to illuminate DTX-1:QD655 conjugates. For antibody colocalization, secondary-Alexafluor488 was excited using an Argon 488nm laser simultaneously with the HeNe 633nm laser used to excite DTX-1:QD655 conjugates. Multiplexing experiments were imaged using single-source excitation via an Argon 488nm laser to excite both CTX:QD525 and DTX-1:QD655 simultaneously.

CHAPTER III

TARGETING NICOTINIC ACETYLCHOLINE RECEPTORS

3.1: Introduction

Nicotinic acetylcholine receptors are a well studied class of ligand-gated ion channels. They are members of the ionotropic receptor Cys-loop superfamily,[100] and are closely related to gamma-amino butyric acid receptors type A ($GABA_A$) and glycine receptors; additionally, they are distant cousins to both serotonin (5HT-3) and glutamate (GluR) receptors. Nicotinic acetylcholine receptors are pentameric transmembrane proteins that consist of subunits surrounding a cation pore. Subunits are classified as α(1-10), β(1-5), δ, and γ (or ε in adult physiology), and found in both muscle tissues and neuronal tissues (Figure 3.1).

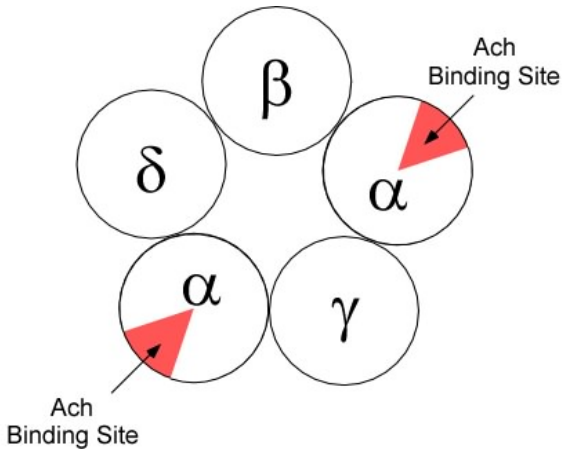

Figure 3.1: Representation of muscle-type nicotinic acetylcholine receptors with designate subunits as viewed from above. Acetylcholine binding sites are highlighted on the α-subunits.

Each subunit has high sequence identity with homologous subunits that combine to form an array of receptor subtypes throughout an organism. These receptors are further categorized as homopentamers or heteropentamers based upon their subunit organization.[76, 78] In vertebrates, dense clusters of nicotinic acetylcholine receptors are found in the *Torpedo* electric organ and in skeletal muscle, such as diaphragm tissue.[74] The muscle-type nicotinic acetylcholine receptors are comprised of an $\alpha_2\beta\gamma\delta$ stoichiometry of subunits. Together, these subunits create a cation pore through which ion flux[78] occurs after acetylcholine binding.

Nicotinic acetylcholine receptors are located on the post-synaptic membrane of the neuromuscular junction. The receptors are anchored in clusters at the peaks of the highly folded post-synaptic membrane by rapsyn. Rapsyn is shown to secure nicotinic acetylcholine receptors to motor endplates during synaptogenesis.[82, 101, 102] The presence of nicotinic acetylcholine receptors at motor endplates of the neuromuscular junction bears important implications in neurological diseases, such as acquired autoimmune myasthenia gravis. Myasthenia gravis is a degenerative neurological disease in which nicotinic acetylcholine receptor antibodies cause loss of the endplate membrane; thereby, significantly reducing nicotinic acetylcholine receptor and Na^+ channel expression at the post-synaptic cleft.[77, 102] Without nicotinic acetylcholine receptor presence at the post-synaptic membrane, the action potential, initiated by an agonist-induced electrochemical gradient, is lost and neuromuscular transmission stops.

An electrochemical gradient is induced through extracellular agonist binding.[75] Nicotinic acetylcholine receptors require that two neurotransmitter molecules bind to non-equivalent binding sites on the α-subunits. Unwin and co-workers demonstrated

through electron microscopy that neurotransmitter binding results in a conformational change, allowing for cation movement.[80] Receptor functionality is gated by the excitatory endogenous agonist, acetylcholine. Exogenous agonists such as (S)-(-)-nicotine, (-)-cyticine, and (±)-epibatidine will additionally induce a receptor response.[78]

3.2: α-Bungarotoxin

Antibody and toxin labeling studies show that muscle-type nicotinic acetylcholine receptors are clustered at the peaks of the highly folded post-synaptic muscle membrane. In the disorder myasthenia gravis, nicotinic acetylcholine receptor antibodies induce a loss of these clusters, thereby producing muscle paralysis and, if untreated, death. Functioning nicotinic acetylcholine receptors are also lost when targeted by certain neurotoxins, such as α-bungarotoxin. α-Bungarotoxin, a 74 amino acid peptide from the snake *Bungarus multicinctus*, has subnanomolar affinity for nicotinic acetylcholine receptors and blocks neuromuscular transmission by preventing binding at the α-subunit interface with the δ and γ subunits.[78] Another venom component, β-bungarotoxin, acts pre-synaptically to trigger massive acetylcholine release and subsequent depletion.[73] The α-bungarotoxin peptide has been used as a high-affinity ligand to label nicotinic acetylcholine receptors for imaging and quantitation. Fluorescent and radiolabeled α-bungarotoxin conjugates are typically used;[103-107] however, biotinylation is also an option as binding to target receptors can be detected with an avidin-linked probe. Coupling of biotin and avidin, or streptavidin, yields an interaction with femtomolar affinity and a long half-life in solution. Common avidin probes include streptavidin-Alexafluor dye conjugates. Recent advances in probe development have generated streptavidin-quantum

dot (streptavidin-QD) conjugates that may be even more suitable for biological applications given their multiplexing capabilities and resistance to photobleaching.[11, 14-16, 22]

Although both live and fixed cells have been labeled with quantum dot conjugates, tissue labeling with quantum dots has been limited to fixed sections[22, 50, 52, 54, 55, 108-111] and illumination tracking during surgical procedures.[25, 51, 67-69, 112] Quantum dot labeling of nicotinic acetylcholine receptors at neuromuscular junctions in mature ex vivo mouse diaphragm is presented. The neuroreceptors were targeted with the α-bungarotoxin conjugate, biotinylated α-bungarotoxin, and used streptavidin-QD655s to visualize the bound biotinylated α-bungarotoxin in the whole mount tissue.

3.3: α-Bungarotoxin Affinity

To examine α-bungarotoxin affinity in ex vivo tissue, mouse diaphragm was dissected and treated with glycine solution for one hour. The tissue was then incubated overnight in blocking solution at 4°C. Following overnight blocking, the tissue was treated with blocking solution containing increasing concentrations of biotinylated α-bungarotoxin for approximately 10 minutes. Overnight incubation in blocking solution containing streptavidin-QD655s (Invitrogen, Inc.) occurred after toxin exposure. Tissue sections were mounted and imaged using invert confocal microscopy, LSM510 Meta (Zeiss, Inc.). Figure 3.2 illustrates the resulting saturation binding curve using the biotinylated α-bungarotoxin and streptavidin-QD655 labeling protocol. The observed biotinylated α-bungarotoxin affinity, K_D of approximately 200fM, indicates that α-bungarotoxin has a much higher affinity for nicotinic acetylcholine receptors at

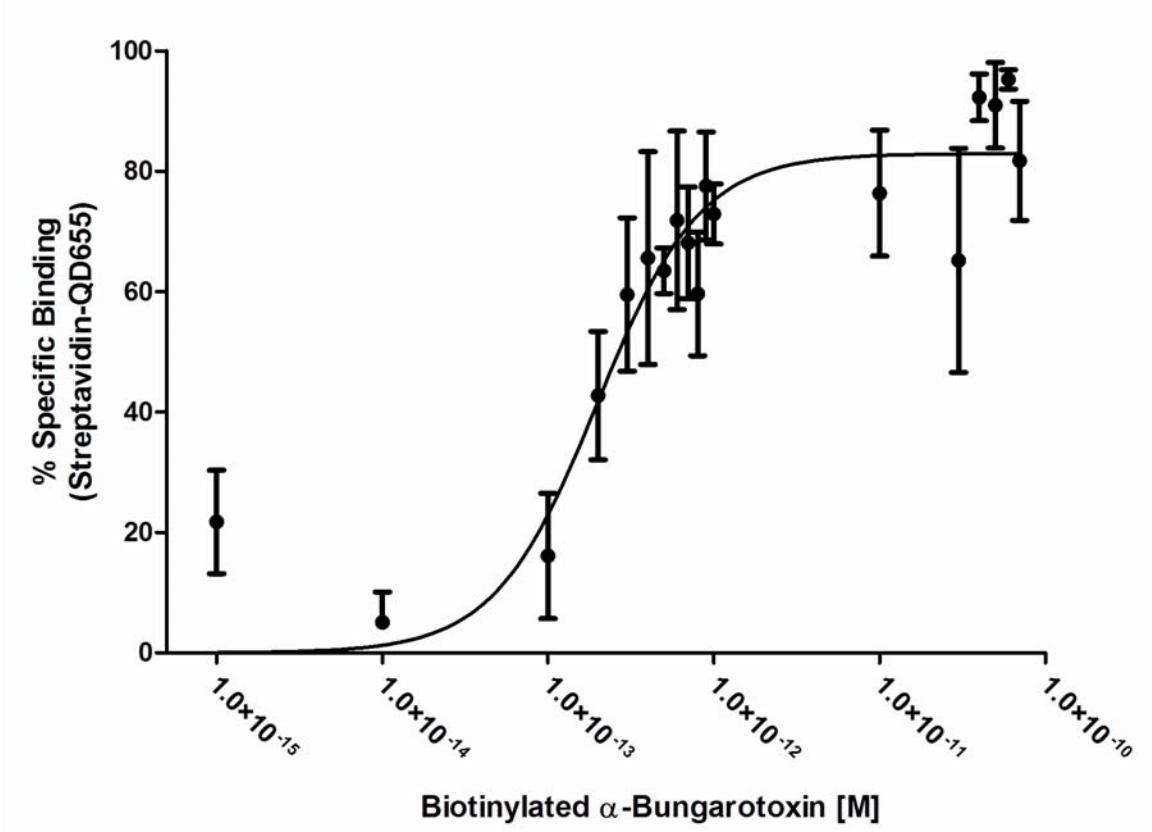

Figure 3.2: Biotinylated α-bungarotoxin saturation binding curve detected with streptavidin-QDs at neuromuscular junction synapses. Tissue was blocked and treated with dilutions of biotinylated α-bungarotoxin for 10 minutes, and labeled with streptavidin-QD655s overnight at 4°C. Data are the mean of three experiments ± S.E.M., with individual points assayed in triplicate for each experiment. K_D is 198fM ± 43fM; B_{max} is 89.93 % ± 4.163%; and, the Hill-slope is 1.402 ± 0.3884. α-Bungarotoxin binds nicotinic acetylcholine receptors with subpicomolar affinity, approximately 1000-fold greater binding affinity than denatured nicotinic acetylcholine receptor assays.

neuromuscular junction synapses than previously observed by Stephenson and coworkers.[83] This finding may indicate that receptors within ex vivo tissue retain higher affinity for the α-bungarotoxin antagonist than homogenized receptors extracted under denaturing conditions. The ability of α-bungarotoxin to bind nicotinic acetylcholine receptors with subpicomolar affinity enables the antagonist to be used as a highly specific probe for quantum dot labeling and imaging to study neuromuscular synapses.

3.4: Quantum Dot Labeling Time-Dependence in Ex Vivo Tissue

To further analyze biotinylated α-bungarotoxin and streptavidin-QD655 efficacy as a probe for nicotinic acetylcholine receptors, we performed time-dependence experiments with unfixed mouse diaphragms. The first experiment was to determine whether length of biotinylated α-bungarotoxin exposure affected visualization with streptavidin-QD655 (Figures 3.3, 3.5A). We treated the tissue as previously described, and exposed the tissue to biotinylated α-bungarotoxin for intervals of 10, 60, 180, 360 (Figure 3.3) and 720 (Figure 3.5A) minutes. Additionally, we co-incubated the tissue with a nicotinic acetylcholine receptor β-antibody and secondary-Alexafluor488 antibody conjugate (Sigma, Inc.) to demonstrate probe specificity. A second experiment analyzed whether receptor viability remained in ex vivo tissue after seven days in blocking conditions prior to labeling with the biotinylated α-bungarotoxin and streptavidin-QD655 probe (Figure 3.4). Figure 3.3 illustrates that biotinylated α-bungarotoxin binds rapidly in fresh ex vivo tissue where essentially full labeling was achieved at 10 minutes. Additionally, we observed that binding was highly specific as demonstrated by colocalization between the streptavidin-QD655 fluorescence, labeling biotinylated α-bungarotoxin, and that of the Alexafluor488 antibody conjugate, labeling anti-nicotinic acetylcholine receptor subunit antibodies. This further substantiates the affinity determined in Figure 3.3 as noted by the lack of dissociation present at 720 minutes of exposure (Figure 3.5A). We also see that binding is equivalent between Figures 2 and 3 at each α-bungarotoxin incubation time. These data suggest that the nicotinic acetylcholine receptor remains viable over time when maintained in an ex vivo

environment, which has potential relevance for production of sample archives for comparative analyses.

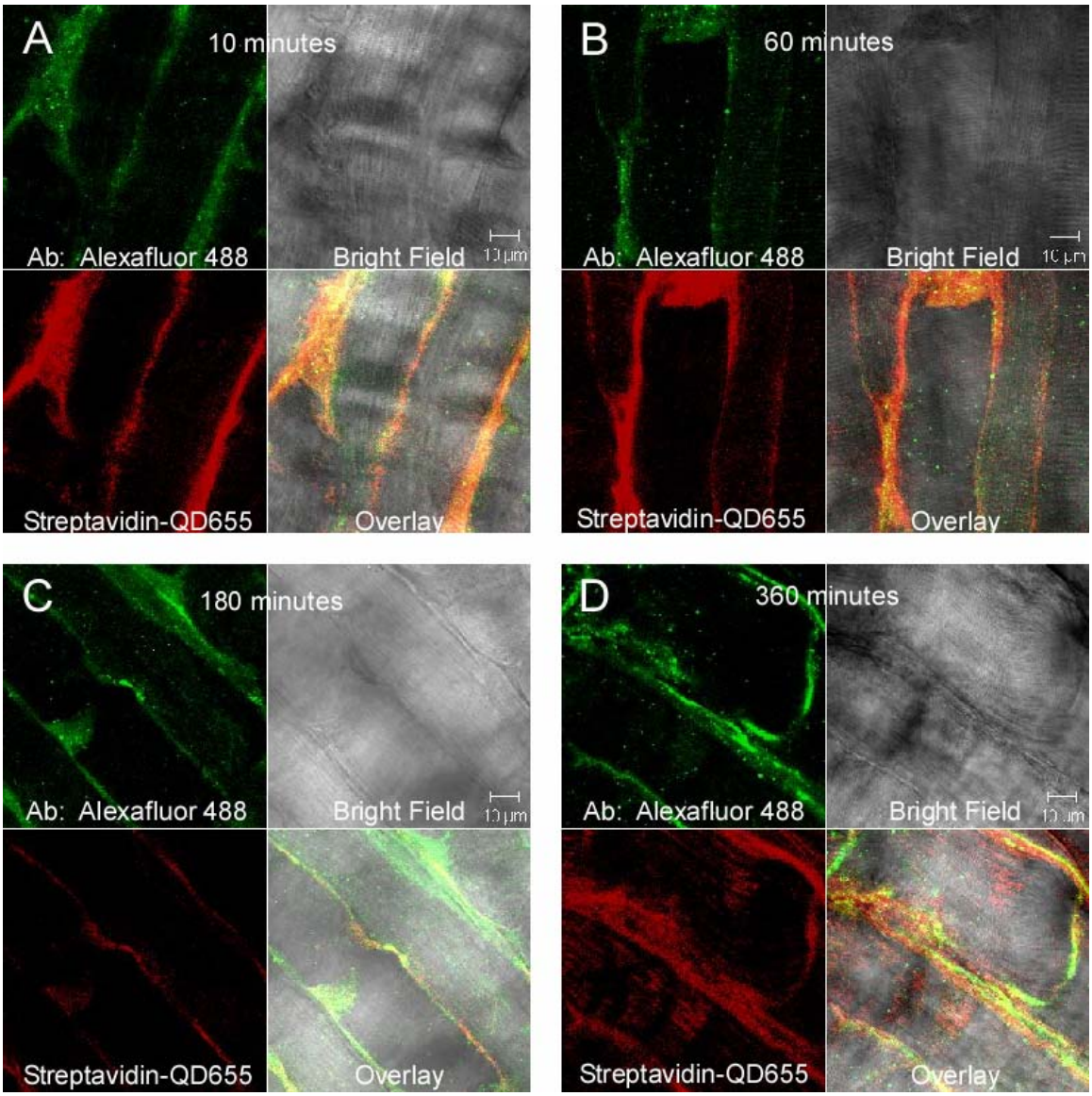

Figure 3.3: Time-dependence labeling of neuromuscular junctions with biotinylated α-bungarotoxin after overnight blocking solution incubation. Images represent tissue incubated with 10nM biotinylated α-bungarotoxin following blocking protocol, and nicotinic acetylcholine receptors detected with streptavidin-QD655 conjugates at (A) 10 minutes, (B) 60 minutes, (C) 180 minutes, and (D) 360 minutes. Experiments were run in triplicate with each piece imaged at least three times. α-Bungarotoxin binding is detected in all sections and all time intervals with streptavidin-QD655s.

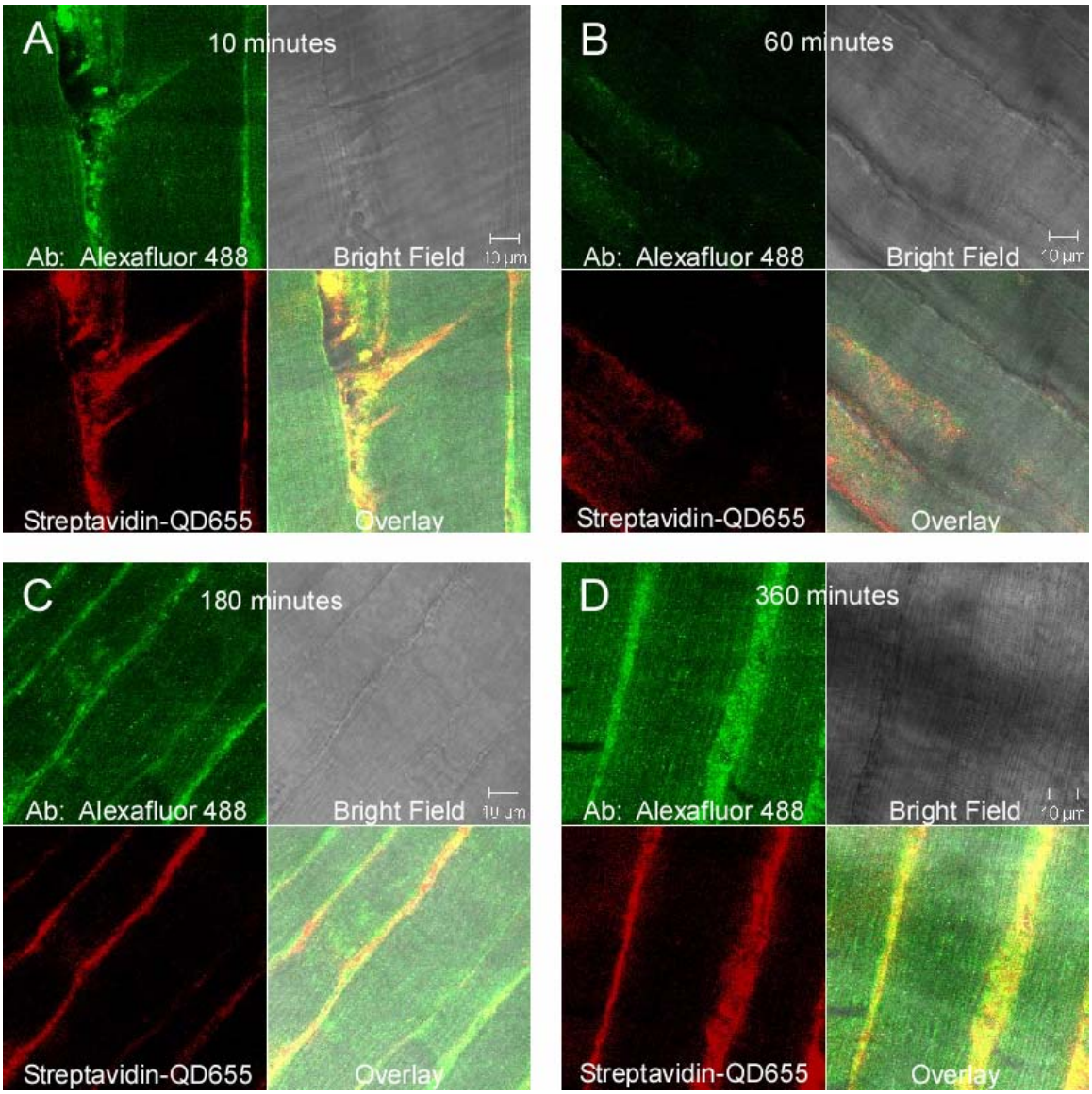

Figure 3.4: Time-dependence labeling of neuromuscular junctions with biotinylated α-bungarotoxin after seven day blocking solution incubation. Tissue was incubated with 10nM biotinylated α-bungarotoxin, and nicotinic acetylcholine receptors were detected with streptavidin-QD655 conjugates at (A) 10 minutes, (B) 60 minutes, (C) 180 minutes, and (D) 360 minutes following seven day blocking protocol. Each time interval was imaged at least three times. Quantum dot detection is unaffected by extended blocking solution incubation prior to α-bungarotoxin labeling.

3.5: Quantum Dot and Alexafluor Comparative Analyses

Next we performed analyses using streptavidin-Alexafluor555 (Invitrogen, Inc.) (Figure 3.5C, D) in place of streptavidin-QD655 (Figure 3.5A, B) to compare quantum dot labeling efficacy versus a commonly used organic fluorophore.[106, 113]

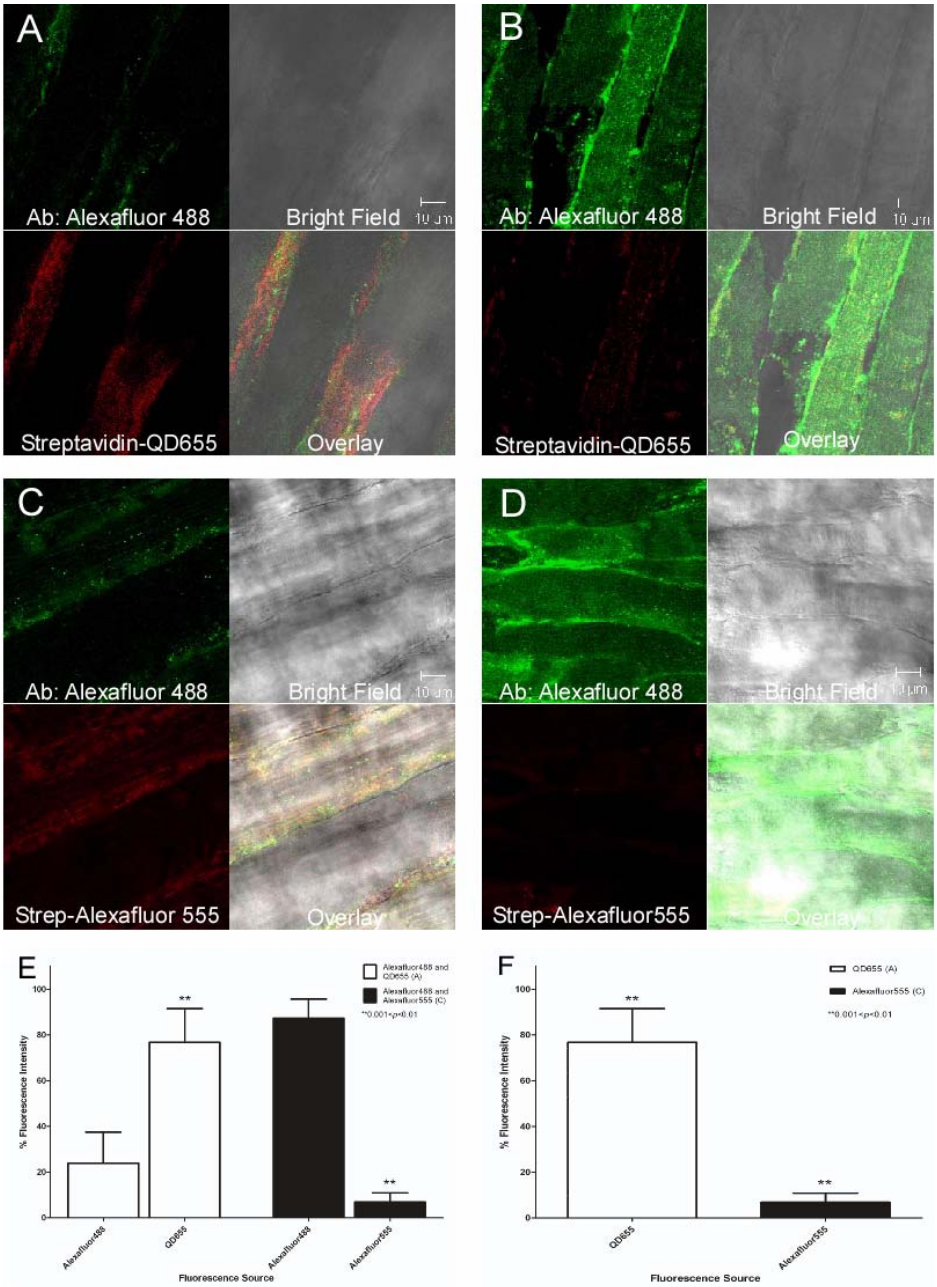

Figure 3.5: Comparative analyses between streptavidin-QD655s and streptavidin-Alexafluor555s detection of biotinylated α-bungarotoxin at neuromuscular junction synapses. All tissue was blocked and exposed to 10nM biotinylated α-bungarotoxin, or blocking solution, for 12 hours; and, treated with streptavidin-QD655 or Alexafluor555 conjugates overnight at 4°C. Images represent a compilation of three experiments. (A, C) 12 hour 10nM biotinylated α-bungarotoxin and primary antibody incubation. (B, D) controls incubated in blocking solution with primary antibody only. Nicotinic acetylcholine receptors detected with 10nM fluorescent probe (A) streptavidin-QD655, (C) streptavidin-Alexafluor555. Alexafluor488 colocalization (A, C) with streptavidin-QD655s (A) and streptavidin-Alexafluor555s (C) indicates effective labeling of nicotinic acetylcholine receptors. Absence of biotinylated α-bungarotoxin (B, D) results in a lack of labeling by both streptavidin-QD655s (B) and streptavidin-Alexafluor555s (D). Relative fluorescence intensity (E, F) reveals statistical significance between streptavidin-QD655 and streptavidin-Alexafluor555 fluorescence ($0.001<P<0.01$, analysis of variance, values are the means ± SEM).

Mouse diaphragms were exposed to biotinylated α-bungarotoxin for 720 minutes, and then labeled overnight in either streptavidin-QD655, or streptavidin-Alexafluor555 conjugates. Although both quantum dots and Alexafluors label neuromuscular junction synapses, imaging revealed that the quantum dots appear much brighter than their fluorophore counterparts. Quantitative analysis of the relative intensities of streptavidin-QD655 versus streptavidin-Alexafluor555 conjugates (Figure 3.5E, F) present statistically significant differences in intensity between the fluorescent probes ($0.001<P<0.01$, analysis of variance). The quantum dots exhibit a higher signal to noise ratio in tissue samples than fluorescent dyes, and adequately label neural targets within an ex vivo system. This is particularly significant in that our experiments are reported at concentrations of biotinylated α-bungarotoxin that are ten times lower than concentrations needed for Alexafluor labeling. To further verify the biotinylated α-bungarotoxin and streptavidin-QD655 labeling system utility, nicotinic acetylcholine receptor α-bungarotoxin binding sites were blocked with unconjugated α-bungarotoxin using a concentration of α-bungarotoxin ten times in excess of the biotinylated α-bungarotoxin used for detecting the neuromuscular junction nicotinic acetylcholine receptors. Figure 3.6 illustrates that labeling at the α-bungarotoxin site is blocked by the presence of α-bungarotoxin prior to introduction of the biotinylated conjugate. These findings also indicate that biotinylated α-bungarotoxin does not displace α-bungarotoxin within the exposure period, and that the labeling is specific to the α-bungarotoxin binding site sequence, a 13-amino acid sequence found on the α-subunit of the nicotinic acetylcholine receptor.[104, 107, 114]

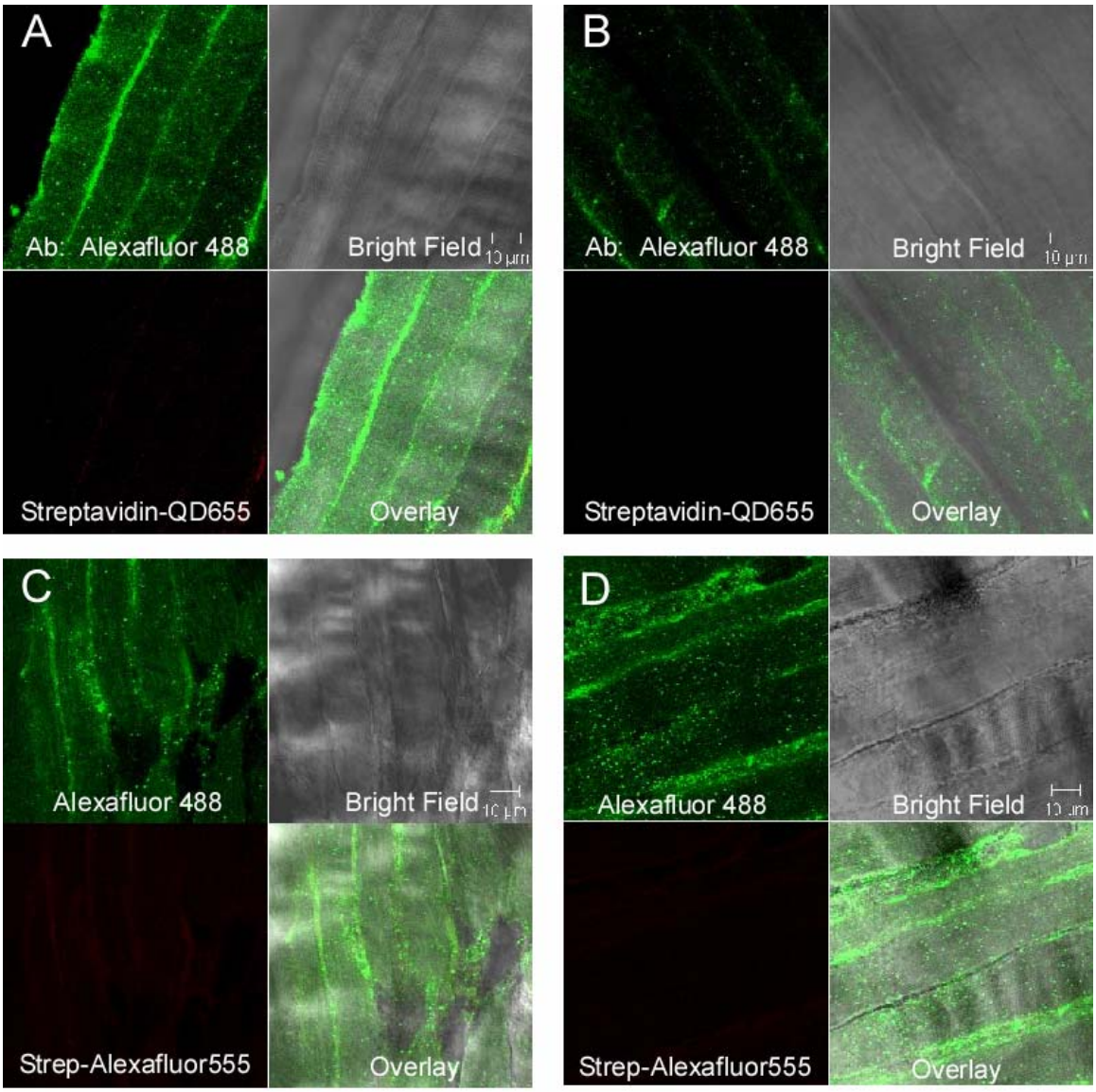

Figure 3.6: Neuromuscular junction synapses pre-treated with 100nM α-bungarotoxin exhibit neither streptavidin-QD655, nor streptavidin-Alexafluor555 labeling after 10nM biotinylated α-bungarotoxin incubation. Tissue was incubated with 100nM α-bungarotoxin overnight, then treated with 10nM biotinylated α-bungarotoxin for 12 hours. Images are representative of three experiments. Presence of biotinylated α-bungarotoxin labeling was not detected after streptavidin-QD655 and Alexafluor555 treatment overnight. Alexafluor488 labeling at the nicotinic acetylcholine receptor β-subunit is unaffected by α-bungarotoxin pre-treatment. This indicates that both streptavidin-QD655 and streptavidin-Alexafluor555 labeling is specific to the α-bungarotoxin binding site.

3.6: Photostability in Ex Vivo Tissue

An additional assessment of the biotinylated α-bungarotoxin and streptavidin-QD655 probe examined quantum dot photostability relative to the Alexafluor dyes.

Resistance to photobleaching is a known characteristic of quantum dots.[53, 104, 105] Figures 3.7A1-3.7A5 demonstrate photobleaching resistance of quantum dots versus the secondary antibody Alexafluor488 conjugate (Figures 3.7A1-3.7A5) and relative to streptavidin-Alexafluor555s (Figures 3.7B1-3.7B5) within ex vivo tissue. The tissue was imaged using an LSM510 Meta inverted confocal microscope (Zeiss, Inc.) and exposed to continuous excitation for approximately 30 minutes. As time progressed, the Alexafluor conjugates, Alexafluor488 and Alexafluor555, photobleached rapidly in ex vivo tissue under continuous excitation. Quantum dots, however, retained their photostability throughout continuous excitation, as illustrated in Figures 3.7A1-3.7A5. There is significant reduction in Alexafluor488 intensity at 180 seconds and no reduction in quantum dot intensity at the same time interval (Figure 3.7A2). After 720 seconds of continuous fluorescence excitation in tissue, quantum dots maintain their brightness, whereas Alexafluor488 is effectively photobleached. Figure 3.7C further supports that quantum dots lose minimal intensity over time during repeated excitation. We measured photobleaching resistance for both fluorophores and quantum dots relative to fluorescein isothiocyanate (FITC) by spin-casting, a solvent evaporation technique that deposits fluorescent probes directly onto a spinning surface, each fluorescent probe and exposing the cast to continuous excitation on a Zeiss Axiovert 200M inverted widefield microscope (Zeiss, Inc.) with Metamorph (MDS, Inc.) for 30 minutes. The trends in Figure 3.7C affirm the photobleaching data obtained using the mouse diaphragms, and suggest that quantum dots are a suitable fluorescent probe for targeting neuroreceptors in ex vivo tissue.

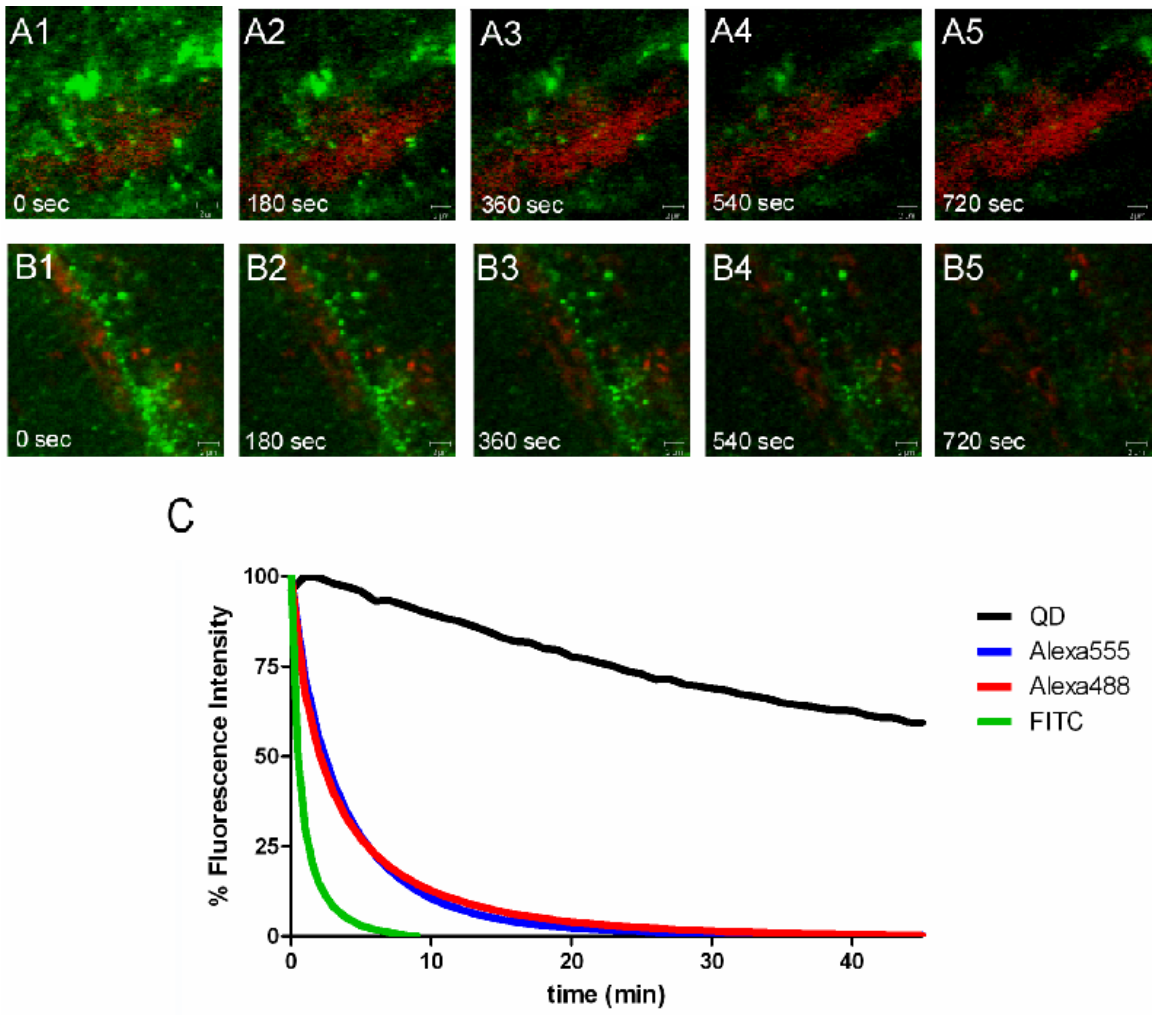

Figure 3.7: Photostability of quantum dots versus Alexafluor dyes in tissue and by spin-casting. The samples were treated with 10nM biotinylated α-bungarotoxin and β-antibody (1:5000) for 10 minutes. Tissue samples were then incubated with secondary-Alexafluor488 antibody and either streptavidin-QD655s (A1-A5), or streptavidin-Alexafluor555s (B1-B5) overnight. Images were captured during continuous excitation of fluorescent probes using an inverted confocal microscope for 30 minutes. At approximately 180 seconds (A2, B2) there is significant photobleaching present in both Alexafluor488 and Alexafluor555, and no photobleaching present in QD655s. By 720 seconds (A5, B5), both Alexafluor dyes are photobleached, and quantum dots maintain their initial intensity. (C) Continuous excitation for 30 minutes using Zeiss Axiovert 200M widefield microscope with Metamorph imaging software of spin-cast, fluorescent probe deposition onto spinning surface for solvent evaporation, streptavidin-QD655s, streptavidin-Alexafluor555s, and secondary-Alexafluor488 antibody conjugate versus FITC. Alexafluor dyes photobleach after less than 10 minutes of continuous excitation; and, quantum dots are photostable after more than 30 minutes of continuous excitation, regardless of medium.

3.7: Summary

Saturation binding analysis revealed that α-bungarotoxin has 1000-fold higher affinity for native nicotinic acetylcholine receptors than previously reported.[83] This

indicates that it is a highly specific ligand that may be used in conjunction with a recombinant α-bungarotoxin binding site to study neural targets lacking suitable high-affinity probes.[104, 107] Biotinylated α-bungarotoxin was shown to maintain high-affinity for nicotinic acetylcholine receptors over time. α-Bungarotoxin also blocked nicotinic acetylcholine receptor detection by biotinylated α-bungarotoxin, when exposed to muscle tissue. Our findings additionally indicate that streptavidin-QD655s are photostable fluorescent probes suitable for detecting nicotinic acetylcholine receptors in ex vivo tissue using biotinylated α-bungarotoxin.

Quantum dots exhibit traits that are not seen with organic fluorophores, such as near 100% quantum yield.[7] Their incorporation into biological experiments has required surface modification for biocompatibility. Reduction of non-specific binding to cell membranes have included modifications such as micelle encapsulation,[29] pegilation,[30] selinization,[31] coating in amphiphilic polymers,[32, 33] and addition of biologically active molecules such as proteins,[22, 34, 35] peptides,[36-38] small molecules,[39-41] and antibodies[42-45] to the surface of the quantum dots. Results of these surface modifications to quantum dots have included successes in cell culture labeling.[22, 23, 30, 46-56] The Ting laboratory recently reported use of streptavidin-QD conjugates through biotin ligase biotinylation of tagged cyan fluorescent protein and epidermal growth factor receptors in HeLa cell cultures and α-amino-3-hydroxy-5-methyl-4-isoxazolepropionate (AMPA) receptors in neurons.[56] Their results demonstrated the utility of biotin-streptavidin quantum dot coupling for targeting neuroreceptors and neurons. Our findings further support biological suitability and provide evidence for quantum dot use in other tissues and neural targets.

Biological applications for quantum dots include live cell-trafficking assays for neural target studies, which require high probe specificity and photostability within unfixed conditions. These data provide preliminary evidence demonstrating the suitability of this approach for labeling nicotinic acetylcholine receptors in the brain following I.C.V. injection of biotinylated α-bungarotoxin. Quantum dot labeling within in vivo neural tissue will advance probe development, and provide real-time data of protein interactions through nanocrystal tracking. Furthermore, our results demonstrate ex vivo labeling efficacy of neuromuscular synapses with quantum dots.

CHAPTER IV

TARGETING ENDOGENOUS TARGETS IN LIVE CANCER CELLS

4.1: Introduction

Peptide-mediated quantum dot detection has been demonstrated to be an effective methodology for probing biological systems with high specificity.[57] Targeted neurotoxin approaches have been employed to selectively label proteins for monitoring,[39] detection,[56, 57] and destruction.[63, 64] Although designed to induce disruption of its targeting system, each toxin provides the possibility to be utilized as a therapeutic vehicle for disease detection and destruction, and as a means to study its target in greater depth. Typically, peptide neurotoxins inhibit ion channels by acting as antagonists, and result in the cessation of neurotransmission propagation and loss of channel functionality.[115] The high affinity characteristic of peptide neurotoxins enables the toxins to be used as ligands for thorough study of their biological targets. Previous studies have demonstrated that a well characterized ion channel may be detected with quantum dots and a high affinity peptide neurotoxin.[57]

4.2: Chlorotoxin

Quantum dot cellular targeting may be mediated with use of toxins that interact and bind to endogenously expressed cell membrane proteins and ion channels. Because quantum dots exhibit characteristics that allow for potential multiplexing analyses, multiple peptide toxins may be utilized toward endogenous labeling of a series of targets simultaneously. One toxin of interest toward these applications is an insect venom toxin

isolated from the scorpion, *Leiurus quinquestriatus*, known as chlorotoxin.[85] Chlorotoxin is 36 amino acids in length with four disulfide bonds, ^{2}Cys-^{19}Cys, ^{5}Cys-^{28}Cys, ^{16}Cys-^{33}Cys, and ^{20}Cys-^{35}Cys.[87] The toxin appears to bind matrix metalloproteinase II,[89, 90] an extracellular matrix enzyme that exhibits gelatinase activity. Additionally, chlorotoxin preferentially binds to cancer cells over non-cancer cells.[62, 89] Of particular biological interest is the primary brain glial cell cancer, glioma. Glioma cells are malignant cancer cells that infiltrate healthy brain tissue, and evade complete surgical resection through yet fully understood mechanisms.[71] Chlorotoxin binds effectively to matrix metalloproteinase-2 endogenously expressed by glioma cells,[71, 89, 90] and exposure results in loss of gelatinase activity, disruption in chloride channel currents, reduction in both matrix metalloproteinase-2 and chloride channel expressions, and internalization of chloride channels.[60, 62, 89-91] In 2003, Sontheimer and colleagues determined that chlorotoxin targets matrix metalloproteinase-2 through recombinant His tagging methodologies coupled with analytical techniques including mass spectrometry.[89] Olson and co-workers provided further evidence in 2007 that matrix metalloproteinase-2 is the chlorotoxin receptor by matrix metallorproteinase-2 antibody fluorescence colocalization with chlorotoxin:Cy5.5 conjugate fluorescence in matrix metalloproteinase-2 transfected MCF7 cells.[90] These studies garner evidence that matrix metalloproteinase-2 is influential in glioma cell proliferation, and raise questions regarding the nature of the chloride channel interactions with matrix metalloproteinase-2. This property indicates that chlorotoxin has the potential to be used as a therapy for gliomas, and affords insights into the understanding of all cancer metastasis and into the poorly characterized chloride channel superfamily.[59, 93] Chlorotoxin conjugates are currently in Phase I/II clinical trials

for tagging glioma cells for surgical resection.[90] These previous studies indicate that chlorotoxin may be a suitable peptide for quantum dot conjugation toward use in live cell detection of endogenous targets.

4.3: Dendrotoxin-1

A second toxin suited for quantum dot applications is a member of the dendrotoxins, a family of high affinity cation channel antagonists. Dendrotoxins are isolated from the venoms of the mamba snake family, and act by blocking various subtypes of voltage-gated potassium channels. The peptides are approximately 7000 Da and range in size from 57-60 amino acids in length.[95] Their mechanism of action results in depletion of acetylcholine at the neuromuscular junction through extension of the action potential.[94] Dendrotoxins interfere with the ability for potassium channels to perform their primary responsibilities: (1) cell membrane potential maintenance, and (2) cell membrane repolarization following action potential propagation. Interference with potassium channel functions results in muscle convulsions and eventual death due to hyperexcitability of the muscles.[96] Dendrotoxin-1, a peptide isolated from the Black Mamba, has been used to target potassium channels on C6 glioma cells. It was found by Allen et al.[97] that unstimulated C6 glioma cells express potassium channels of the subtype, Kv1.1, which are targeted by dendrotoxin-1. Dendrotoxin-1 also targets two other Shaker family potassium channels, Kv1.2 and Kv1.6. In the study by Allen et al.,[97] only Kv1.1 was detected to be present within the cells. Dendrotoxin-1 blockade caused significant reduction in potassium currents, and not all cells recovered completely from exposure.[97] Significant reduction in potassium currents is indicative of impact on

potassium channel functionality. Loss of potassium channel functionality results in the possibility that this channel subclass contributes to glioma metastasis through motility mechanisms. These outcomes to dendrotoxin-1 exposure enable the peptide to be utilized as a high affinity ligand for quantum dot studies of the intricate interplay between potassium channels and other cellular targets.

4.4: Preliminary Experiments with Chlorotoxin and Glioma Cells

The objective of these preliminary experiments with chlorotoxin and glioma cells was to determine the overall viability of the approach to apply quantum dots as a versatile fluorescent probe capable of detecting ion channel disruptive neurotoxins within cell cultures with high specificity. The aims of the preliminary chlorotoxin and glioma cell experiments were to determine if chlorotoxin is able to be detected in C6 glioma cells by avidin-linked quantum dots when biotinylated; and, to assess if quantum dot detection of chlorotoxin is dependent on culture age, labeling temperature, vehicle solution, and time of exposure to the toxin and quantum dots.

4.5: Biotinylated Chlorotoxin Detection by Streptavidin Quantum Dots

Following our previous success with biotinylated peptide neurotoxins and streptavidin-QD655 conjugates,[57] we biotinylated chlorotoxin for detection with streptavidin-QD655s in cell culture. We estimated approximately four potential biotinylation residues in the peptide based upon its sequence. Those are ^{1}Met, ^{15}Lys, ^{23}Lys, and ^{27}Lys of the 36 amino acids that compose the toxin.[87] Peptide biotinylation was performed using the Pierce EZ-link NHS biotin (succinimidobiotin) with chlorotoxin

reconstituted in bicarbonate buffer (pH 8.5). The reaction was performed based upon the protocol provided within the kit, but modified to be effective with the low concentration of our peptide (2μM). Briefly, the lyophilized peptide was reconstituted in bicarbonate buffer to a concentration of 2μM. To compensate for the low concentration, the succinimidobiotin was added to the peptide with a 50 molar excess to drive the reaction to completion. The reaction vial was allowed to sit for 2 hours on ice, and was loaded into the Pierce Dialysis Cassette (MWCO 3500 Da) according to equipment specifications. We then dialyzed the solution to remove unreacted succinimidobiotin and NHS present in the solution. The dialysis cassette was suspended in 1-L of phosphate buffered saline (1x PBS, pH 7.4) for 2 hours two times at 4°C with constant stirring of the PBS solution. After the second buffer change, the cassette was allowed to spin overnight in the same conditions to finish the dialysis process. Following dialysis, the biotinylated chlorotoxin was removed from the cassette according to manufacturer's instructions and prepared for analysis to assess biotinylation efficiency. The biotinylated chlorotoxin solution was compared to a HABA solution using UV/Vis analysis. We were able to determine that the chlorotoxin was biotinylated approximately 2.38 moles of biotin : 1 mole of chlorotoxin. This indicates that we were successful at biotinylating chlorotoxin for our studies.

C6 glioma cells (courtesy of and purchased by Dr. Daryl Bornhop via Lynn E. Samuelson of Vanderbilt University from American Type Culture Collection) were cultured in Dulbecco's Minimum Essential Media (DMEM) with glucose and sodium pyruvate, 1% L-glutamate, 1% penicillin/streptomycin, and 10% heat-inactivated fetal bovine serum (FBS) at 37°C and 5% CO_2. C6 glioma cells are a tumorigenic cell line

derived from rat gill cells that were transformed into tumor cells through N-nitrosomethylurea induction by Benda et al. in 1968.[116] Chlorotoxin has been successfully used on C6 glioma cells for patch-clamp experiments with chloride conductance.[60, 117] Additionally, they endogenously express voltage-gated potassium channels, Kv1.1, when unstimulated, along with other potential targets.[97]

Preliminary experiments with chlorotoxin have yielded results indicative that the toxin appears to be amenable to streptavidin-linked probe detection when biotinylated. C6 glioma cells were cultured for 72 hours in six-well plates at 37°C and 5% CO_2 and allowed to propagate until nearly 100% confluent. This was an attempt to mimic the conditions of a tumor. We then exposed the cells at 37°C and 5% CO_2 to 10nM biotinylated chlorotoxin in 1x PBS with Ca^{2+} and Mg^{2+} for five minutes, and followed the toxin exposure with 1nM streptavidin-QD655s in 1x PBS with Ca^{2+} and Mg^{2+} for five minutes (Figure 4.1). We then washed the cells with room temperature 1x PBS with Ca^{2+} and Mg^{2+} three times and imaged.

The cells exposed only to streptavidin-QD655s are without fluorescence (Figure 4.1, B1); however, cells exposed to the biotinylated chlorotoxin conjugate reveal quantum dot fluorescence (Figure 4.1, A1). The fluorescence observed was seen uniformly throughout the entire well, and in each well exposed to biotinylated chlorotoxin and streptavidin-QD655s. This is significant in that the exposure time was minimal and the cells were not cooled to impede internalization of the target. The cells were imaged in solution and the images captured using a Zeiss Axiovert 200M widefield microscope at 20x. It is also significant to note that non-specific binding is absent from these cells.

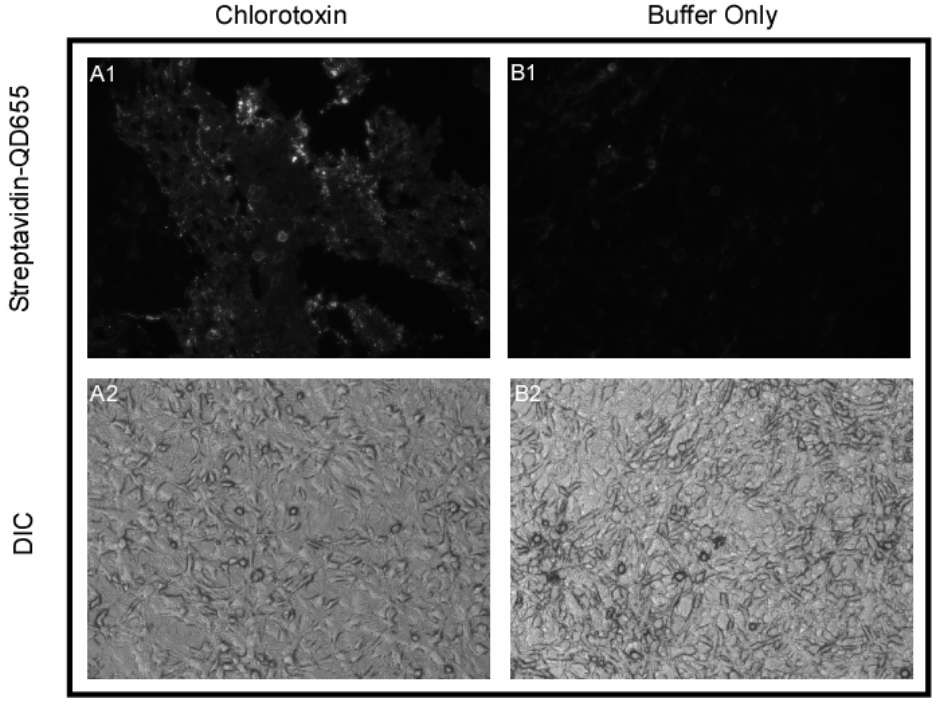

Figure 4.1: Preliminary evidence of biotinylated chlorotoxin effectiveness as a peptide label using streptavidin-QD655. C6 glioma cells were plated and allowed to propagate in a six-well plate for 3 days. Cells were treated for five minutes at 37°C with both 10nM biotinylated chlorotoxin in 1x PBS with Ca^{2+} and Mg^{2+} (A) and 1xPBS with Ca^{2+} and Mg^{2+} (B). The biotinylated peptide was detected with 1nM streptavidin-QD655s in 1xPBS with Ca^{2+} and Mg^{2+} for five minutes at 37°C. The cells were washed with the same buffer at room temperature three times, and imaged in the buffer. Cells were imaged at 20x using a Zeiss Axiovert 200M widefield microscope with Metamorph imaging software. Quantum dot fluorescence (A1) and lack of quantum dot fluorescence (B1) indicates chlorotoxin is a high affinity probe that may be used to enable quantum dot detection for further studies. The experiment was performed in triplicate.

4.6: Conditions Influencing Biotinylated Chlorotoxin Detection

We next wanted to examine labeling with cells that were allowed to propagate for shorter periods of time. This was to see if quantum dot detection maintained its integrity and lack of non-specific binding with cells that had few, if any, daughter cells. It was also to determine whether the necessary target is expressed so soon after trypsinizing the culture, since trypsin is an enzyme that cleaves all proteins at the carboxyl side of arginine and lysine, unless either is followed by proline. This eliminates surface

expression of proteins until the cells have had adequate time to recover from the trypsin process. It is apparent that the cells have recovered the chlorotoxin target by 72 hours in culture, as evident by the fluorescence present in Figure 4.1 (A1).

To continue our preliminary examination of quantum dot detection of chlorotoxin using a two-step methodology, we cultured C6 glioma cells for 24 hours after trypsinizing and plating the cells. This was accomplished by examining the cultures in a variety of buffer solutions to optimize quantum dot detection of chlorotoxin's cellular target, matrix metalloproteinase-2. The cells were treated with ice cold Kreb's-Ringer-HEPES (KRH) buffer before exposing the cultures to multiple buffer solutions, including 1x KRH buffer with and without a percent bovine serum albumin (BSA), containing the labeling agents. We chose KRH because it contains salts and glucose, which may aid in examining shuttling events, and to maintain cell life during the hours of incubation at 4°C. We added 10nM biotinylated chlorotoxin and 1nM streptavidin-QD655 conjugates to KRH with 1% BSA, KRH with 2% BSA, KRH with 3% BSA, and DMEM complete culture medium with 10% fetal bovine serum. Additionally, we ran parallel control experiments to determine if our methods yielded quantum dot non-specific binding interactions. The solutions were added to the cells for two hours at 4°C with constant agitation. Following the two hour incubation, the cells were washed 4-times in ice cold KRH buffer and imaged. These experiments yielded no obvious binding events, but also demonstrated a lack of non-specific binding interactions. This indicates that the blocking components may be hindering the streptavidin quantum dot detection of biotinylated chlorotoxin. This supports the development of one-step probes, toxin:quantum dot

conjugates, for live cell detection. It may also indicate that the target is not expressed at 24 hours following the trypsin treatment, although this is not the favored conclusion.

To determine if the blocking proteins were inhibiting biotinylated chlorotoxin labeling from being detected by streptavidin-QD655s, we repeated the experiment but used KRH buffer, 1x PBS with Ca^{2+} and Mg^{2+}, and tissue buffer with Ca^{2+} and Mg^{2+}. Unlike the previous experiments with increasing amounts of blocking proteins, we washed the cells in ice cold KRH buffer three times to acclimate the cells to the 4°C environment. We then added the labeling solutions and proceeded as previously described. Imaging was performed with a Zeiss 200M Axiovert microscope with Metamorph software.

We observed binding events with all three solutions; however, KRH buffer appeared to have the highest number of events. Figure 4.2 shows labeling events in C6 glioma cells plated for 24 hours before treatment in KRH buffer. The cells maintained their morphology throughout the labeling process at 4°C, and showed some quantum dot fluorescence (Figure 4.2, A2). The most encouraging data is that quantum dot non-specific binding was not a factor (Figure 4.2, B2). This indicates that both the toxin and quantum dots retain high specificity with their binding events, and do not present with cross-reactivity.

Figure 4.2 indicates that chlorotoxin targeting may be culture-age dependent such that an older culture (Figure 4.1) shows more fluorescence labeling in a shorter amount of time. Increased labeling may also be a factor of the temperature difference between the experiments, or the increased number of cells present due to longer propagation. Cell confluency may effect target expression such that the culture in Figure 4.1 resembles

tissue in its confluency. There may be a correlation between chlorotoxin target, matrix metalloproteinase-2, expression and confluency. Further studies are needed to derive definitive conclusions relating these results. These preliminary finding provide additional evidence to substantiate the use and suitability of quantum dots for biological labeling applications, and provide evidence that high affinity neurotoxin mediated quantum dot detection may be a viable tool for disease identification and therapies.

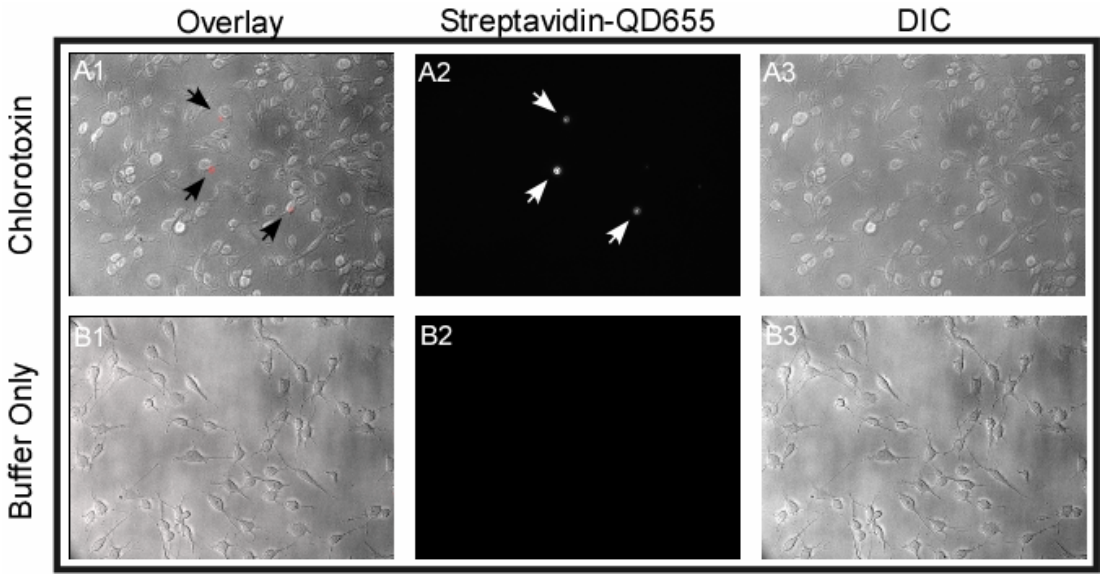

Figure 4.2: Additional evidence that chlorotoxin is an effective probe for use in quantum dot detection studies. C6 glioma cells were plated and allowed to propagate in a six-well plate for 1 day. Before toxin exposure, cells were washed three times for 10 minutes with ice-cold KRH buffer. The cells were then treated with both 10nM biotinylated chlorotoxin and 1nM streptavidin-QD655 in KRH buffer, and 1nM streptavidin-QD655 in KRH buffer for 2 hours at 4°C with constant agitation. Imaging was performed at 20x using a Zeiss Axiovert 200M widefield microscope with Metamorph imaging software following four washes with ice-cold KRH buffer. Detection was reduced compared with cells allowed to propagate for a longer period of time, yet present. Experiments were performed in triplicate.

4.7: Neurotoxin Conjugated Quantum Dots

Quantum dot labeling utilizing high affinity peptide toxins has been demonstrated to provide increased sensitivity for probing biological systems in their native environment.[57] Multiplexing experiments using two high affinity peptide toxins,

chlorotoxin and dendrotoxin-1, conjugated to quantum dots were performed. Each toxin was conjugated directly to quantum dots, and used to visualize endogenous expression of matrix metalloproteinase-2 and voltage-gated potassium channels, Kv1.1, in C6 glioma cells, along with expression of these cellular targets within a series of representative cell types.

4.8: Neurotoxin Nanoconjugates and Antibody Colocalization Analyses

Quantum dot conjugates for chlorotoxin and dendrotoxin-1 were synthesized according to the reaction scheme in Figure 2.2 (A-C).[72] The toxins were cross-linked to both QD525 and QD655 for chlorotoxin and dendrotoxin-1, respectively, to produce CTX:QD525 and DTX-1:QD655 for labeling. Quantum dot conjugate detection of endogenous cellular targets was determined through antibody colocalization analyses. Live C6 glioma cells were incubated with either 10nM CTX:QD525 or QD525, and either 5nM DTX-1:QD655 or QD655, at 37°C and 5% CO_2 for 120 and 180 minutes, respectively. Following incubation cells were post-fixed in 4% paraformaldehyde and permeabilized in 0.1% Triton X-100 prior to primary antibody exposure and subsequent secondary Alexafluor conjugated antibody labeling. Figure 4.3 illustrates the colocalization of CTX:QD525 conjugates (Figure 4.3A) with anti-matrix metalloproteinase-2 antibodies detected with secondary-Alexa594 antibodies versus exposure to QD525 in lieu of the toxin conjugate (Figure 4.3B). The presence of colocalization between CTX:QD525 and secondary-Alexa594 antibodies indicates that CTX:QD525 has labeled MMP-2 in the live cell, and demonstrates probe suitability for the specified target.

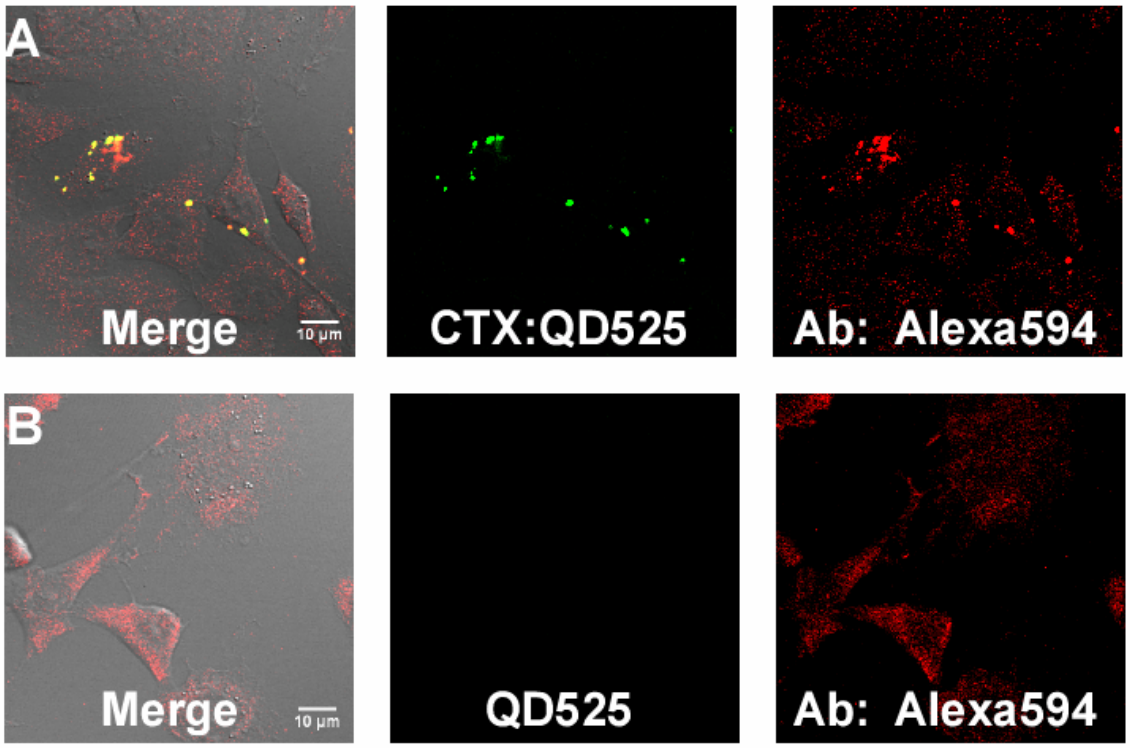

Figure 4.3: Antibody colocalization of endogenous matrix metalloproteinase-2 expression in live C6 glioma cells. CTX:QD525 (A) and QD525 (B) were exposed to live C6 glioma cells for 2 hours at 37°C and 5% CO_2. Cells were post-fixed in 4% paraformaldehyde, and permeabilized in 0.1% TritonX-100. CTX:QD525 and QD525 exposed cells were incubated with matrix metalloproteinase-2 (1:500) primary antibody in 1% normal goat serum for 20 hours at 4°C, and then exposed to Alexa594 secondary antibody (1:500) for 1 hour at room temperature. Imaging was performed on an LSM510 Meta inverted confocal microscope following mounting with Aqua Polymount. CTX:QD525 labels endogenous matrix metalloproteinase-2 expression in live cell culture, indicating effectiveness as a probe for live detection studies.

DTX-1:QD655 and secondary-Alexafluor antibody colocalization is similarly observed with fluorescence colocalization achieved using an anti-voltage-gated potassium channel, Kv1.1, antibody and secondary-Alexa488 antibody system, and compared with exposure to QD655s only (Figure 4.4).

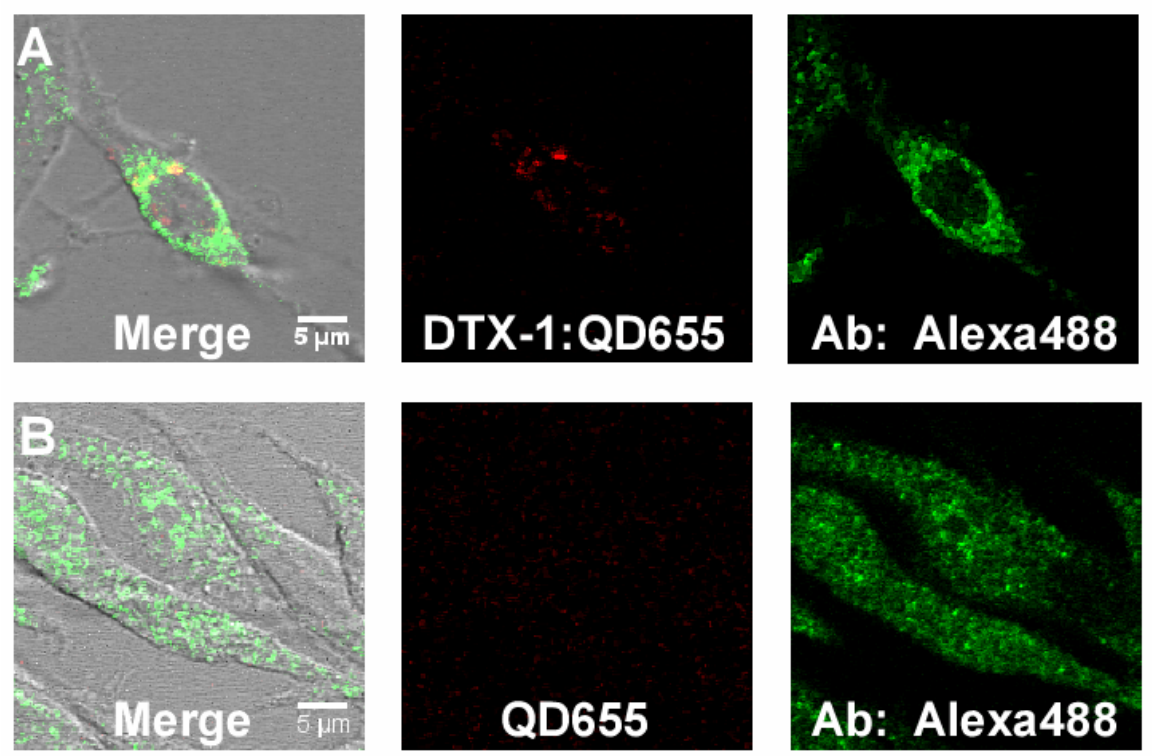

Figure 4.4: Antibody colocalization of endogenous Kv1.1 expression in live C6 glioma cells. DTX-1:QD655 (A) and QD655 (B) were exposed to live C6 glioma cells for 3 hours at 37°C at 5% CO_2. Cells were post-fixed in 4% paraformaldehyde, and permeabilized in 0.1% TritonX-100. DTX-1:QD655 and QD655 exposed cells were incubated with potassium channel, Kv1.1, (1:500) primary antibody in 1% normal goat serum for 24 hours at 4°C, and then exposed to Alexa488 secondary antibody (1:500) for 1 hour at room temperature. Imaging was performed on an LSM510 Meta inverted confocal microscope following mounting with Aqua Polymount. Potassium channel, Kv1.1, expression is effectively detected using DTX-1:QD655 in live cell culture, which indicates probe effectiveness for live detection studies of endogenously expressed targets.

Comparable to CTX:QD525, secondary-Alexa488 fluorescence colocalization with DTX-1:QD655 emission is observed (Figure 4.4A) without the presence of QD655 non-specific binding (Figure 4.4B). This supports DTX-1:QD655 specificity for the potassium channel target, Kv1.1, making the conjugate a suitable probe for endogenous potassium channel detection in living cells. Colocalization of secondary-Alexafluor fluorescence with CTX:QD525 and DTX-1:QD655 emission enabled labeling efficacy to be determined as specific to the cellular targets, matrix metalloproteinase-2 and voltage-gated potassium channel, Kv1.1. Additionally, lack of secondary-Alexafluor

colocalization when present in the system exposed only to QD525 or QD655 further substantiates probe specificity via CTX:QD525 and DTX-1:QD655 affinity for the endogenous cellular targets, and supports that fluorescence is not the result of QD525 or QD655 non-specific binding within C6 glioma cells.

4.9: Chlorotoxin Quantum Dot Conjugate Time-Dependent Blocking

Following examination utilizing antibody colocalization analyses for positive determination of target detection, verification that CTX:QD525 binds to the specified target was further tested through time-dependent blocking assays. C6 glioma cells were incubated in media containing 200nM unconjugated chlorotoxin overnight. The cultures were then treated with 10nM CTX:QD525 or QD525 for time intervals of 30, 60 and 120 minutes at 37°C and 5% CO_2. Figure 4.5 illustrates representative images of effective chlorotoxin blocking of CTX:QD525 labeling for the designated time intervals. Comparatively, CTX:QD525 detection of matrix metalloproteinase-2 increases with time in C6 glioma cultures left unexposed to unconjugated chlorotoxin, which further substantiates CTX:QD525 probe specificity for the target. There is a significant increase at 120 minutes in CTX:QD525 labeling of native matrix metalloproteinase-2 in live culture, which was established to be the optimal incubation time for the CTX:QD525 conjugate for additional studies utilizing the probe.

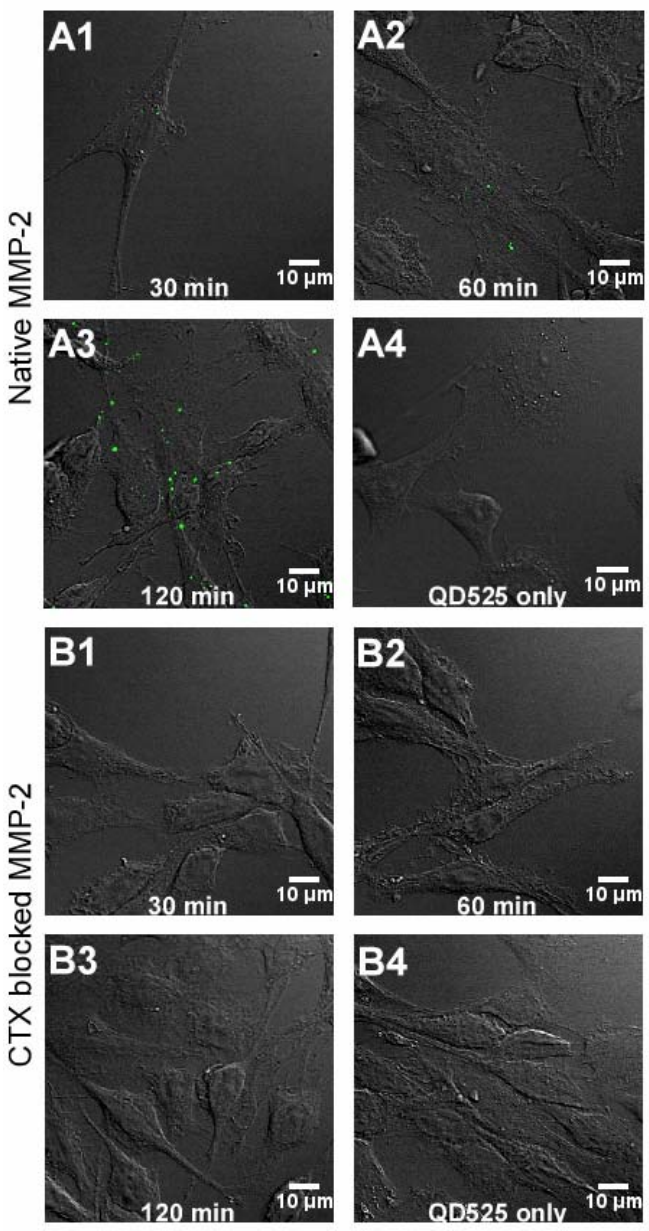

Figure 4.5: Chlorotoxin pre-incubation blocks CTX:QD525 detection in live culture for up to 2 hours. C6 glioma cells were exposed to 200nM chlorotoxin in complete media overnight at 37°C at 5% CO_2 prior to exposure to 10nM CTX:QD525 (B1-B3) and 10nM QD525 (B4) for time intervals of 30, 60, and 120 minutes. Each time interval was performed in triplicate with at least six images acquired per replicate.

Incubation times greater than 120 minutes appeared to result in cell death, possibly due to the toxin's lethal effects. At 120 minutes, chlorotoxin blocked the matrix metalloproteinase-2 remains undetected by CTX:QD525, Figure 4.6 (P<0.001, analysis

of variance, values are the means ± SEM). Quantitative analysis that CTX:QD525 detection in live culture is effectively blocked for 120 minutes, in addition to antibody colocalization (Figure 4.3A), confirms CTX:QD525 target specificity, and concurs with qualitative microscopic evidence.

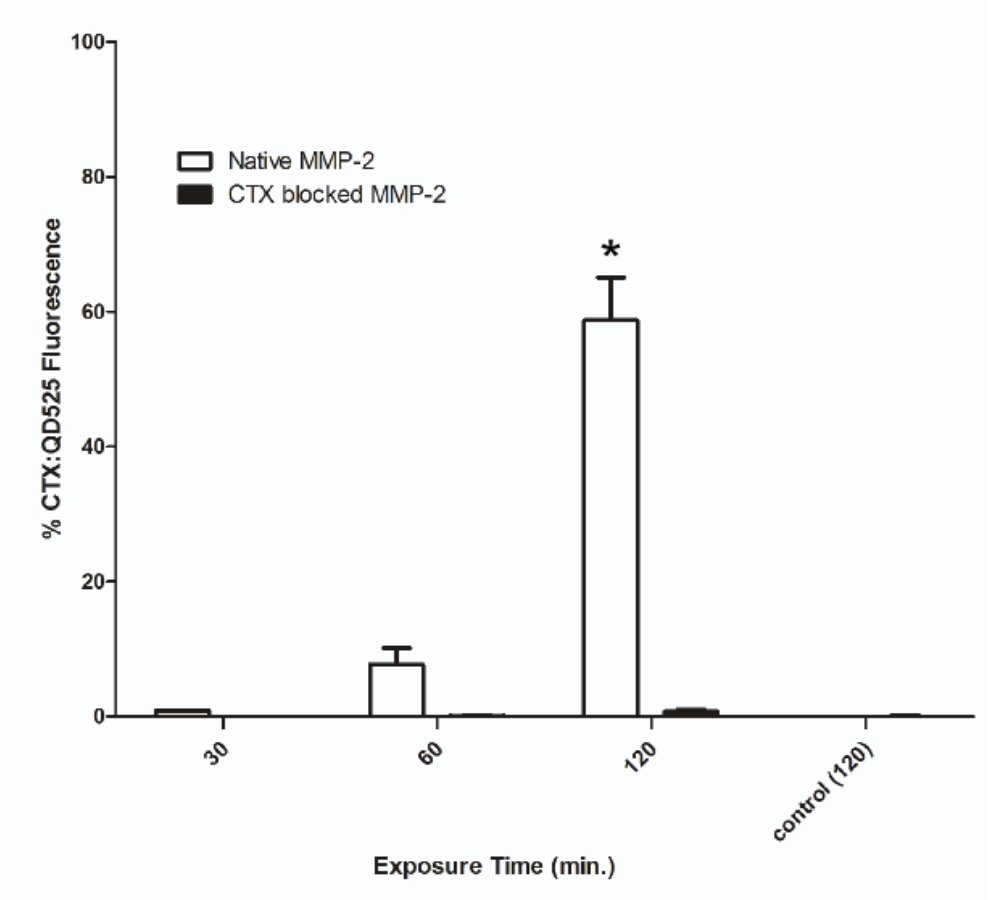

Figure 4.6: Chlorotoxin pre-incubation blocks CTX:QD525 detection in live culture for up to 2 hours. Chlorotoxin effectively blocked CTX:QD525 endogenous detection in live culture for up to 2 hours ($P<0.001$, analysis of variance, values are the means ± SEM), and further indicates probe suitability for live assays. Each time interval was performed in triplicate with at least six images acquired per replicate.

4.10: Dendrotoxin-1 Nanoconjugate Time-Dependent Blocking

This methodology of unconjugated toxin blocking was repeated using DTX-1:QD655 to ascertain endogenous specificity for potassium channels, Kv1.1, in C6 glioma culture (Figure 4.7).

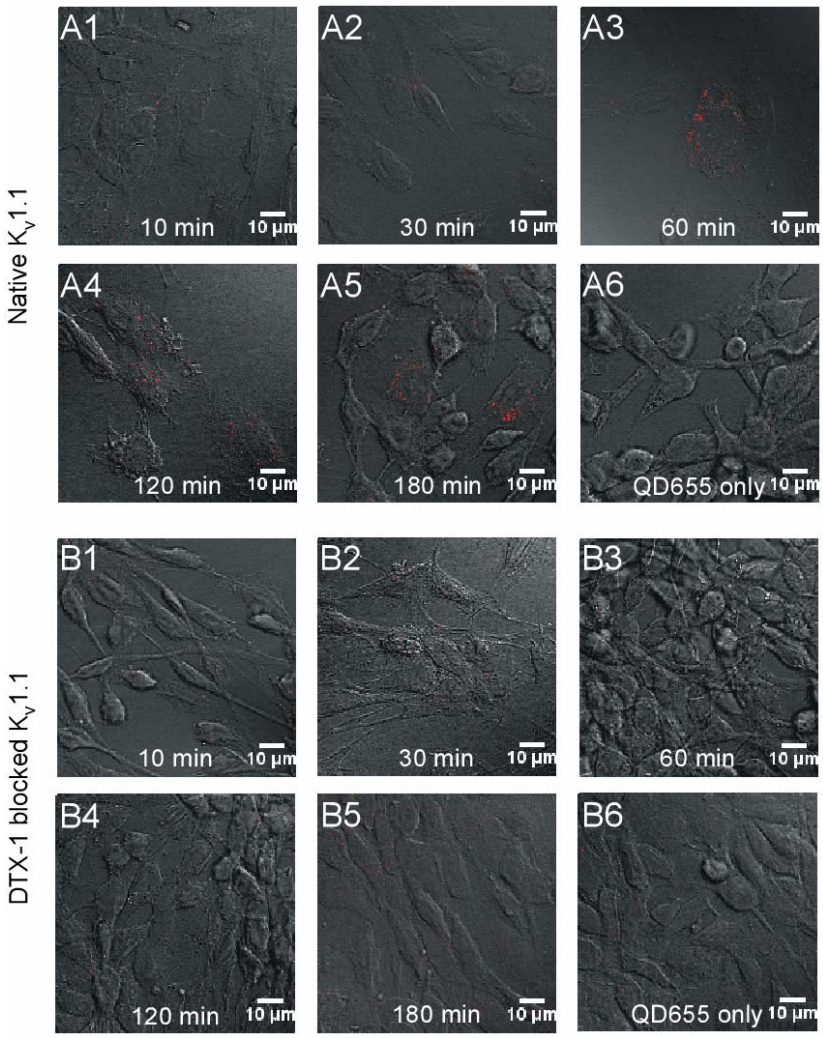

Figure 4.7: Dendrotoxin-1 pre-incubation blocks DTX-1:QD655 detection in live culture for up to 3 hours. C6 glioma cells were exposed to 100nM dendrotoxin-1 in complete media overnight at 37°C at 5% CO_2 prior to exposure to 5nM DTX-1:QD655 (B1-B5) and 5nM QD655 (B6) for time intervals of 10, 30, 60, 120, and 180 minutes. Each time interval was performed in triplicate with at least six images acquired per replicate.

Cells were treated similarly to the chlorotoxin assays, and blocked with 100nM unconjugated dendrotoxin-1 overnight. Following blocking with unconjugated dendrotoxin-1, C6 glioma cells were incubated with 5nM DTX-1:QD655 for time intervals of 10, 30, 60, 120, and 180 minutes. Subsequent comparison to native Kv1.1 potassium channels, illustrated in Figure 4.7, reveals the rapidity of DTX-1:QD655 labeling of native Kv1.1 potassium channels in live culture. Both quantitative, Figure 4.8, and qualitative analyses, Figure 4.7, reveal that dendrotoxin-1 blocks DTX-1:QD655 detection of voltage-gated potassium channels, Kv1.1, for approximately 180 minutes.

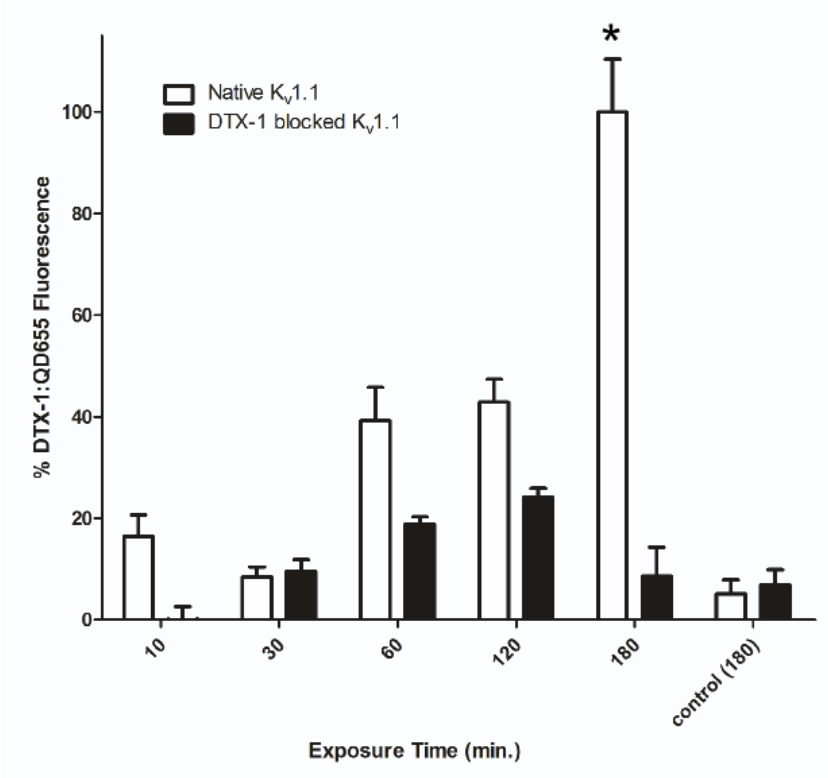

Figure 4.8: Dendrotoxin-1 pre-incubation blocks DTX-1:QD655 detection in live culture for up to 3 hours. Dendrotoxin-1 effectively blocked DTX-1:QD655 endogenous detection in live culture for up to 3 hours ($P<0.001$, analysis of variance, values are the means ± SEM), and further indicates probe suitability for live assays. Each time interval was performed in triplicate with at least six images acquired per replicate.

At approximately 180 minutes, DTX-1:QD655 fluorescence in cells not exposed to unconjugated dendrotoxin-1 is significantly greater and more widely distributed throughout the culture than at other time points, Figure 4.8 ($P<0.001$, analysis of variance, values are the means ± SEM); however, at both 60 and 120 minutes, labeling is significant for adequate detection. The lack of DTX-1:QD655 labeling in cells incubated with unconjugated dendrotoxin-1, denotes that the toxin effectively blocks DTX-1:QD655 detection of Kv1.1 potassium channels at all time intervals. This is further confirmed by quantitative analysis in Figure 4.8. DTX-1:QD655 utility and specificity as a probe to effectively target endogenous Kv1.1 are revealed at each time point by the ability to block detection. This evidence, paired with antibody colocalization, indicates a suitable probe for Kv1.1 detection in a dynamic living environment.

4.11: Peptide Toxin Quantum Dot Conjugate Saturation Binding Analyses

Affinity for cellular targets in live culture was determined using saturation binding curve analysis for both CTX:QD525 and DTX-1:QD655 conjugates. C6 glioma cells were incubated with increasing concentrations of CTX:QD525 (Figure 4.9) and DTX-1:QD655 (Figure 4.10), independently, for 120 and 180 min, respectively. Cells were fixed, mounted, and imaged using invert confocal microscopy, LSM510 Meta (Zeiss, Inc.). Figure 4.9 illustrates the resulting saturation binding curves for CTX:QD525 conjugates in C6 glioma live cell culture. The Hill-slope was also calculated to be approximately 2.620, which indicates that there may be more than one binding site on matrix metalloproteinase-2.

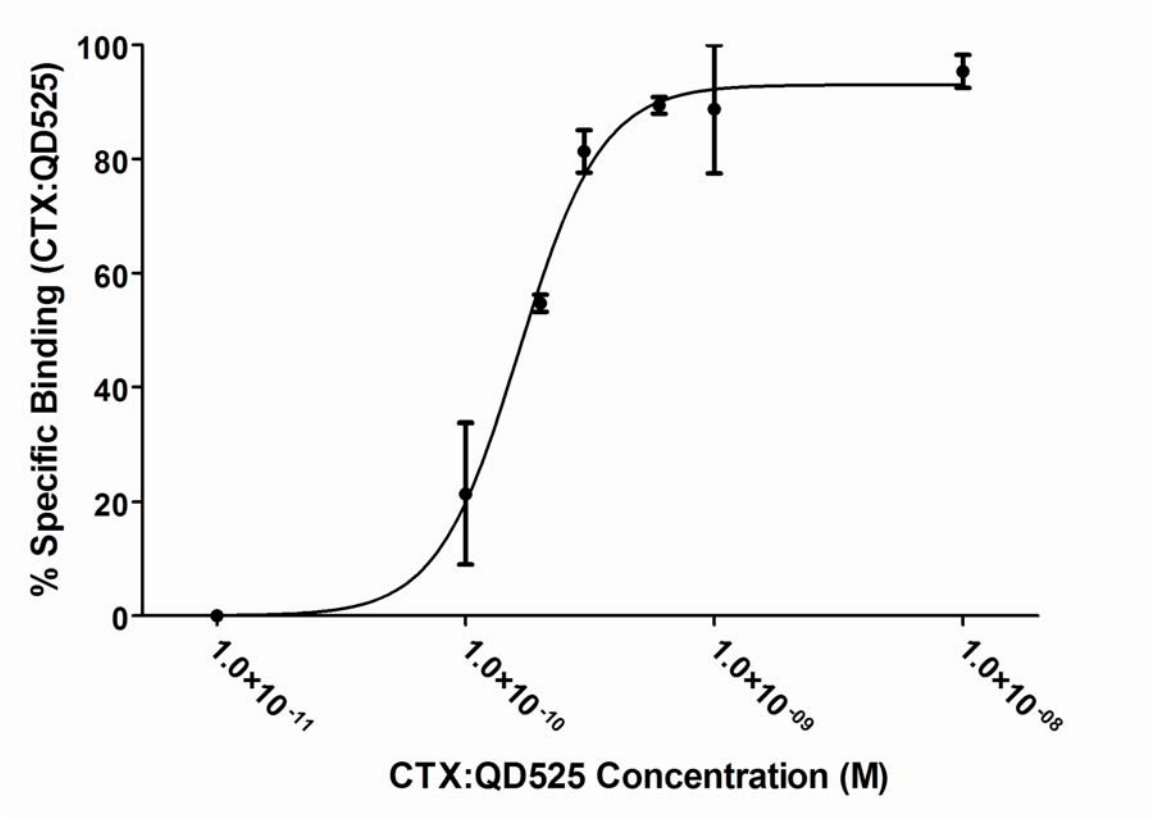

Figure 4.9: Saturation binding curve for CTX:QD525. Points represent experiments run in triplicate and imaged at least five times. Live C6 glioma cells were exposed to 10nM CTX:QD525 for approximately 120 minutes prior to post-fixing with 4% paraformaldehyde for imaging. Data are the mean of three experiments ± S.E.M. The CTX:QD525 saturation binding curve yielded the chlorotoxin affinity to be approximated as: K_D = 164.5pM ± 8.712pM; B_{max} is 93.02% ± 2.333%; and, the Hill-slope is 2.620 ± 0.3269. Toxin conjugation to quantum dots produces high affinity probes for target detection.

Saturation binding analysis for DTX-1:QD655 conjugates (Figure 4.10) also supported the data presented in Figure 4.7 and Figure 4.8. The binding curve indicated a K_D for DTX-1:QD655 in C6 glioma live cell culture to approximately 3.7nM. Although this is in agreement with the observed data in Figure 4.7 and Figure 4.8, the affinity was determined to be less for the conjugate than previously reported for unconjugated DTX-1.[94] Lower affinity may be the result of the conjugation process in that the residues used to conjugate the quantum dot to the toxin may be critical to the interaction with the

binding site on Kv1.1; thus, the loss of the free residues may weaken binding with the channel and result in a lower affinity. Despite the lower observed affinity, the conjugate maintains nanomolar affinity for the potassium channel, and therefore is a sufficient probe for detecting the presence of Kv1.1 in live culture.

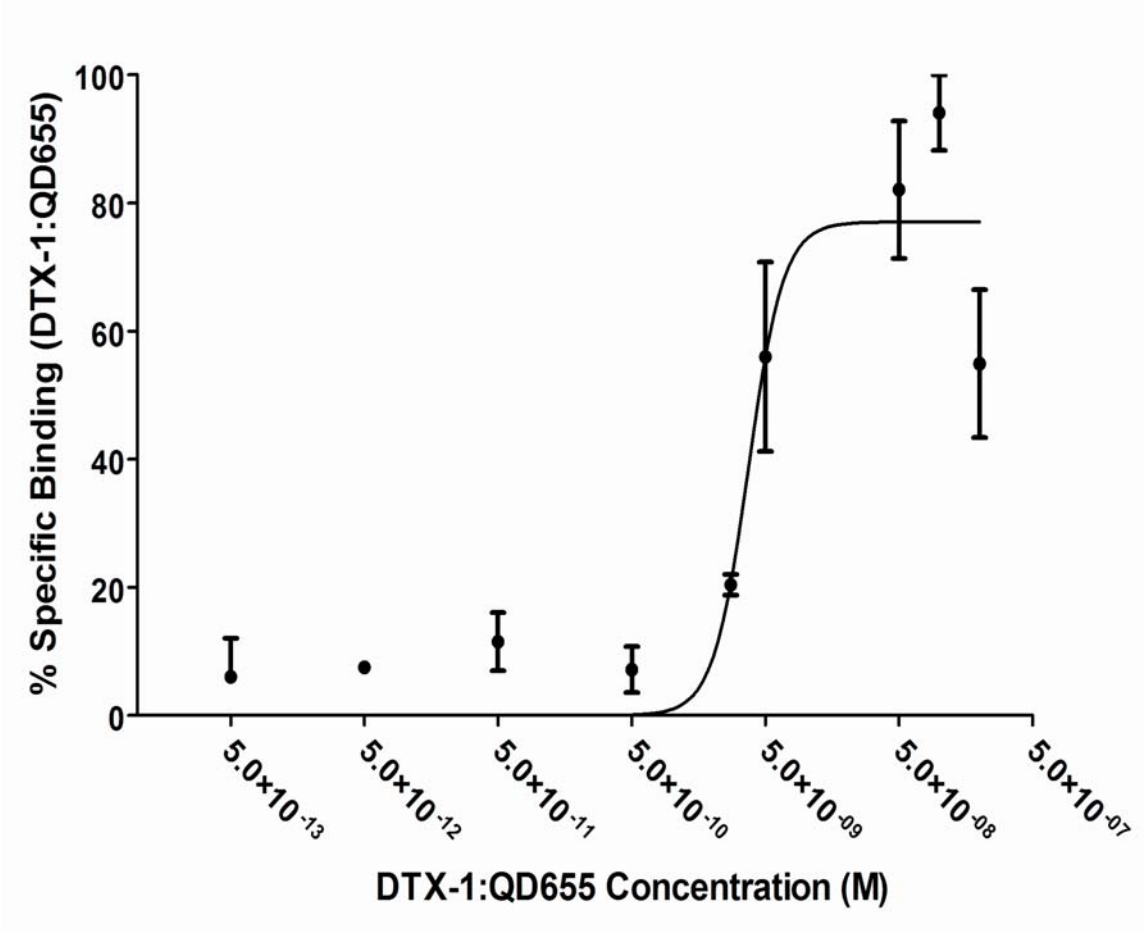

Figure 4.10: Saturation binding curve for DTX-1:QD655. Points represent experiments run in triplicate and imaged at least five times. Live C6 glioma cells were exposed to 5nM DTX-1:QD655 for approximately 180 minutes prior to post-fixing with 4% paraformaldehyde for imaging. Data are the mean of three experiments ± S.E.M. Dendrotoxin-1 affinity for Kv1.1, as assessed through DTX-1:QD655 detection, was determined to be: K_D = 3.729nM ± 0.7581nM; B_{max} is 77.06% ± 7.759%; and, the Hill-slope is 3.316± 2.124. Peptide neurotoxin conjugation to quantum dots produces high affinity probes for target detection.

4.12: Quantum Dot Conjugate Multiplexing Detection in Live Cells

Multiplexing capacity is a characteristic of quantum dots which enables multiple targets to be illuminated simultaneously with the same excitation source. To demonstrate multiplexing using quantum dot conjugates, C6 glioma cells were simultaneously incubated with CTX:QD525 and DTX-1:QD655 (Figure 4.11A).

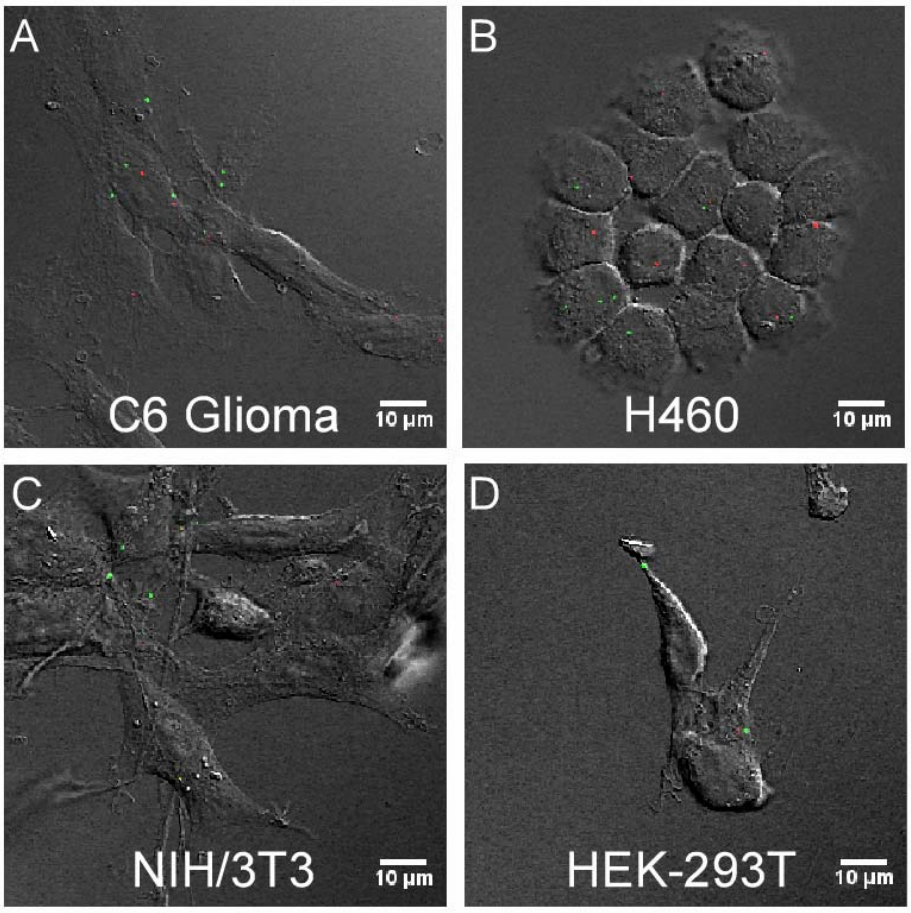

Figure 4.11: CTX:QD525 and DTX-1:QD655 multiplexing detection differs between cancer and non-cancer cells in live culture. C6 glioma (A), H460 (B), 3T3/NIH (C), and HEK-293T(D) cells were co-incubated with 10nM CTX:QD525 and 5nM DTX-1:QD655 for 2h at 37°C at 5% CO_2. Cells were post-fixed in 4% paraformaldehyde and imaged using an LSM510 Meta confocal microscope. Each experiment was performed in triplicate with approximately six images in each sample. CTX:QD525 and DTX-1:QD655 show increased detection within cancer cells at low concentrations, and may serve as high affinity probes for distinguishing cancer presence in live culture.

The cells were exposed to the conjugates for 120 minutes at 37°C and 5% CO_2, and fixed and mounted for imaging. Source excitation was a 488nM Argon laser in conjunction with an inverted confocal microscope, LSM510 Meta, for image collection. Figure 4.11 reveals the multiplexing images resulting from co-incubation of CTX:QD525 and DTX-1:QD655 in C6 glioma cells. Both CTX:QD525 and DTX-1:QD655 detection is observed, and indicates that the toxin nanoconjugates are suitable not only for target detection in live cells, but also are amenable to multiplexing experimentation. This trait provides the potential to monitor multiple targets simultaneously within living systems for in depth analyses concerning an array of cellular functions.

Chlorotoxin is reported to preferentially bind to cancer cells over non-cancer cells. To test this, comparative multiplexing experiments were performed to ascertain the proclivity other cell types have for both toxin:quantum dot conjugates. Collectively, two rodent cell types, C6 glioma (Figure 4.11A) and 3t3/NIH (Figure 4.11C), and two human cell types, H460 (Figure 4.11B) and HEK-293T (Figure 4.11D), were chosen to be examined for endogenous expression of matrix metalloproteinase-2 and potassium channel, Kv1.1. Each cell type couple consisted of a cancer cell line and a non-cancer cell line for direct comparison. The cells were treated with the toxins as previously described for the multiplexing experimentation, and imaged using the same conditions. Figure 4.11 illustrates the results of the comparison. Quantitation reveals that the differences between endogenous matrix metalloproteinase-2 detection are greater in C6 glioma cells and H460 cells, than in 3t3/NIH cells and HEK-293T cells (Figure 4.12). This indicates that these cells likely express higher levels of matrix metalloproteinase-2 on their cell membranes, which is detected and visualized by CTX:QD525 fluorescence.

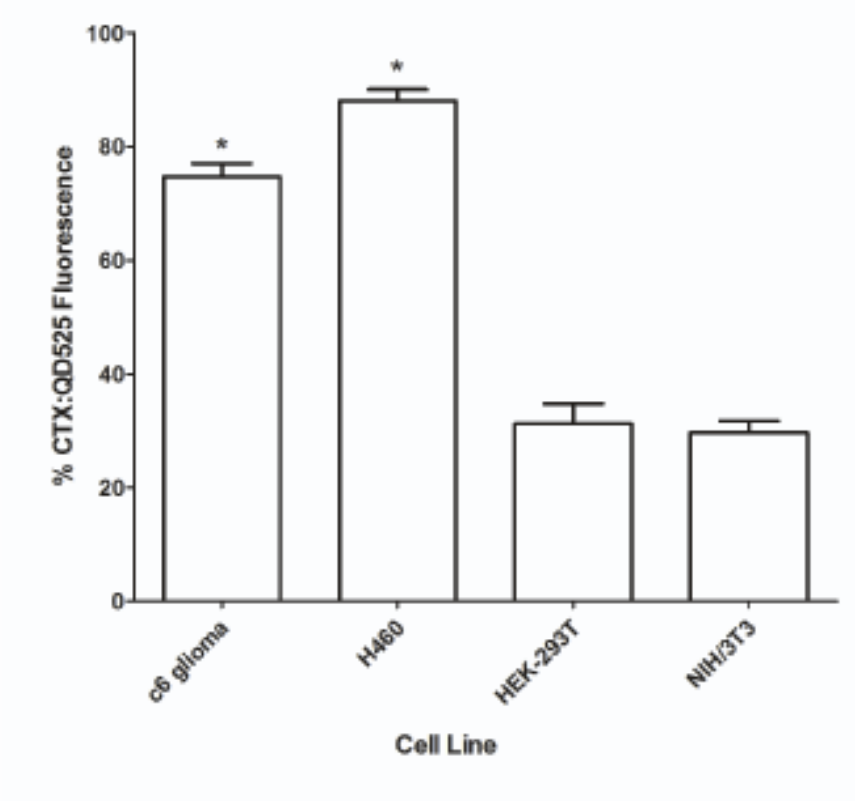

Figure 4.12: CTX:QD525 fluorescence is statistically greater in the two cancer cell lines examined than in the two non-cancer cell lines. C6 glioma, H460, 3T3/NIH, and HEK-293T cells were co-incubated with 10nM CTX:QD525 for 2 hours at 37°C at 5% CO_2. Cells were post-fixed in 4% paraformaldehyde and imaged using an LSM510 Meta confocal microscope. Each experiment was performed in triplicate with approximately six images in each sample. Relative fluorescence intensity for CTX:QD525 reveals statistically significant differences between quantitated fluorescence within cancer cells, C6 glioma and H460, versus non-cancer cells, HEK-293T and 3T3/NIH (P<0.001, analyses of variance, values are the means ± SEM).

Similar results are observed for DTX-1:QD655 detection of voltage-gated potassium channels, Kv1.1, in all cell types (Figure 4.13). There is a quantifiable difference between detectable cancer cell expression levels of Kv1.1 potassium channels and non-cancer cell expression levels. The voltage-gated potassium channel, Kv1.1, was detected in both C6 glioma cells and H460 cells at levels approximately four times that of the non-cancer cells tested. This suggests that there may be a marked increase in Kv1.1 potassium channel expression within cancer cells, along with the increased expression of

matrix metalloproteinase-2, that DTX-1:QD655 and CTX:QD525 detect, respectively, within 120 minutes. These results support that CTX:QD525 and DTX-1:QD655 conjugates may serve as a highly sensitive visible spectrum labeling system capable of distinguishing between diseased and healthy cells, and possibly tissue, for diagnostic purposes.

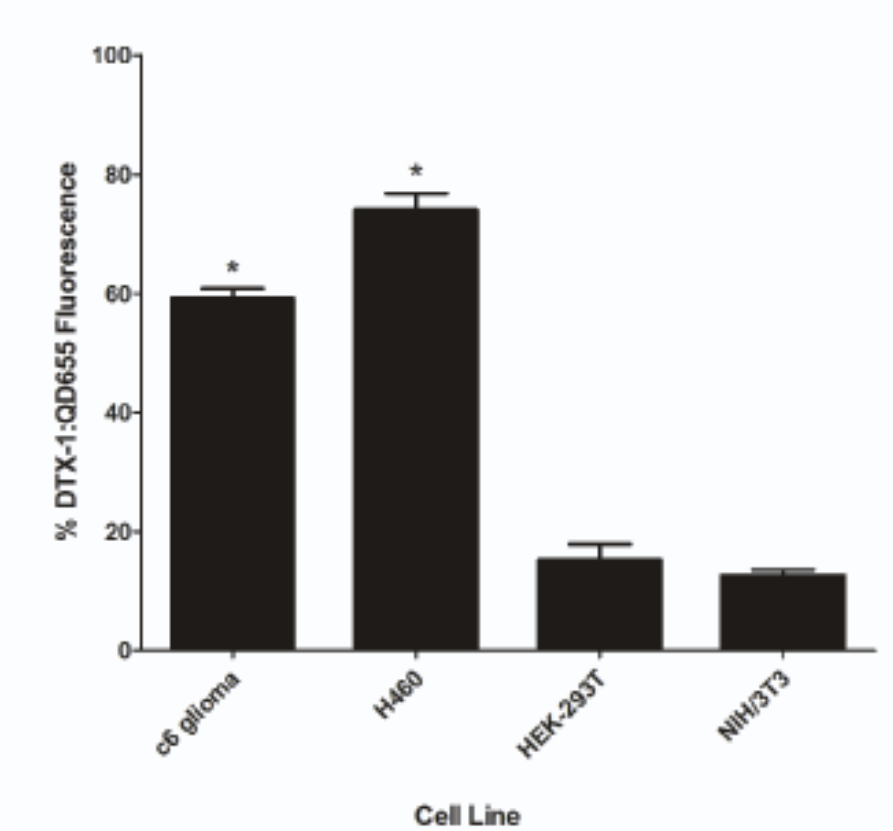

Figure 4.13: DTX-1:QD655 fluorescence is statistically greater in the cancer cell lines examined than in the non-cancer cell lines. C6 glioma, H460, 3T3/NIH, and HEK-293T cells were co-incubated with 5nM DTX-1:QD525 for 2 hours at 37°C at 5% CO_2. Cells were post-fixed in 4% paraformaldehyde and imaged using an LSM510 Meta confocal microscope. Each experiment was performed in triplicate with approximately six images in each sample. Relative fluorescence intensity for DTX-1:QD655 reveals statistically significant differences between quantitated fluorescence within cancer cells, C6 glioma and H460, versus non-cancer cells, HEK-293T and 3T3/NIH (P<0.001, analyses of variance, values are the means ± SEM).

4.13: Flow Cytometry

Flow cytometry was performed to assess the CTX:QD525 and DTX-1:QD655 labeling efficacy throughout the populations of the cell lines examined. Additionally, CTX:QD525 and DTX-1:QD655 specificity was examined using flow cytometry through blocking analyses with unconjugated chlorotoxin and dendrotoxin-1, respectively. Figure 4.14 illustrates the histogram data comparing CTX:QD525 labeling of native matrix metalloproteinase-2 and chlorotoxin blocked matrix metalloproteinase-2.

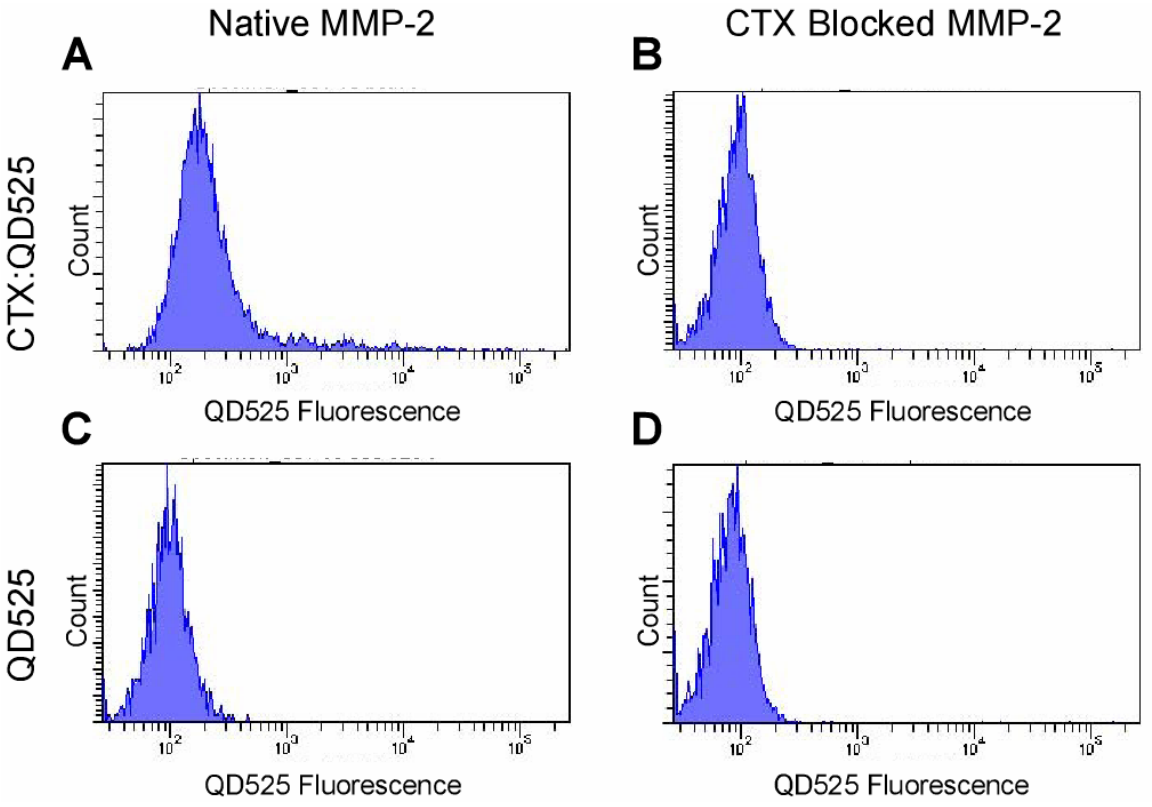

Figure 4.14 Flow cytometry histograms describing CTX:QD525 detection of matrix metalloproteinase-2 within C6 glioma cell populations. Matrix metalloproteinase-2 (MMP-2) is labeled by 10nM CTX:QD525 (A) when the conjugate is exposed to native, untreated cells. CTX:QD525 detection of matrix metalloproteinase-2 is blocked by previous exposure to 200nM unconjugated chlorotoxin (CTX) overnight (B). Labeled cell populations for chlorotoxin blocked CTX:QD525 are comparable to 10nM QD525 in both untreated (C) and chlorotoxin treated (D) C6 glioma cells.

Chlorotoxin blocking analyses histograms reveal that CTX:QD525 detection of cells exposed to 200nM chlorotoxin overnight is approximately comparable to QD525 control assays for both native matrix metalloproteinase-2 and chlorotoxin blocked matrix metalloproteinase-2. These qualitative assessments are affirmed by quantitative analysis (Figure 4.15).

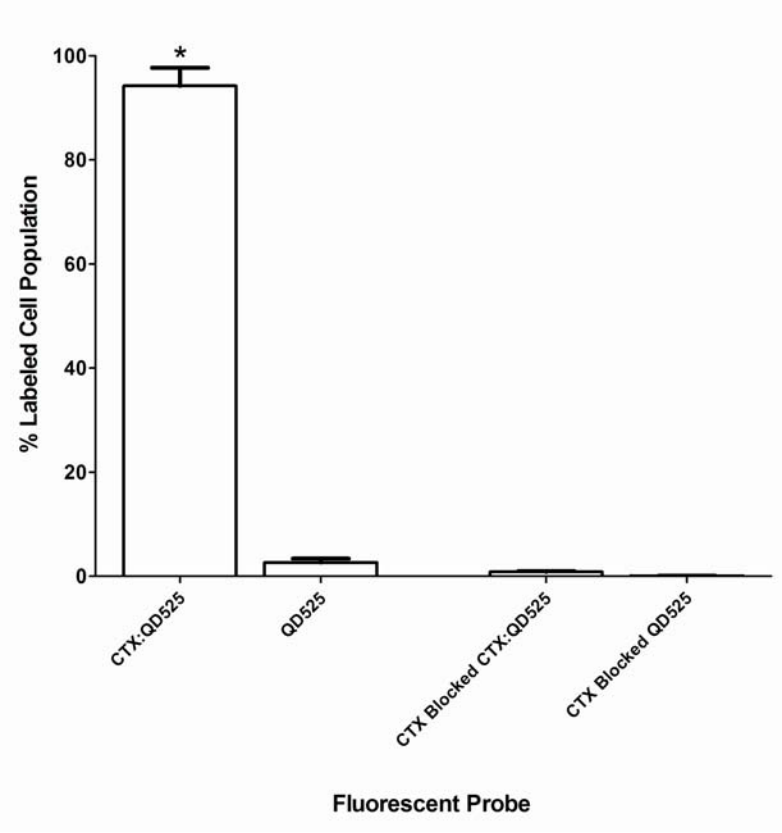

Figure 4.15: Flow cytometry supports CTX:QD525 detection of matrix metalloproteinase-2 in C6 glioma cells. The percentage of cells labeled with CTX:QD525 only within the cell population is statistically significant ($P<0.001$, analysis of variance, values are the means ± SEM), as compared with cells incubated with unconjugated chlorotoxin prior to CTX:QD525 exposure at 120 minutes.

Flow cytometry experimentation further supports CTX:QD525 specificity by providing quantitative evidence reflecting the number of C6 glioma cells labeled at 120

minutes, relative to cells exposed to unconjugated chlorotoxin prior to CTX:QD525 incubation. The CTX:QD525 labeled cells were present in approximately 80% of the culture; whereas, unconjugated chlorotoxin incubation resulted in cell labeling levels similar to the cells exposed only to QD525 ($P<0.001$, analysis of variance, values are the means ± SEM).

As with CTX:QD525, DTX-1:QD655 detection was examined using flow cytometry analyses. Figure 4.16 illustrates the histogram data highlighting DTX-1:QD655 detection of native Kv1.1 and dendrotoxin-1 blocked Kv1.1.

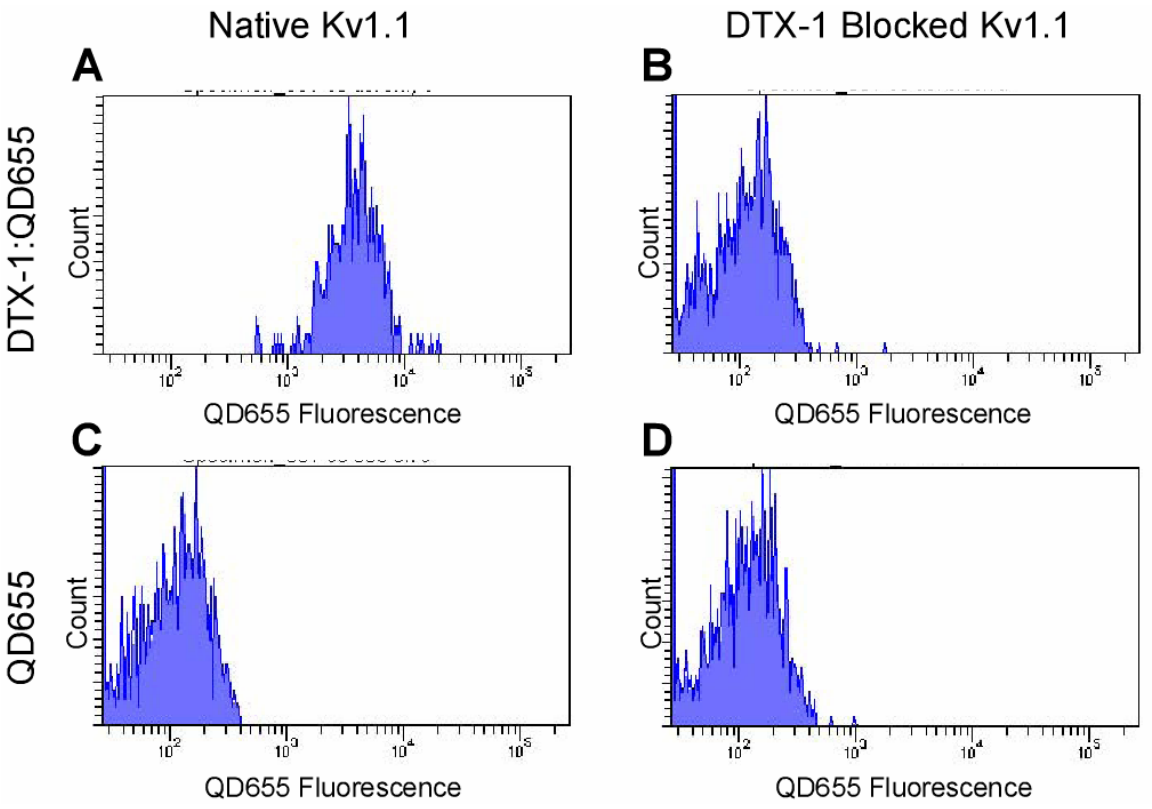

Figure 4.16: Flow cytometry histograms describing DTX-1:QD655 detection of Kv1.1 within C6 glioma cell populations. Kv1.1 is labeled by 5nM DTX-1:QD655 (A) when the conjugate is exposed to native, untreated cells. DTX-1:QD655 detection of Kv1.1 is blocked by previous exposure to 100nM unconjugated DTX-1 overnight (B). Labeled cell populations for DTX-1 blocked DTX-1:QD655 are comparable to 5nM QD655 in both untreated (C) and DTX-1 treated (D) C6 glioma cells.

As with chlorotoxin blocking analyses, dendrotoxin-1 blocking analyses histograms reveal that DTX-1:QD655 detection of cells exposed to 100nM dendrotoxin-1 overnight is approximately comparable to QD655 control assays for both native Kv1.1 and dendrotoxin-1 blocked Kv1.1 potassium channels. These qualitative assessments are affirmed by quantitative analysis (Figure 4.17).

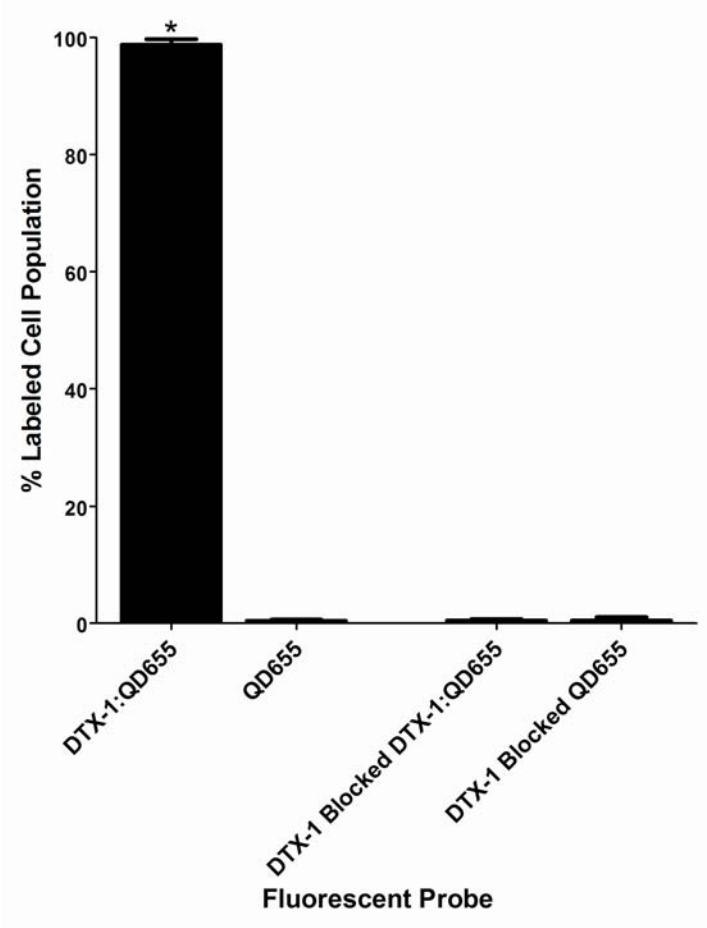

Figure 4.17: Flow cytometry supports DTX-1:QD655 detection of Kv1.1 in C6 glioma cells. The percentage of cells labeled with DTX-1:QD655 only within the cell population is statistically significant ($P<0.001$, analysis of variance, values are the means ± SEM), as compared with cells incubated with unconjugated dendrotoxin-1 prior to DTX-1:QD655 exposure at 180 minutes. Each time interval was performed in triplicate.

DTX-1:QD655 detection of Kv1.1 potassium channels is also supported by flow cytometry experimentation. As with CTX:QD525, DTX-1:QD655 labeled cells were present at statistically significant numbers within culture (P<0.001, analysis of variance, values are the means ± SEM) versus the number of labeled cells previously exposed to unconjugated dendrotoxin-1. At 180 minutes, the number of DTX-1:QD655 labeled cells in culture was approximately <90% of the population.

To complement the multiplexing microscopy analyses, flow cytometry was utilized to examine the cell populations labeled with CTX:QD525 and DTX-1:QD655 (Figure 4.18). C6 glioma, H460, NIH/3T3, and HEK-293T cells were incubated with 10nM CTX:QD525 and 5nM DTX-1:QD655 for 120 min. The cells were suspended in 1x DPBS without Mg^{2+} and Ca^{2+} and examined using BD 5-laser LDRII flow cytometer.

Flow cytometry quantitation of the dual labeling experimentation is illustrated in Figure 4.19. These analyses revealed that statistically significant cell populations (P<0.001, analysis of variance, values are the means ± SEM) of both C6 glioma cells and H460 cells were labeled with both CTX:QD525 and DTX-1:QD655 together and independently.

Flow cytometry analyses supports microscopy qualitative and quantitative data for the blocking assays and the multiplexing experimentation examined. Both chlorotoxin and dendrotoxin-1 were able to effectively block CTX:QD525 and DTX-1:QD655, respectively, from labeling their cellular targets in C6 glioma cells.

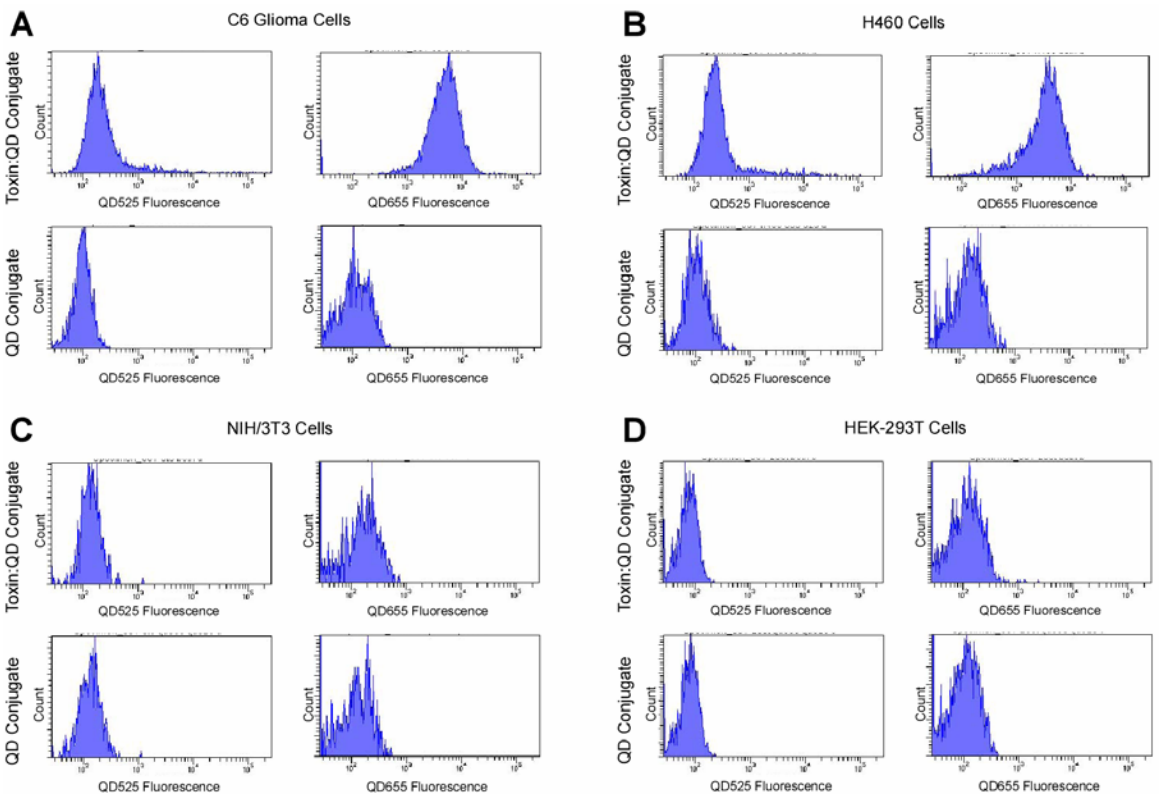

Figure 4.18: Flow cytometry histograms describing CTX:QD525 and DTX-1:QD655 detection of matrix metalloproteinase-2 and Kv1.1 potassium channels, respectively, within C6 glioma (A), H640 (B), NIH/3T3 (C), and HEK-293T (D) cell populations. Both C6 glioma (A) and H460 (B) reveal labeling of matrix metalloproteinase-2 by CTX:QD525 and Kv1.1 potassium channels by DTX-1:QD655 conjugates in their cell populations. CTX:QD525 and DTX-1:QD655 detection of matrix metalloproteinase-2 and Kv1.1 potassium channels, respectively, is less in NIH/3T3 (C) and HEK-293T (D) cells. Labeling levels in NIH/3T3 (C) and HEK-293T (D) cell lines were similar to 10nM QD525 and 5nM QD655 levels in all cell lines examined. The cells were exposed to 10nM CTX:QD525 and 5nM DTX-1:QD655 for 120 min. at 37°C and 5% CO_2.

Low percentages of labeled cells within the populations evince the efficacy of the fluorescent nanocrystal probes to detect their endogenous targets in live culture. Comparative analyses between cell lines revealed that CTX:QD525, detecting matrix metalloproteinase-2, and DTX-1:QD655, detecting Kv1.1 potassium channels, are present in higher percentages of the C6 glioma and H460 populations than in the NIH/3T3 and HEK-293T populations. This may further support the utility of these

cellular targets, when detected by quantum dot conjugates, to be indicative of altered cell states.

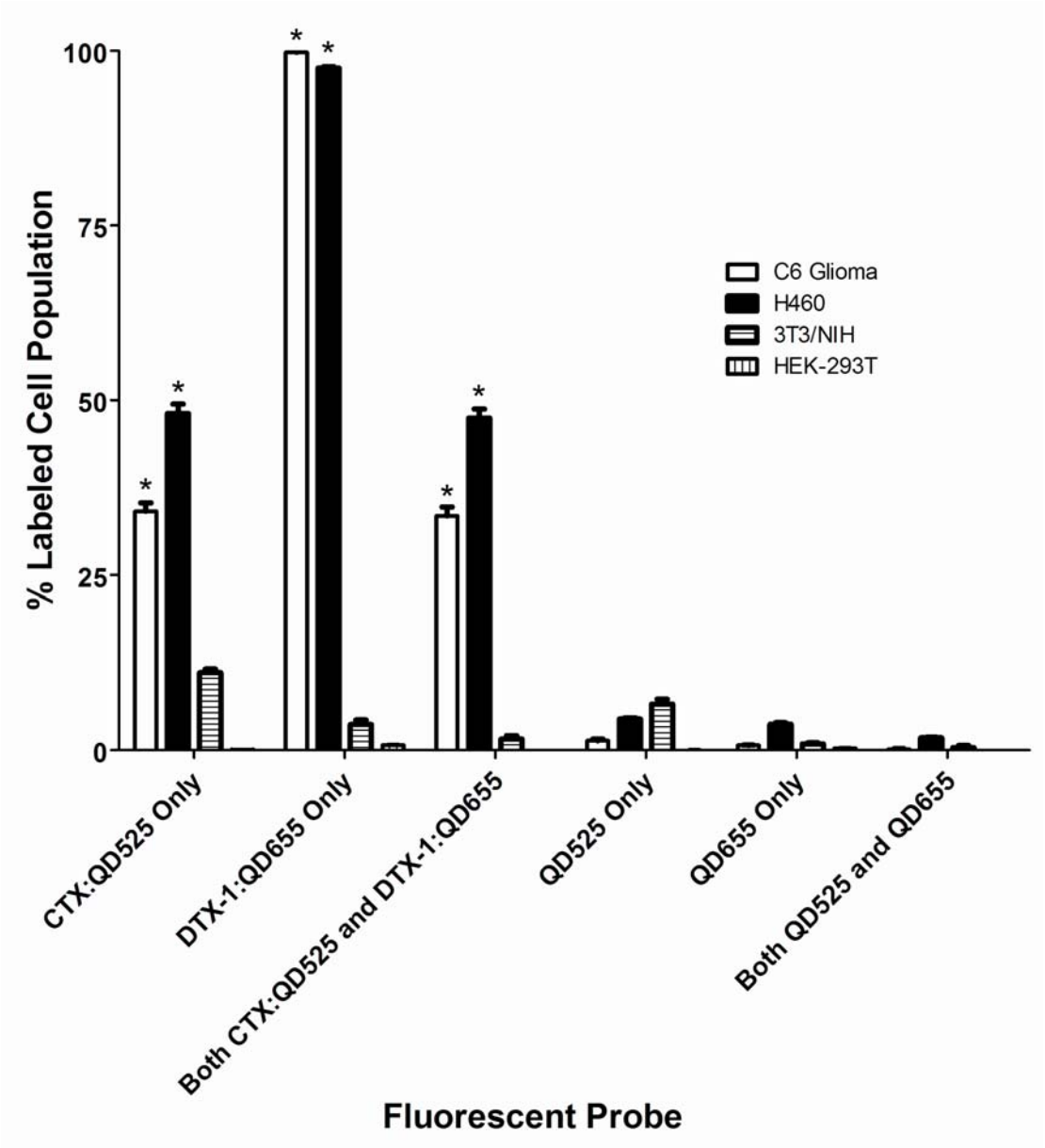

Figure 4.19: Flow cytometry analyses reveal the percentage of the cell populations labeled with both CTX:QD525 and DTX-1:QD655 together, and separately, in each cell line examined. CTX:QD525 detection of matrix metalloproteinase-2 and DTX-1:QD655 detection of Kv1.1 potassium channels in C6 glioma cells and H460 cells is statistically significant, relative to respective detection in NIH/3T3 cells and HEK-293T cells ($P<0.001$, analysis of variance, values are the means ± SEM), at 120 minutes. Each assay was run in triplicate.

4.14: Summary

Utilization of high affinity peptide neurotoxins as ligands for labeling tissue and cellular targets for quantum dot detection has been shown to be an effective means of visualizing proteins for qualitative and quantitative analyses. Quantum dots exhibit unique photophysical properties, capable of near 100% quantum yield,[7] and are resistant to photobleaching typically seen by fluorophore complements. Recently, ex vivo mouse diaphragm was successfully labeled using streptavidin quantum dot conjugates to detect native nicotinic acetylcholine receptors with biotinylated α-bungarotoxin.[57] The study demonstrated that the nanocrystals are not only able to detect biotinylated α-bungarotoxin on a post-synaptic membrane receptor ex vivo, but also capable of being highly sensitive probes in conjunction with a suitable ligand. High affinity peptide toxins provide ample means to integrate quantum dots with biological protocols to study dynamic processes in living systems.

Direct conjugation of isolated high affinity peptide toxins to quantum dots facilitates quantum dot detection of disease states in cells. Qualitative and quantitative analyses revealed that CTX:QD525 and DTX-1:QD655 labeled endogenous matrix metalloproteinase-2 and Kv1.1 potassium channels in living cells at rates of three and four times greater, respectively, in cancer versus non-cancer cells. Dynamic detection of disease state markers by high affinity peptide toxin conjugated quantum dots enables increased sensitivity, and introduces the capacity for long-term tracking in live cell culture due to quantum dot photostability. This allows for diagnostic and therapeutic development to occur utilizing real-time cell tracking, thus providing the potential for

functionality evidence within a living system not observed through static, fixed conditions.

Introduction of technological advances into biological studies enables sample archiving, live-cell tracking techniques, and multiplexing experimentation to be more productive. Quantum dot technology grants significant advantages over existing fluorescent probes in that the nanocrystals are much brighter, even in whole-mount ex vivo tissue, and are capable of detecting biologically interesting targets within living cells and at the synapse with high specificity. Continued development of endogenous cellular targeting utilizing neurotoxin quantum dot conjugates to detect disease state markers expands current quantum dot applications. Furthermore, neurotoxin nanoconjugate studies demonstrate the suitability of high affinity peptide toxins to serve as adequate ligands for targeting a broad array of cellular proteins gauged at broadening the understanding of the interplay between healthy and diseased cells with their endogenously expressed proteins.

CHAPTER V

CONCLUSIONS

It is of technological and pharmacological interest to develop methodologies that engage nanotechnology with the pursuit of biologically interesting objectives. Induction of nanotechnology toward biological applications has required the development of chemical modifications which meet the needs of the system being studied. These modifications are necessary to enable adequate binding and system compatibility. Importance, for biological labeling with nanomaterials, has been placed upon determination and classification of suitable ligands for inclusion with nanotechnology initiatives. Ligands must be of the characteristics of high target affinity, and low cross-reactivity with other biological targets present within the system of interest. Additionally, ligands must be amenable to chemical modifications that serve to promote probe detection without eliciting unwanted responses from the biology. The central focus of this research was upon the development and execution of endogenous biological target detection using fluorescent nanocrystals, commonly known as quantum dots. To detect endogenous targets in both ex vivo tissue and living cells, quantum dots were paired with high affinity peptide neurotoxins. The overall advantages to developing strategies combining the use of high affinity peptide neurotoxins with highly fluorescent nanocrystals are numerous. Some of the advantages associated with the use of peptide neurotoxins, isolated from the venom of various animal sources, for quantum dot ligands include the low propensity for cross-talk between targets and high affinity for their respective targets. These advantages were demonstrated through the research presented,

in that endogenously expressed cellular proteins were detected and quantified within ex vivo tissue and within living cells. Each of the high affinity peptide neurotoxins served as a ligand for effective quantum dot detection of the endogenously expressed target. Both the high affinity for the cellular proteins and the superior photoemission and photostability inherent in the quantum dot nanomaterial, enable visualization of biological targets in their native environment.

To establish method efficacy, a high affinity peptide neurotoxin that has been used to classify ligand-gated ion channels was used. Biotinylated α-bungarotoxin served as a ligand to facilitate streptavidin-quantum dot detection of nicotinic acetylcholine receptors (Figure 5.1). This methodology demonstrated that the biotin-(strept)avidin dual step approach is sufficient for labeling endogenous receptor expression within ex vivo tissue. Protocol development resulted in prompt detection of nicotinic acetylcholine receptor expression within unfixed mouse diaphragm tissue. Due to the superior photoemission exhibited by quantum dots, α-bungarotoxin affinity for nicotinic acetylcholine receptors was determined to be 1000-fold greater than previously reported. Quantum dot detection enabled toxin affinity to be measured against a model of a native receptor environment with unfettered endogenous expression. Additionally, quantum dots were shown to be sensitive enough to detect a ligand bound to a receptor at the post-synaptic cleft of the neuromuscular junction. This gauges the sensitivity of the nanocrystals to be great enough to distinguish targets at the synaptic cleft in ex vivo tissue. It was also determined that quantum dots are significantly brighter than their fluorophore complements; thus, supporting desirability for usage of quantum dot technology toward biological applications.

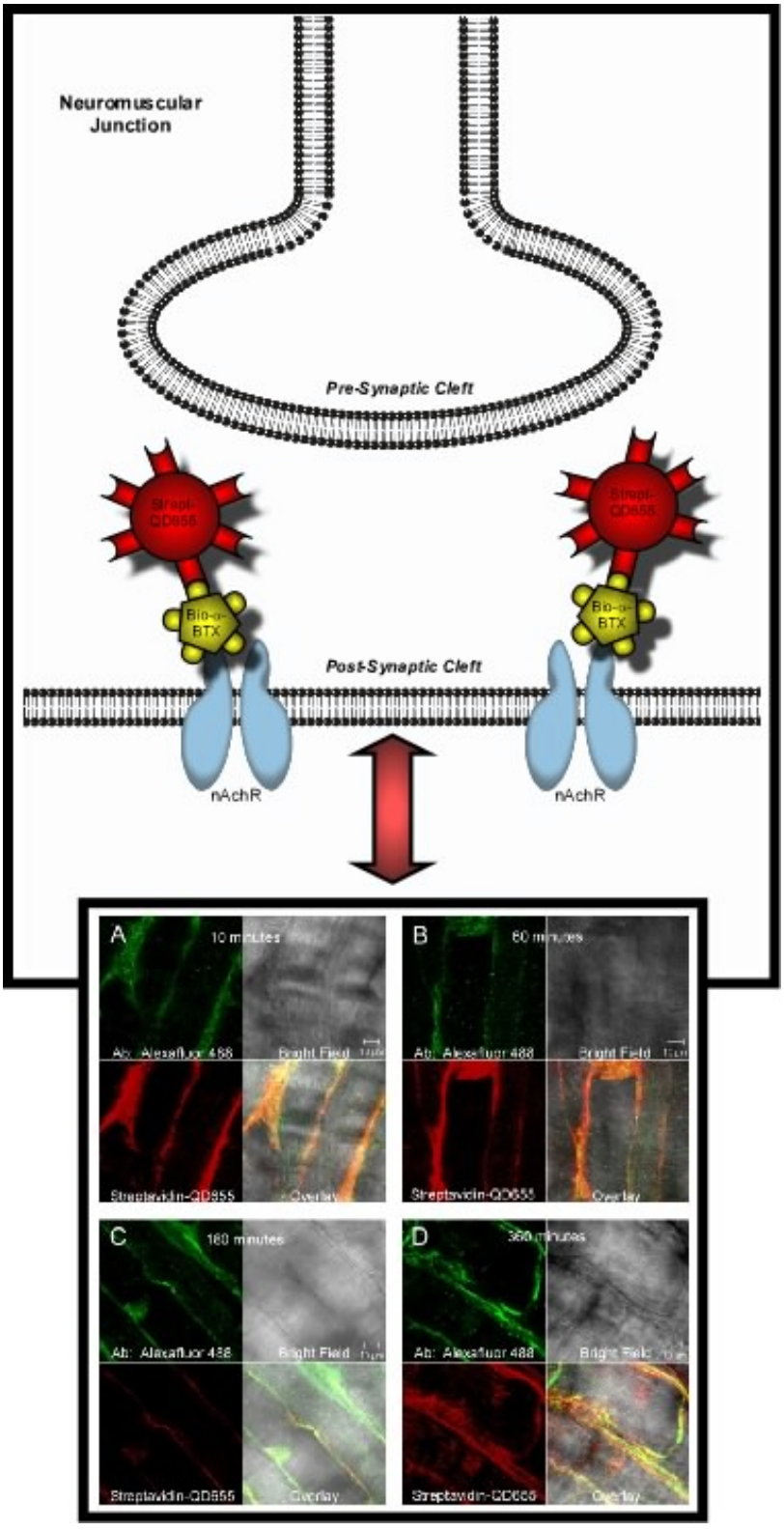

Figure 5.1: Biotinylation of the high affinity peptide neurotoxin, α-bungarotoxin, bound nicotinic acetylcholine receptors at the post-synaptic cleft of the neuromuscular junction—enabling streptavidin-linked quantum dot detection within ex vivo tissue.

Through binding analyses, native nicotinic acetylcholine receptors were shown to be capable of being blocked by biotin-free α-bungarotoxin, which prevented biotinylated α-bungarotoxin from serving as a means for streptavidin quantum dot detection. Confocal microscopy revealed that streptavidin quantum dot fluorescence was only present when diaphragm tissue was exposed to biotinylated α-bungarotoxin (Figure 5.2). Quantum dot detection was determined to be specific to native nicotinic acetylcholine receptors by analysis utilizing Alexafluor conjugated anti-β nicotinic acetylcholine receptor subunit antibody colocalization. Saturation binding analysis served as a further demonstration of quantum dot sensitivity by providing support toward α-bungarotoxin being a ligand with much greater affinity for nicotinic acetylcholine receptors than previously realized. Quantum dots were also shown to be capable of detecting biotinylated α-bungarotoxin at a series of time points, and within both fresh and seven day ex vivo tissue. Biotinylated α-bungarotoxin was able to label nicotinic acetylcholine receptors for subsequent streptavidin quantum dot detection when the ex vivo tissue was treated with blocking solution for seven days. This indicates that the protocol for usage of high affinity peptide neurotoxins with quantum dots to detect endogenous targets within ex vivo tissue is suitable for preserving the native expression of nicotinic acetylcholine receptors. Potential utilization of this methodology lends itself toward the possible incorporation of quantum dots for sample archiving. Sample archiving provides a means of tracking a disease state, as well as documenting and monitoring arrays of native protein interactions effected by various stimuli. These studies demonstrated that quantum dots are potentially well suited for such applications.

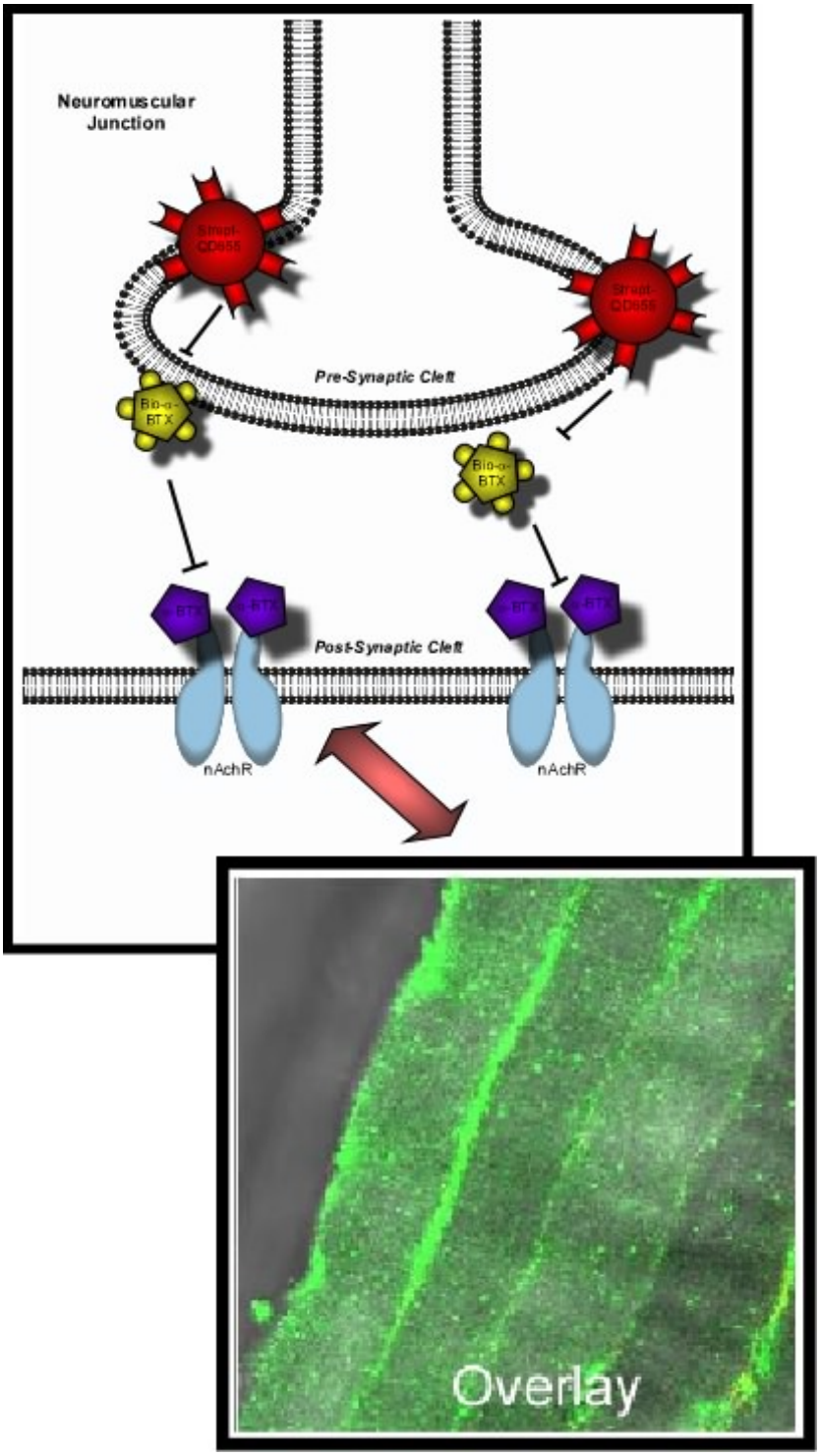

Figure 5.2: Streptavidin quantum dot detection is blocked within ex vivo diaphragm tissue due to previous exposure to α-bungarotoxin. The unconjugated α-bungarotoxin prevents biotinylated peptide from labeling nicotinic acetylcholine receptors expressed within the tissue. Because binding capacity for biotinylated α-bungarotoxin is lost, streptavidin quantum dot fluorescence is absent. The presence of the green fluorescence indicates that nicotinic acetylcholine receptors are expressed due to anti-β-subunit antibody detection.

Peptide neurotoxins were coupled with quantum dots again to demonstrate endogenous detection of multiple targets within live cells. Criteria for the neurotoxins consisted of the peptides being chosen based upon size and cellular target. The purpose of these studies was to demonstrate specificity in targeting cellular proteins within living cells using multiple quantum dot probes simultaneously. Multiplexing is a characteristic inherent in quantum dots that makes them desirable for use as biological probes. Use of multiple high affinity neurotoxin conjugated quantum dots in live cells proved to be a successful demonstration of this unique characteristic. It was not only able to be shown that endogenous cellular targets could be detected simultaneously and illuminated with a single excitation source, but also that the fluorescence could be quantified. The relative quantified fluorescence was determined to be indicative of potential markers for the presence of cancerous cells.

Initial studies using chlorotoxin followed the biotin-(strept)avidin dual step labeling methodology. Chlorotoxin was biotinylated, exposed to C6 glioma cells, and labeled with streptavidin quantum dots. Although evidence supported that this is a viable strategy for detecting chlorotoxin's cellular target, matrix metalloproteinase-2, it was deduced that dual labeling approaches were not well suited for use with multiple probes. It was determined that production of novel toxin:quantum dot conjugates was likely to be the best strategy for achieving dual detection of two independent endogenous cellular targets and visualization using quantum dot multiplexing properties. To achieve this, both chlorotoxin (Figure 5.3) and dendrotoxin-1 (Figure 5.4) were coupled to quantum dots of different emission spectra. High affinity peptide neurotoxin conjugation was achieved using 2-iminothiolane (Traut's reagent) and N-succinimidyl iodoacetate (SIA)

as cross-linking reagents with polyethylene amino terminated quantum dots. Each neurotoxin was conjugated to a specific size dot, and thus correlated to a specific emission color when visualized.

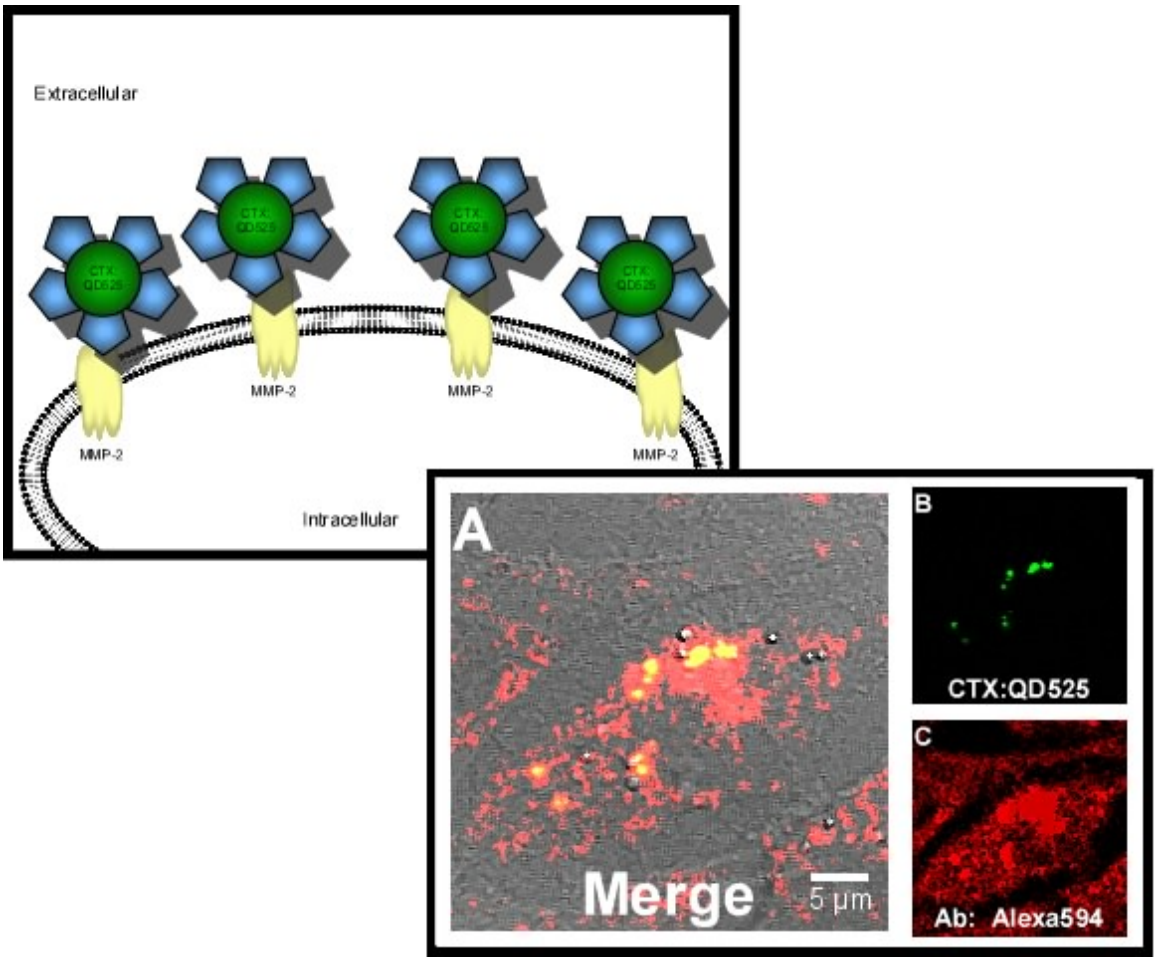

Figure 5.3: Chlorotoxin conjugated quantum dots (525s) bind to matrix metalloproteinase-2 (MMP-2) within live C6 glioma cells.

Both conjugates were tested, independently, within C6 glioma cells for specificity using Alexafluor conjugated target antibodies. Each toxin:quantum dot conjugate target detection was also shown to capable of being blocked within living cells for a period of

time when the cells were exposed previously to unconjugated neurotoxin. This further substantiated the specificity that the nanomaterials maintain for their targets, but also supported the suitability of high affinity peptide neurotoxins to serve as ligands.

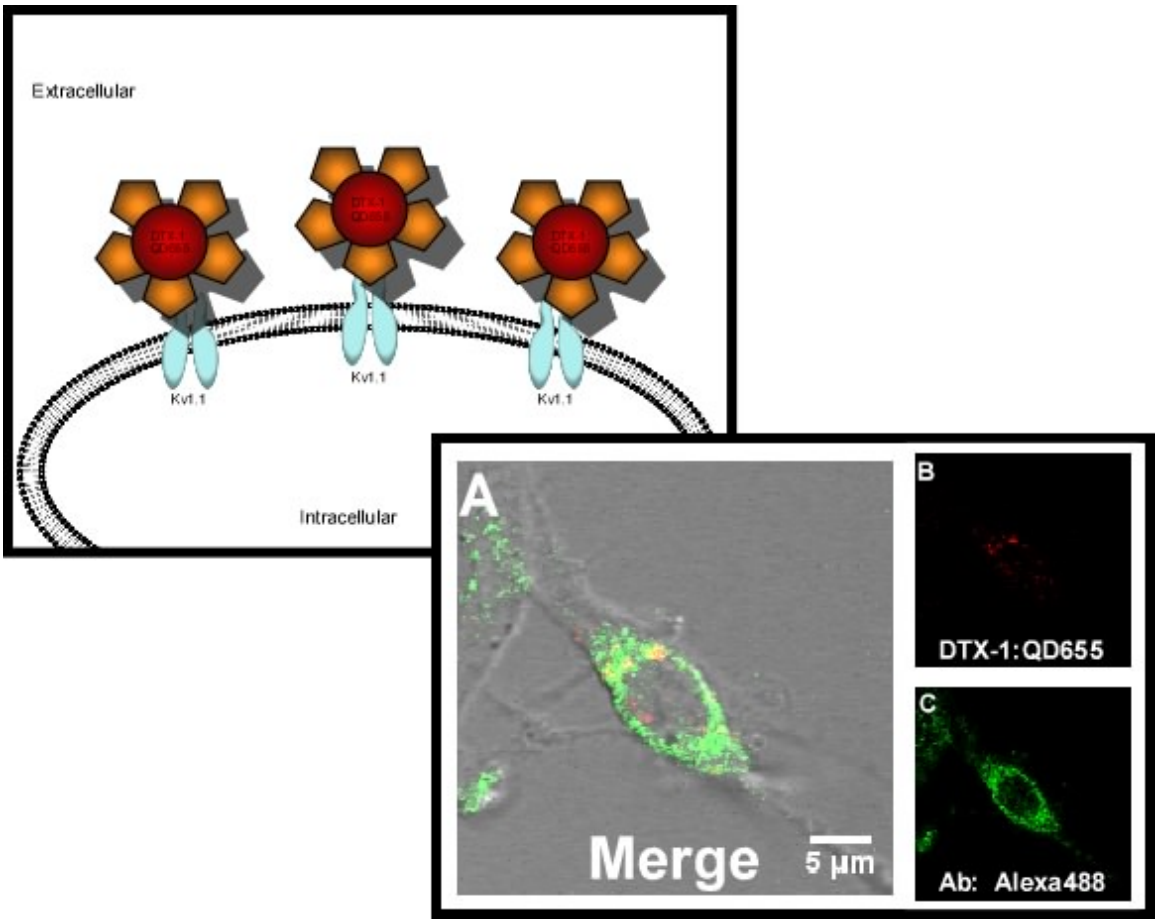

Figure 5.4: Dendrotoxin-1 conjugated quantum dots (655s) bind to voltage-gated potassium channels 1.1 (Kv1.1) in live C6 glioma cells.

There was no evidence of cross-talk between different targets, and no evidence of non-specific binding within living cells for up to two hours for chlorotoxin and three hours for dendrotoxin-1 of continuous exposure at cell maintenance conditions (Figure 5.5). Each toxin's affinity was measured using confocal microscopy through quantification of

quantum dot fluorescence. The affinity was determined using microscopy within a living cell environment, and thus reflects the affinity the toxin and toxin:quantum dot conjugates exhibit for the respective targets.

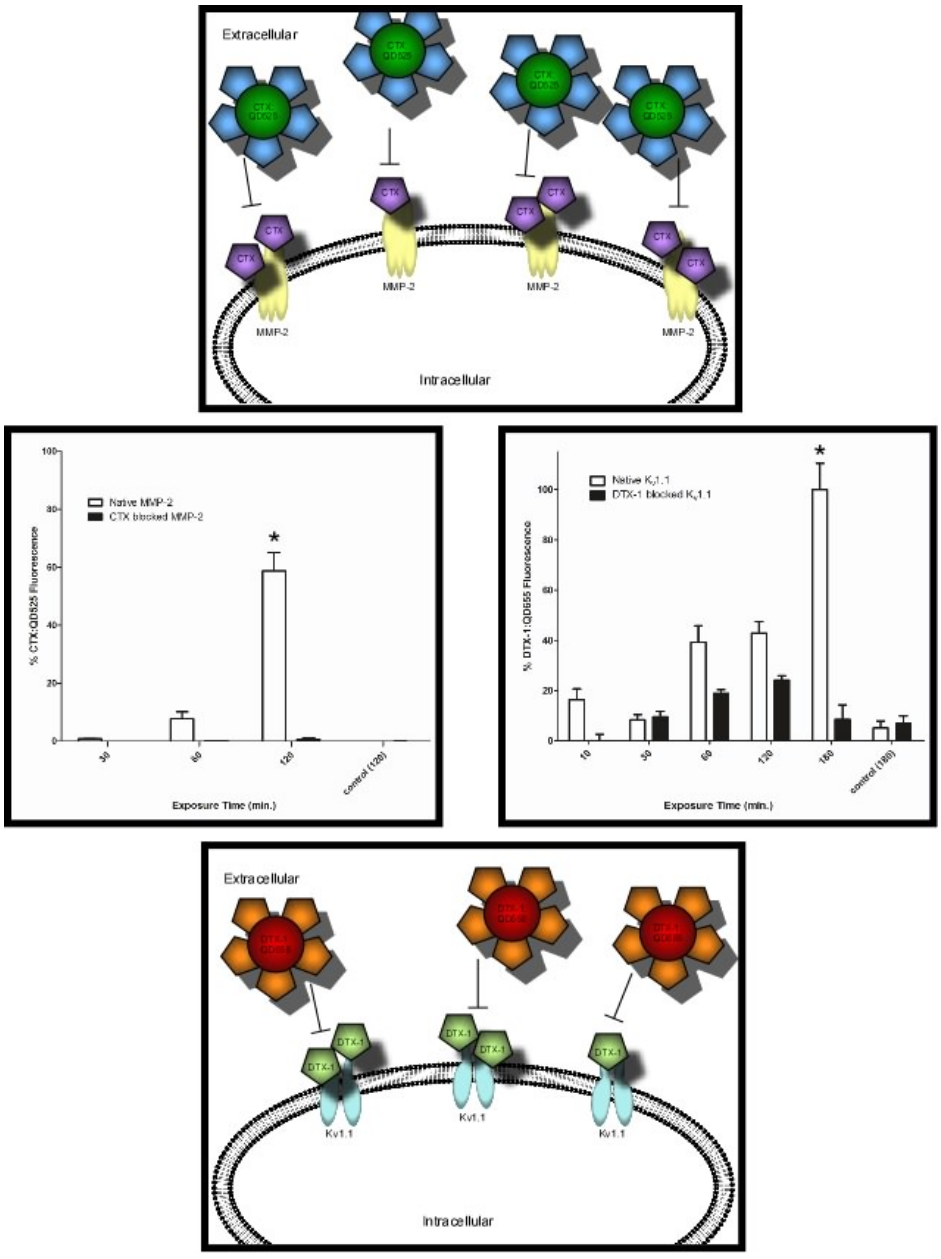

Figure 5.5: Both chlorotoxin and dendrotoxin-1 block free binding sites within live C6 glioma cell cultures. Consequently, the ability for both chlorotoxin quantum dot conjugates (CTX:QD525s) and dendrotoxin-1 quantum dot conjugates (DTX-1:QD655s) to detect their targets is effectively inhibited.

To demonstrate quantum dot multiplexing, C6 glioma cells were incubated with both chlorotoxin:quantum dot conjugates and dendrotoxin-1:quantum dot conjugates simultaneously (Figure 5.6).

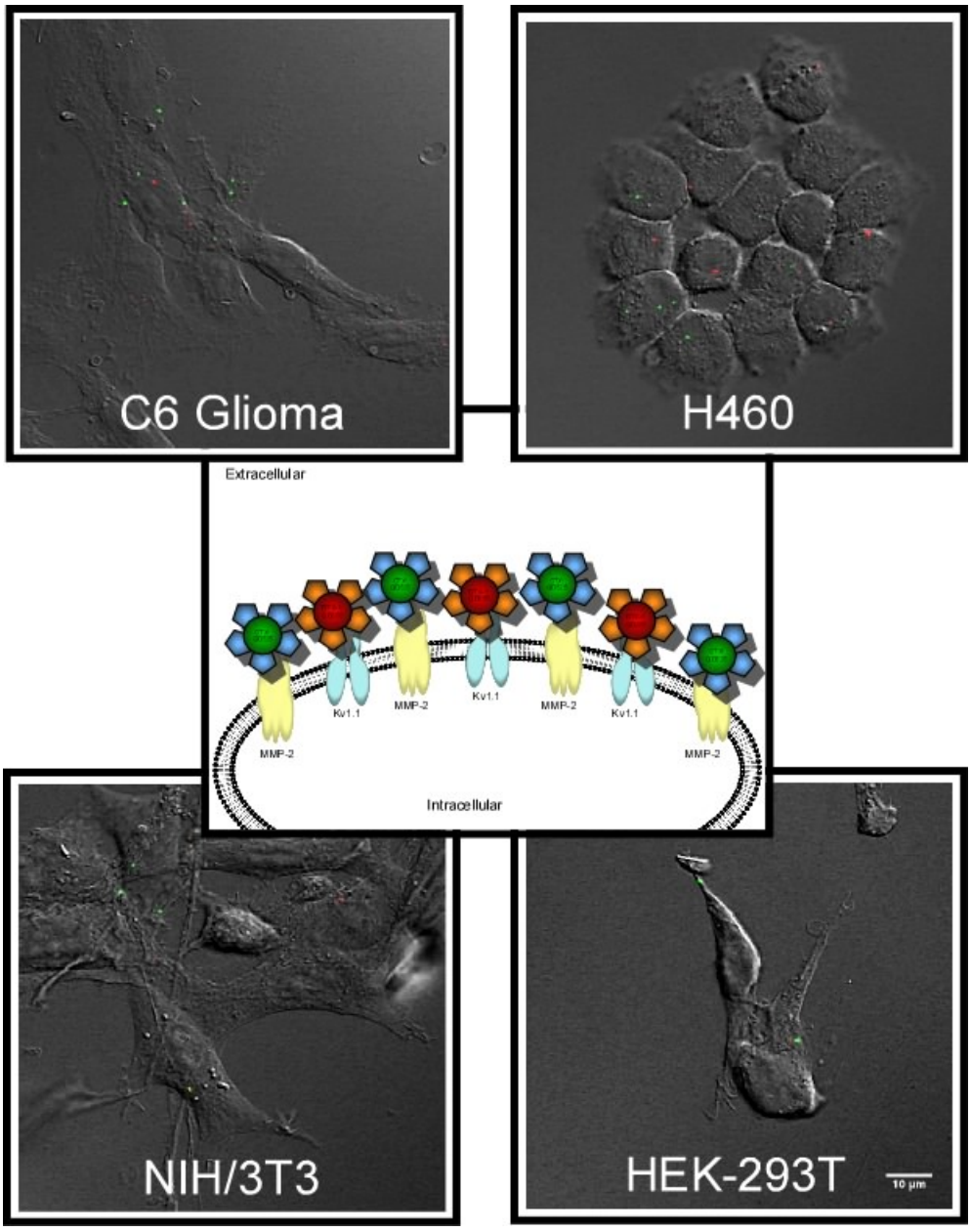

Figure 5.6: Multiplexing experimentation visually reveals that matrix metalloproteinase-2 (MMP-2) and voltage-gated potassium channels 1.1 (Kv1.1) appear to be expressed in higher concentrations within cancer cells (rat C6 glioma and human Lewis lung carcinoma, H460) than in non-cancer cells (mouse 3T3/NIH and human embryonic kidney, HEK-293T).

These studies revealed punctuate labeling from each toxin:quantum dot conjugate emanating from a single excitation source. Because chlorotoxin is reported to have increased activity associated with glioma cells, additional cell types were examined to compare endogenous expression levels of matrix metalloproteinase-2 and Kv1.1 within each representative cell line. The cells chosen were human and rodent cell lines. The human lines were H460, a Lewis lung carcinoma; and, HEK-293T, human embryonic kidney cells. The additional rodent line was a normal cell line, 3T3/NIH, which is a mouse embryonic kidney cell line. The results indicate that both toxin:quantum dot conjugates are sensitive enough to detect endogenous expression within cell lines other than C6 rat glioma cells. They also indicate that endogenous expression varies between cancerous and normal cells. Both expressions, matrix metalloproteinase-2 and Kv1.1, are detected in statistically significant higher percentages in cancer cells than in normal cells. This may indicate that matrix metalloproteinase-2 and Kv1.1 are potential markers that may be detected rapidly for identification of cancer cells within culture. Further development and analyses utilizing these toxin:quantum dot probes may serve to aid in future methodologies to understand cancer or abnormal cell behaviors.

Advantages to incorporating high affinity peptide neurotoxins with nanotechnology initiatives include real-time monitoring of biological targets (Figure 5.7). Huganir and coworkers demonstrated the use of the α-bungarotoxin binding site as a means of tagging cellular proteins that lack adequate ligands for analysis. The idea that high affinity peptide neurotoxin binding domains may serve as ubiquitous tags for poorly understood proteins lends itself to nanotechnology incorporation. Not only does α-bungarotoxin serve as an adequate ligand for quantum dot detection, but also chlorotoxin

and dendrotoxin-1 are revealed to be suitable for quantum dot detection of endogenous cellular proteins.

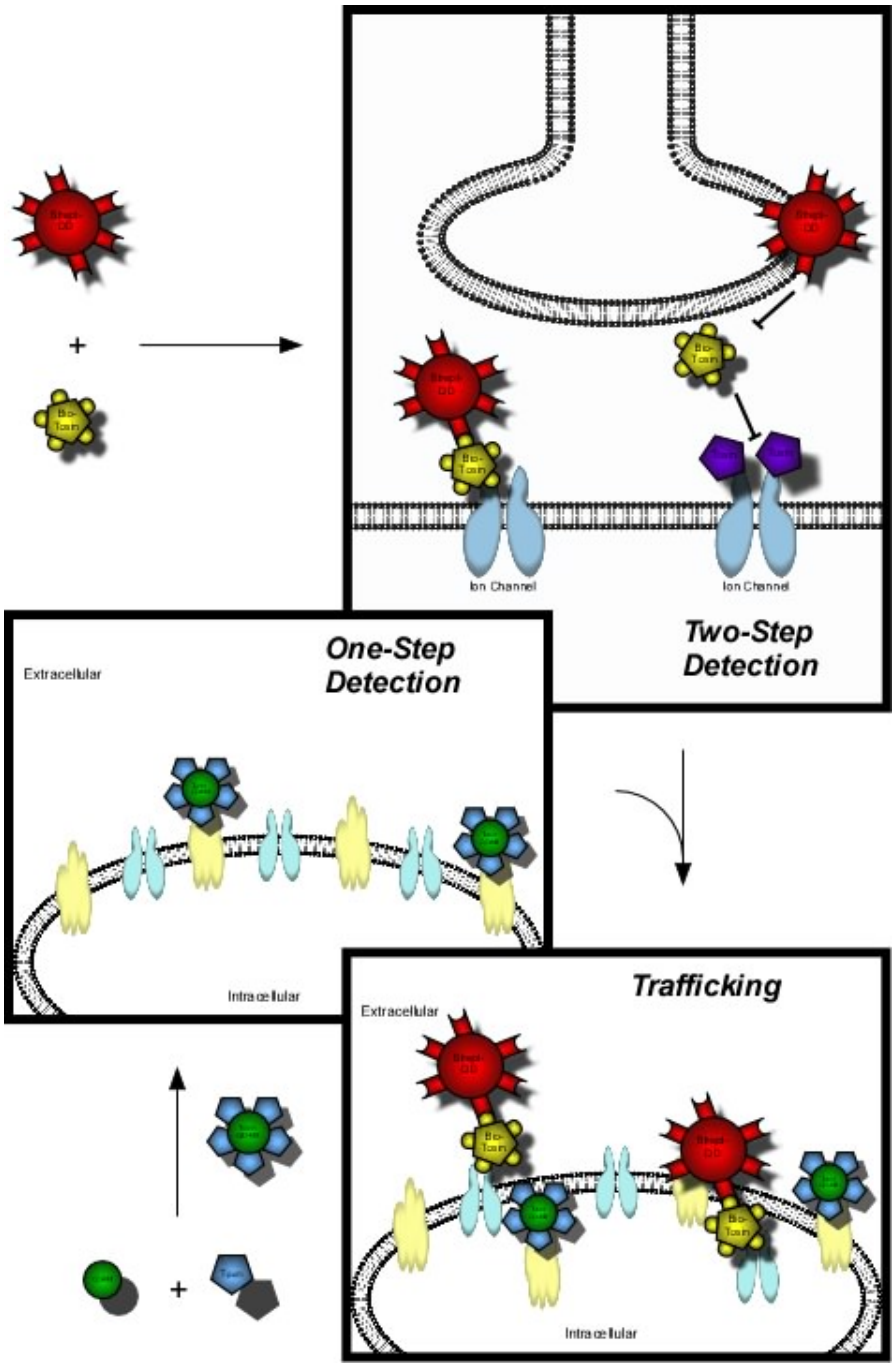

Figure 5.7: Two methodologies for quantum dot detection of endogenous biological targets. Each method has the potential to further biological understanding through high affinity detection leading to trafficking studies.

Quantum dot detection was achieved in live cells using three separate peptide neurotoxins, isolated from different venom sources, conjugated to nanocrystals. Two probe methodologies were employed that enabled quantum dot detection: (1) direct peptide conjugation to quantum dots, and (2) streptavidin-quantum dot labeling of biotinylated ligand. Both methodologies were amenable to quantitation in addition to qualitative analyses. These studies provide evidence to support the universality of high affinity peptide neurotoxins to serve as viable ligands for utilization as components of nanomaterials.

The applications for such nanomaterials are numerous. There is significant emphasis that has been placed upon the use natural products for research and therapeutic purposes. Both organic products and isolated peptides possess the potential to be used to treat a variety of conditions. When coupled with nanotechnology, they may also be used to study biological targets in real-time. Such information provides a better understanding of the environment that influences the protein under examination. A better understanding affords the capacity to possibly design more efficient therapies for a multitude of conditions. Future studies using these peptides may include in vivo monitoring and tracking of multiple isolated peptide neurotoxins coupled to quantum dots. These data will provide information relating the nature of the biological response to the presence of each peptide. Disruption of cellular processes due to bound neurotoxin quantum dot conjugates enables monitoring of both the neurotoxin blocked target and additional targets present in the biological system being investigated. General disruption to a biological system bestows a plethora of information regarding the balance each component has in maintaining the functionality of the system. The photostability

characteristic of quantum dots enables these induced imbalances to be monitored for extended periods of time, thus affording knowledge of the system previously unseen. Quantum dots may also serve as a means of monitoring delivery of a therapeutic molecule. During initial phases of development, therapeutic molecules may be attached to quantum dots to assess delivery efficacy through fluorescence monitoring. This methodology provides the advantage of visualizing the presence of molecules targeting specific cell types within an array of differentiated cells in vivo. Additional studies using quantum dots as both detection probes, as well as delivery vehicles, will further nanotechnology toward biological purposes.

Future studies using high affinity peptide neurotoxins as ligands for nanocrystal visualization have the potential to span a variety of disciplines. Quantum dots have been shown to be versatile for biological labeling. Expansion of nanocrystal technology into biological research will include monitoring in vivo. In vivo monitoring will allow tracking of responses to stimuli in real-time, making nanotechnology a critical tool for endeavors examining the basic principles governing a biological system. Because many cellular proteins are without ligands, either endogenous or exogenous, that are capable of being used for fluorescence assessment, the binding domain for peptide neurotoxins may be genetically incorporated into the protein being studied. By creating a fusion of the binding site of a high affinity peptide neurotoxin with a protein of interest, the cellular target may potentially being examined using fluorescence microscopy. This was demonstrated previously by Huganir and colleagues who fused the α-bungarotoxin binding site to the N-terminus of glutamate receptor-2 neural protein. Their work demonstrated the potential for using peptide binding sequences as ubiquitous regions for

fluorescence tagging and visualization. These studies, demonstrating the multiplicity of quantum dots for these purposes by detecting three different high affinity peptide neurotoxins seeking endogenous targets, reveal the suitability of applying this technology to sensitive biological targeting schemes. Quantum dots exhibit superior photostability to common fluorophores, thereby permitting longer monitoring capacity than their fluorescent counterparts. The nanocrystals may provide information regarding cellular responses and native behaviors that previous technology has failed to currently provide.

Quantum dot detection within biological systems is effectively mediated by the use of high affinity peptide neurotoxins. Peptide neurotoxins serve as suitable ligands to facilitate the utilization and advancement of quantum dots as probes for various biological studies. Advancement of quantum dot technology for biology incorporation with nanotechnology mitigates the advancement of nanotechnology toward potential uses as weapons against disease through rapid detection and therapy delivery. These studies have demonstrated the versatility of fluorescent semiconductor nanocrystals as detection probes through conjugation with multiple high affinity peptide neurotoxins. These nanoconjugates were shown to be sensitive enough to detect endogenous receptors at the post-synaptic cleft of the neuromuscular junction in ex vivo tissue, and proteins expressed within living cells. Further development will yield an arsenal of probes that represent a new class of tagging devices capable of examining living biology from a renewed perspective.

APPENDIX

COMPUTATIONS FOR MASS SPECTROMETRY

A.1: Introduction

Computational support was performed to examine the correlation between bond energies and MALDI-TOF/TOF CID fragmentation patterns of organic polymers. The general methodology entailed determining a representative monomeric portion of the polymer to represent the large molecule. The first polymeric system examined was polystyrene. Following polystyrene, calculations on polystyrene derivatives, poly(α-methylstyrene), poly(t-butylstyrene), and poly-(4-methyl)-styrene, were performed. Some additional calculations were prepared, and some performed examining poly-aramid structures. These included polymers labeled: PBO, PBO-amide, PPD-T, and MP-amide. The calculations followed the general methodology outlined in Figure A.1.

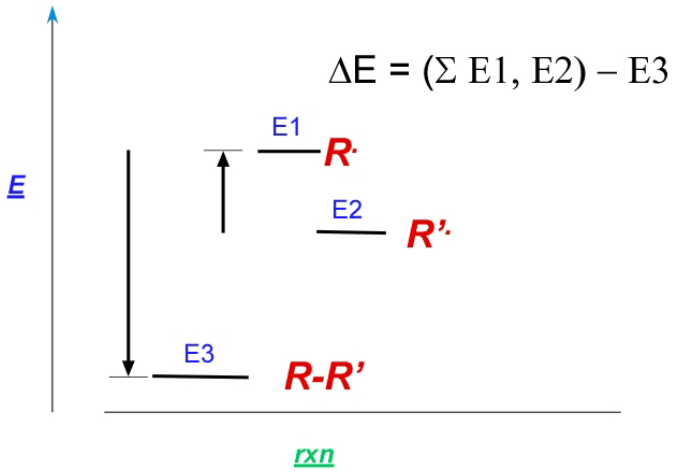

Figure A.1: Calculation diagram representing general methodology utilized for organic polymer bond energy calculations. All computations were performed using the Gaussian3.0 computation suite, and GaussView3.09 and GaussView4.0 for model building.

A.2: Computation Methods

Polystyrene models were built using GaussView3.09. Fragmentation was simulated by homolytic bond cleavage of the parent structure. The fragments were moved approximately 15Å apart in space. Optimization was performed using the ONIOM feature of Gaussian03 program package.[118] Optimization about the carbon radical was performed using DFT/B3LYP[119, 120]/6-31G* level of theory. The remaining portions of the fragments were optimized using DFT/B3LYP/STO-3G* level of theory. Overall multiplicity for systems calculated with both fragments present was determined to be of triplet character. For systems independently calculated for each fragment, multiplicity was determined to be of doublet character. Following optimization, single-point energy calculations were performed, assuming a single layer for the system, using DFT/B3LYP/6-31G* level of theory. Additional calculations were performed using DFT/B3LYP/6-31G* theory for both the triplet and doublet systems without the layering. All computations were performed *in vacuo* at the ground state.

A.3: Polystyrene Summary of Experimental Results

In support of experimental results, we performed calculations using Gaussian03, following model building in GaussView3.09. The parent structure was optimized using DFT/B3LYP/6-31G* level of theory (Figure A.2). To simulate fragmentation, the bond of interest was broken. We performed a series of calculation types to mimic homolytic cleavage. The first series of calculations involved bond cleavage followed by movement of the fragments to approximately 15Å apart, designated as Triplet (Table A.1). Each new system was determined to have triplet multiplicity. Additionally, each fragment was

calculated independently and given doublet multiplicity (Doublet, Table A.1). This series of calculations was determined using DFT/B3LYP/6-31G* theory.

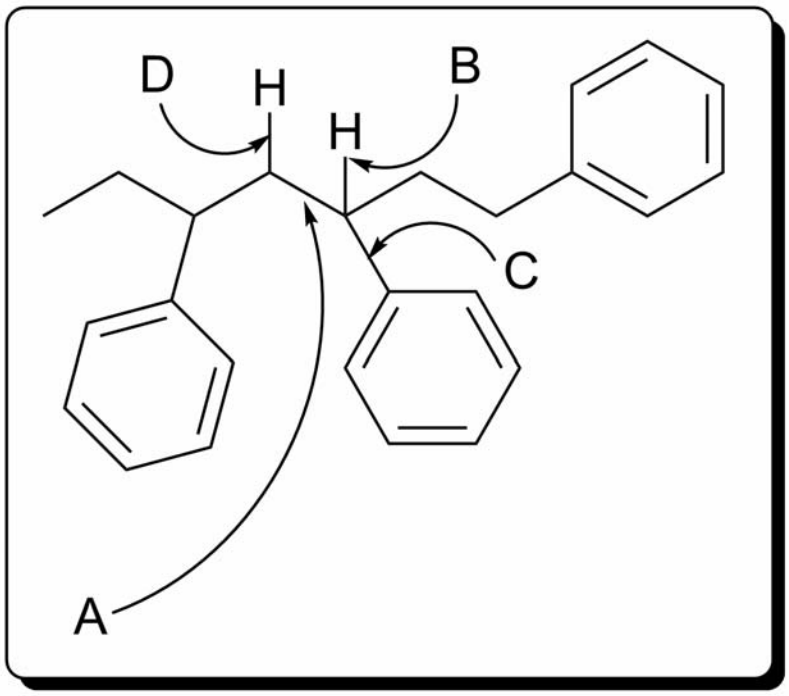

Figure A.2: Polystyrene fragment used to determine atomization energies for specified bonds.

Another set of calculations sought to determine whether the carbon radical geometry affected the energy difference between the fragments and the parent molecule. To achieve this, we layered the molecules within the calculations using the ONIOM feature of Gaussian03. Each carbon radical was optimized using DFT/B3LYP/6-31G*, and the remainder of the molecule was optimized using DFT/B3LYP/STO-3G* level of theory. The experimental protocol described previously was repeated.

Table A.1: Calculated atomization values using DFT/B3LYP/6-31G* level of theory in Gaussian03 for polystyrene. All triplet calculations were performed with the fragments approximately 15Å apart. Values are in kcal/mol.[121]

Calculation	A	B	C	D
Doublet	71.87	91.66	96.21	103.69
ONIOM Layered Doublet	77.22	106.53	96.21	103.76
Triplet	98.97	108.30	109.55	110.46
ONIOM Layered Triplet	77.55	107.90	100.65	108.31

Overall, the values obtained from the layered experimental method were higher than expected (Table A.1). It is possible that this is in part due to the global minimum failing to be found on account of differences in the level of theory between the layers used in the calculation. It is also noted that the calculations inclusive of both fragments, and designated as triplet systems, yielded atomization values much higher than anticipated from experimentation. This further supports the values obtained from the doublet calculations. The doublets determined using DFT/B3LYP/6-31G* are representative of the minimum of each fragment upon cleavage.

A.4: Results for Polystyrene Derivatives

The doublet calculation method was repeated for derivatives of polystyrene—poly(α-methylstyrene),[122] poly(*t*-butylstyrene) and poly(4-methylstyrene)[123]. The calculations for poly(*t*-butylstyrene) and poly(4-methylstyrene) were performed based upon the representative molecule in Figure A.3.

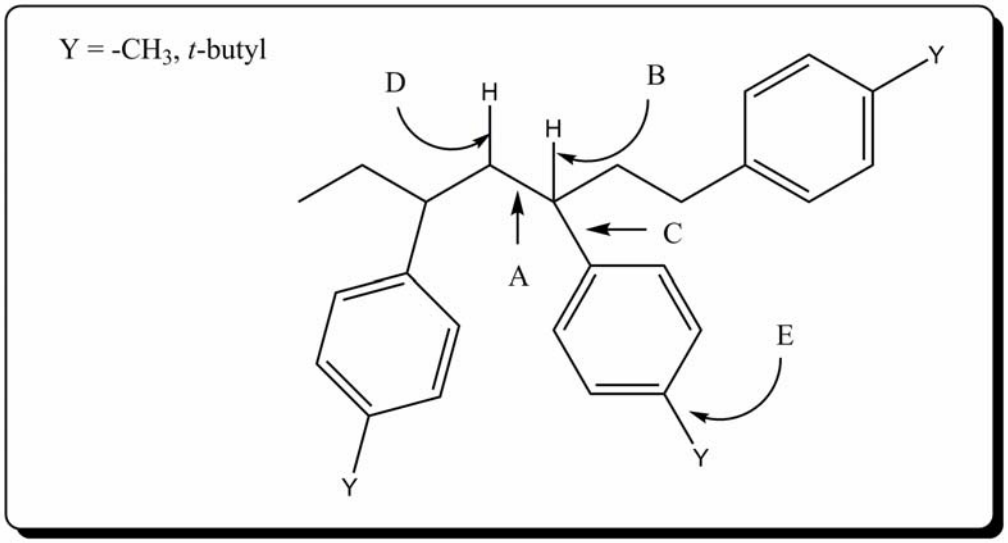

Figure A.3: Polystyrene derivative fragments used to calculate energies of the indicated bonds.

These calculations yielded values for the specified bonds reflected in Table A.2. Fragmentation patterns were consistent with theoretical values, and indicated that dominant fragmentation occurred at the carbon backbone bond (Figure A.3, bond A).

Table A.2: Polystyrene and polystyrene derivatives calculated values for specified bonds. Computations reflect density functional theory methods: B3LYP/6-31G* level of theory. All values are in kcal/mol.[123]

Calculation	A	B	C	D	E
Polystyrene	71.87	91.66	96.21	103.69	117.17
Poly(4-methylstyrene)	71.61	91.42	96.47	103.72	105.13
Poly(*t*-butylstyrene)	71.64	91.20	96.64	103.72	90.65

Additionally, calculated values were consistent between polystyrene derivatives. The bond values were reflective of the fragmentation patterns observed through mass spectrometry experimentation on the full length polymer. The largest variance between values was observed at bond "E" where the bond reflected the loss of either H, $-CH_3$, or *t*-butyl functional groups, with the most favored loss being that of the *t*-butyl moiety.

Intuitive chemical analysis indicates that this is most likely the result of the *t*-butyl group, as a tertiary carbon radical, having the capacity to stabilize the free radical to a greater extent compared with the primary carbon and hydrogen groups. This indicates that the *t*-butyl functional group is favored for fragmentation, relative to the methyl and hydrogen.

Another polystyrene derivative, poly(α-methylstyrene), was analyzed under the similar conditions. The model molecule used for the calculations is illustrated in Figure A.4. This model varies from the previous polymeric molecules by the presence of the methyl group bound to the α-carbon, which additionally has a phenyl substituent.

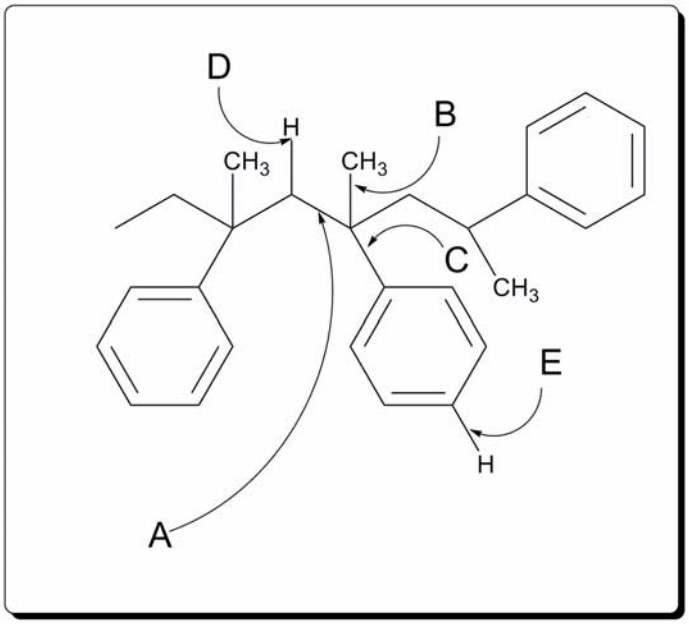

Figure A.4: Poly(α-methylstyrene) representative molecule used for DFT calculations.

The electronic influence that the methyl group imposes upon the chain is reflected in the values obtained from the density functional theory calculations (Table A.3). The values indicate that the α-methyl contributes to the reduction in the bond energy. The

1,2-phenyl shift reaction was also examined using computational methods to predict the relative bond stability and fragmentation probability (Figure A.5).

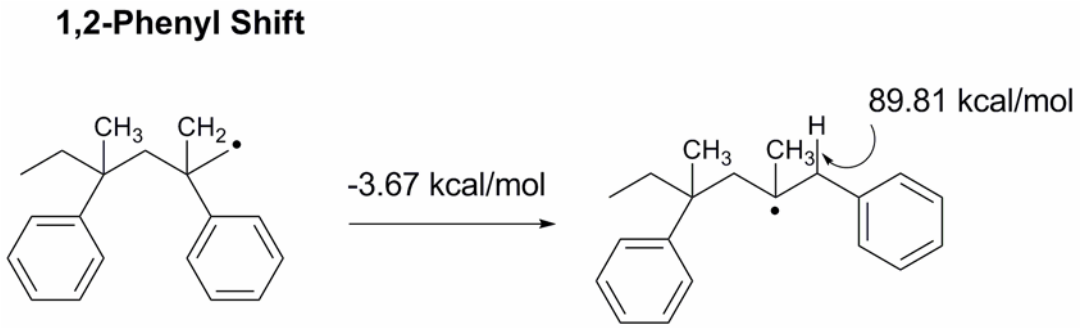

Figure A.5: Representation of the 1,2-phenyl shift reaction observed during poly(α-methylstyrene) fragmentation. The reaction results in the rearrangement of the phenyl substituent on the alkyl backbone, which results in the stabilization of the free radical.

The theoretical results predicted that the shift resulted in a tertiary free radical that was more stable than the initial primary free radical. The monomer reversion reaction (Figure A.6) was also analyzed to assess the likelihood that this reaction plays an important role within these systems.

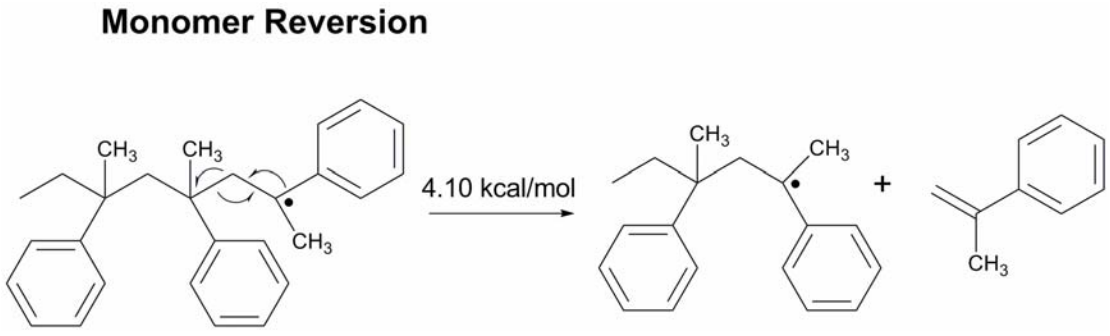

Figure A.6: Monomer reversion reaction for poly(α-methylstyrene). The reaction results in the formation of a tertiary free radical and an alkene species.

The values obtained from the density functional theory calculations agree with expectations and experimental values (Table A.3). Additionally, calculated values for both polystyrene and poly(α-methylstyrene) (Table A.3) follow similar cleavage patterns, which is indicative of resonance stabilization due to both phenyl substitution along the alkyl backbone and also within the phenyl rings. As observed previously, the methylene hydrogen is predicted to undergo homolytic cleavage to a lesser extent due to its higher calculated bond energy (Site D, Figure A.4) relative to carbon backbone cleavage (Site A, Figure A.4). The determined theoretical values are also supportive of known radical stability trends, such that lower energies were observed where cleavages resulted in tertiary radicals, and higher energies were observed where cleavages resulted in primary or alkyl radicals. This theoretical trend additionally substantiates the interpretation of relative fragment populations obtained through MALDI-TOF/TOF CID spectra.

Table A.3: Poly(α-methylstyrene) and polystyrene calculated values for specified bonds and reactions. Computations reflect density functional theory methods: B3LYP/6-31G* level of theory. All values are in kcal/mol.[122]

Calculation	A	B	C	D	E	1,2 Phenyl Shift	Monomer Reversion
Polystyrene	71.87	91.66	96.21	103.69	117.17	*N/A*	17.13
Poly(α-methylstyrene)	56.68	81.87	67.68	101.52	89.81	-3.76	4.10

Values obtained for poly(α-methylstyrene) versus polystyrene show significant differences in energy (Table A.3). Sites A-C (Figure A.4) on poly(α-methylstyrene) are predicted to have much lower bond energy values than equivalent sites on its parent polymer, polystyrene, which further indicates fragmentation pattern variance due to radical stabilization. It is noted that the poly(α-methylstyrene) phenyl loss (Site C, Table

A.3) is predicted to have a relative bond energy value approximately 29 kcal/mol less than that bond cleavage site for polystyrene. This is attributed to the additional stabilization for the formed radical along the alkyl backbone; the methyl substituent at Site C aids in stabilizing the delocalized free radical formed in the fragmentation process.

Additionally, computations indicate the alkyl backbone (Site A, Table A.3) is expected to present more fragmentation in poly(α-methylstyrene) than polystyrene. Methyl substitutions contribute to this by allowing for tertiary radical formation either directly through the bond cleavage process or resonance delocalization with the neighboring phenyl ring. Based on theoretical predictions presented in Table A.3, the methyl substitutions on poly(α-methylstyrene) add significant stability to radical formation along sites on the polymer; thereby, allowing for site specific fragmentation more readily than that seen with polystyrene.

A.5: PPD-T, MP-Amide, PBO, and PBO-Amide

Cation influence on fragmentation patterns was examined for various industrial polymers. All models were built using GaussView4.0, and all computations were executed using the Gaussian3.0 suite of programs. Calculations were performed using density functional theory methods employing the B3LYP/6-31G* level of theory. Because the B3LYP basis set includes only elements up to sodium, Na^+ was substituted for Ag^+ within the calculations. This was agreed to be a reasonable substitution in order to maintain consistency between molecules and previous calculations.

Initial calculations for PPD-T and MP-Amide did not include Na^+ within the model design. Figure A.7 provides the structures of both representative molecules for the polymers.

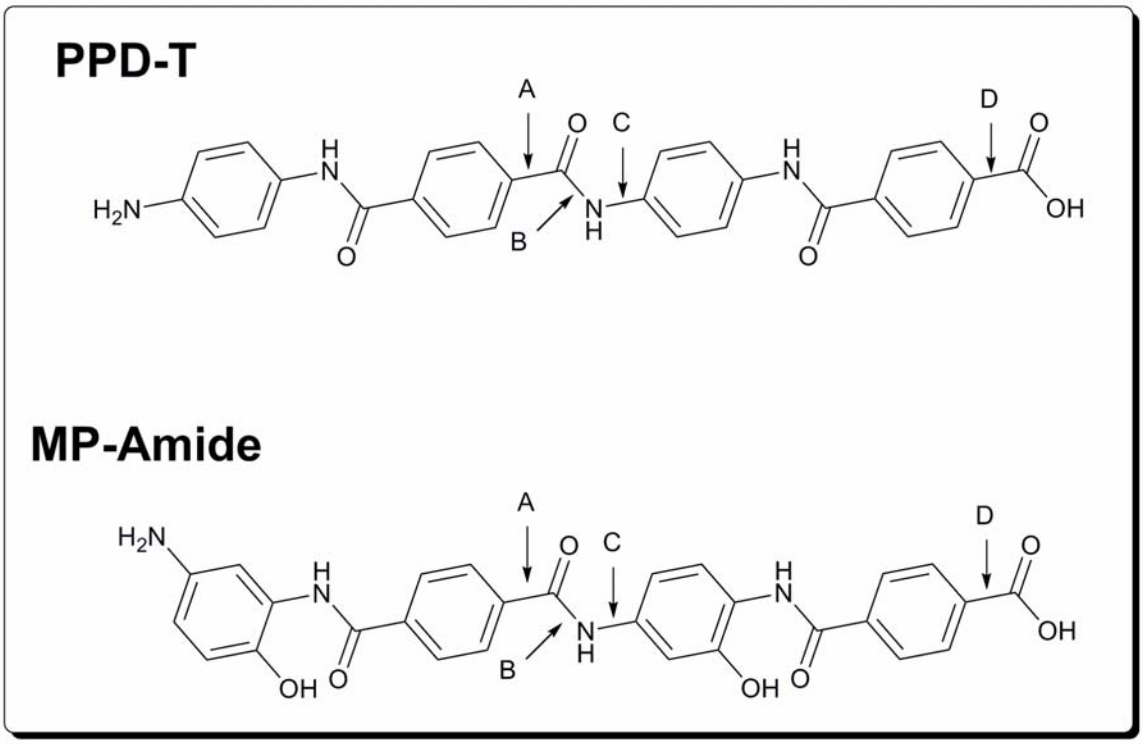

Figure A.7: Model molecules for PPD-T and MP-Amide industrial polymers. Labeled arrows indicate sites examined for potential fragmentation points along the length of the molecule.

The computation results are outlined in Table A.4. The values indicate that Site B will be the site of most frequent fragmentation because of its lower predicted atomization energy.

Table A.4: Initial calculated values of the bonds specified for representative PPD-T and MP-Amide structures. All values were obtained using DFT/B3LYP/6-31G* theory, and are in kcal/mol.

Calculation	A	B	C	D
PPD-T	95.786	76.979	103.449	107.683
MP-Amide	95.275	63.143	102.420	110.204

Following initial calculations performed based upon these models, additional models were built for computations focusing around the influence of Na^+ on the fragmentation potential of the chains. The models for PPD-T with Na^+ are outlined in Figure A.8.

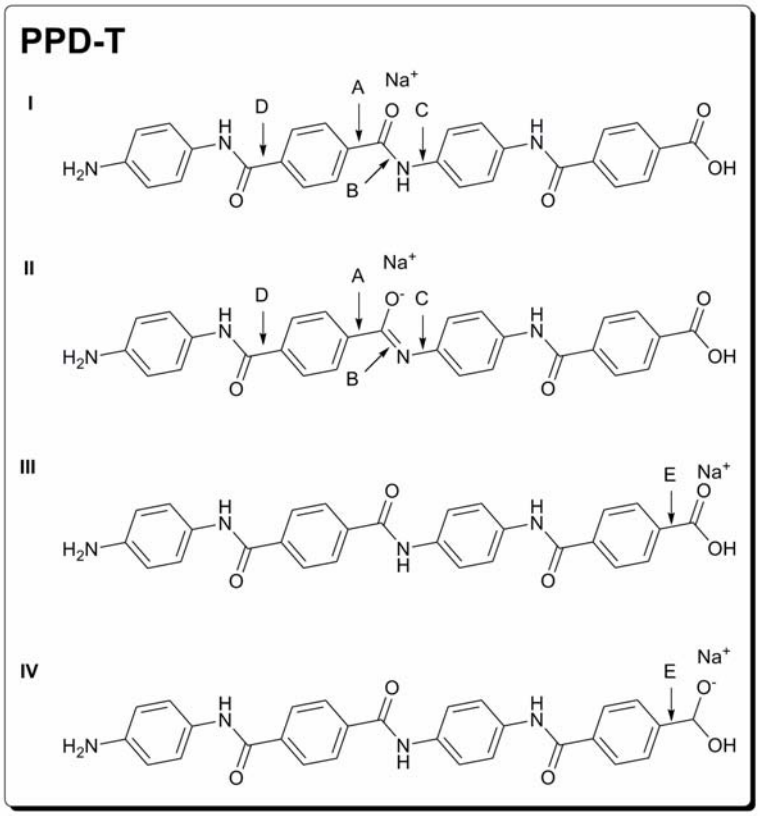

Figure A.8: PPD-T structures for calculations to determine the cationic influence on fragmentation.

These models differ through both the fragmentation sites examined, and also the placement of Na^+ associated with the amide and terminal carboxylic acid oxygen species. These should yield results indicative of the preferred cleavage point within the polymer backbone.

In relation to the MP-Amide species previously examined through computation, models for a cation influenced homolytic cleavage were built. Figure A.9 reflects the MP-Amide structures built for computational studies.

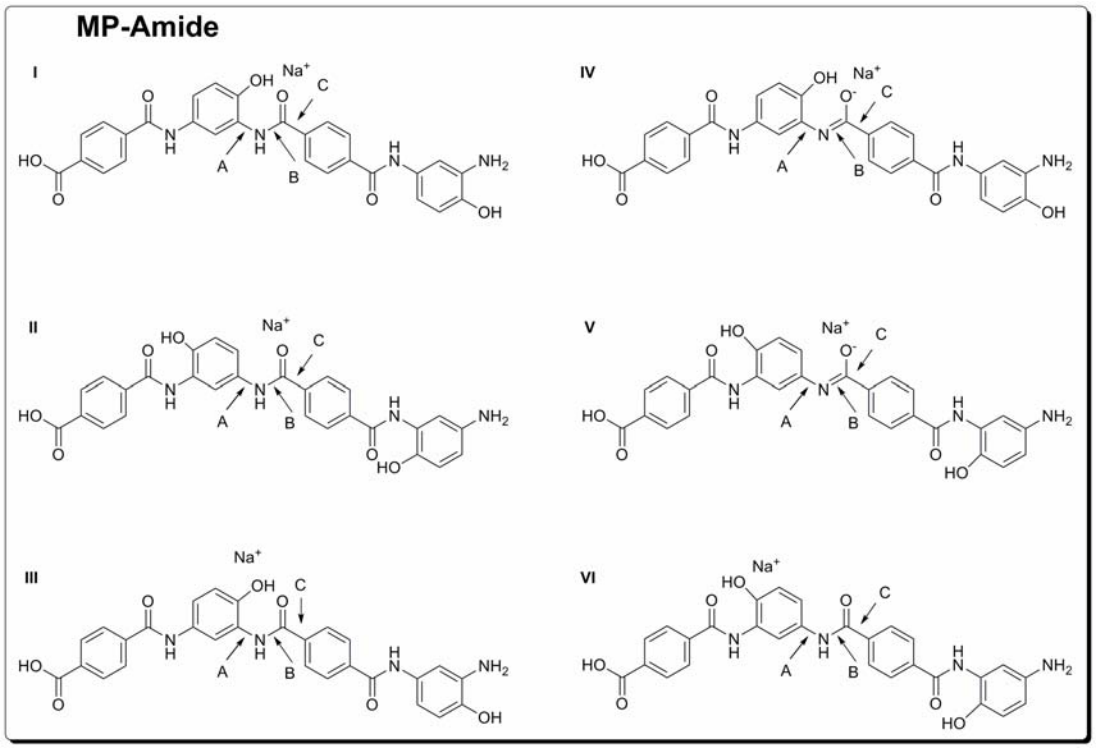

Figure A.9: MP-Amide structures for calculations to determine the cationic influence on fragmentation.

As with PPD-T, MP-Amide models also make use of a Na^+ associating with both hydroxyl oxygen species and amide species. The bonds examined differ from the non-cation influenced calculations, in that only the terminal carboxylic acid group present on the representative molecule is not under consideration for homolytic cleavage.

Further calculations relating to this class of industrial polymers were produced, namely for the polymers coded as PBO (Figure A.10) and PBO-Amide (Figure A.11).

Again, Na^+ was used to simulate the effects of Ag^+ on the fragmentation patterns observed using MALDI/TOF TOF CID MS.

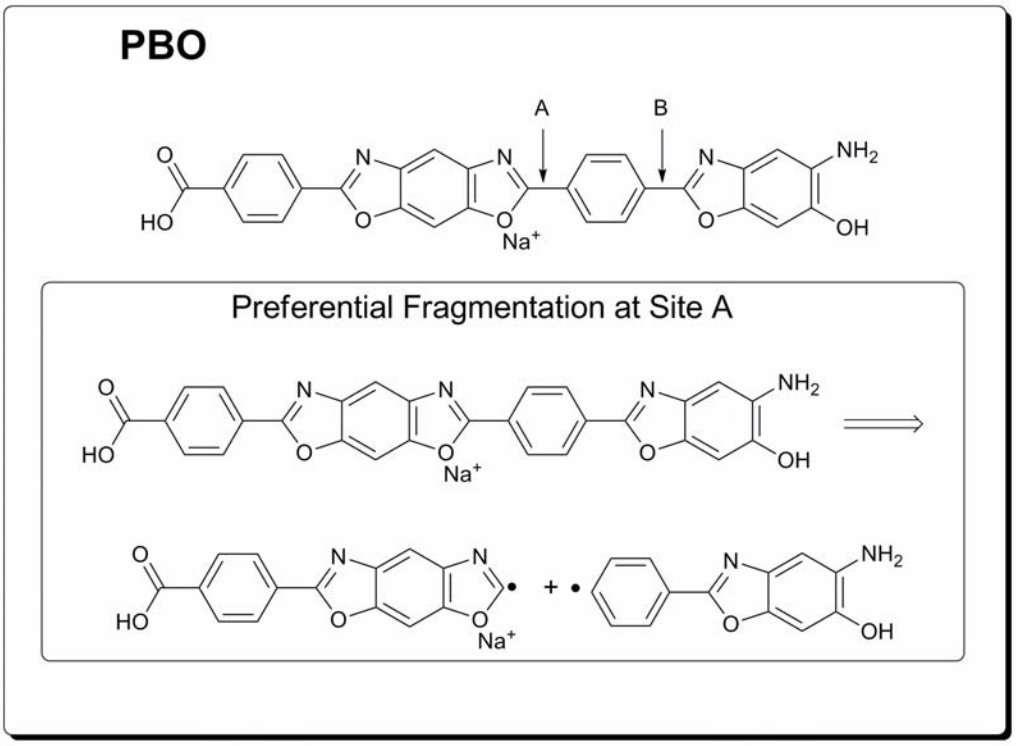

Figure A.10: Representative structure of PBO polymer and preferential fragmentation site illustrating homolytic cleavage of the molecule. The two bonds examined are highlighted with arrows.

The calculations yielded results supporting the hypothesis that the Site A (Figure A.10) will be favored for fragmentation. Table A.5 shows the predicted energies for each bond.

Table A.5: PBO predicted homolytic cleavage bond energies. All calculations were performed using DFT/B3LYP/6-31G* level of theory. All values are in kcal/mol.

Calculation	PBO
Site A	98.698
Site B	121.460

There is a difference of approximately 22 kcal/mol between Sites A and B (Figure A.10), which reflects a relative energy barrier necessary to overcome for induction of fragmentation.

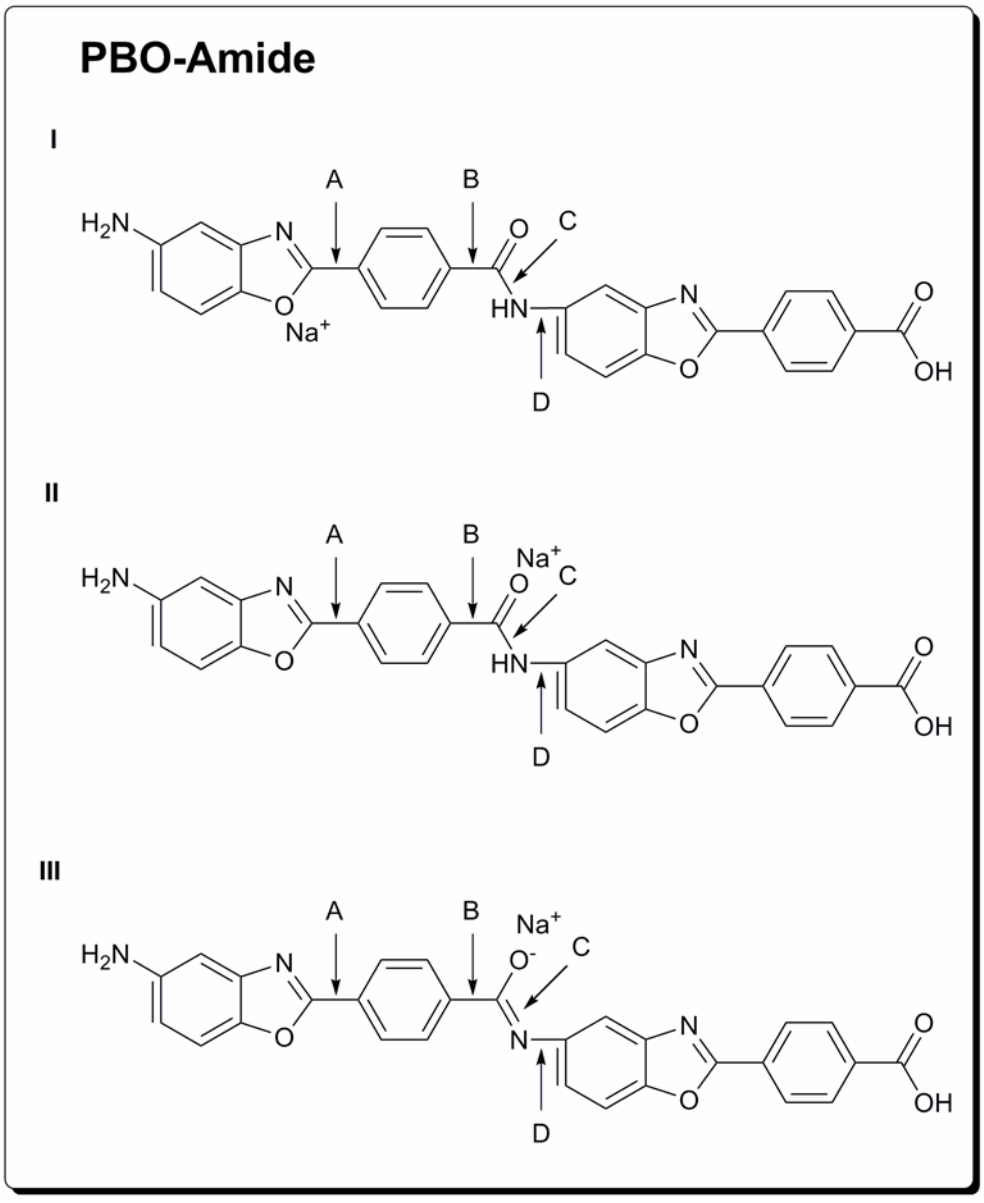

Figure A.11: PBO-Amide models for computations to discern the probable fragmentation sites along the polymer.

A.6: Summary

Computational modeling for mass spectrometry has been shown to be a useful tool toward predicting probable fragmentation patterns based upon electronic and chemical configuration. These methods have been tested using a series of molecules, some varying only by addition of a single functional group, and have produced results that support mass spectrometry data. Although currently limited to the elements addressed within the B3LYP basis set, the methodology may be further tested using other basis set parameters that reflect and are better suited for the model being studied. Expansion of the computational approach will provide additional support and further integrate theoretical techniques into analytical analyses.

REFERENCES

(1.) Dong, C.; Qian, H.; Fang, N.; Ren, J., Study of Fluorescence Quenching and Dialysis Process of CdTe Quantum Dots, Using Ensemble Techniques and Fluorescence Correlation Spectroscopy. *J. Phys. Chem. B* **2006,** 110, 11069-11075.

(2.) Wuister, S. F.; Donega, C. d. M.; Meijerink, A., Luminescence Temperature Antiquenching of Water-Soluble CdTe Quantum Dots: Role of the Solvent. *J. Am. Chem. Soc.* **2004,** 126, 10397-10402.

(3.) Wolcott, A.; Gerion, D.; Visconte, M.; Sun, J.; Schwartzberg, A.; Chen, S.; Zhang, J. Z., Silica-Coated CdTe Quantum Dots Functionalized with Thiols for Bioconjugation to IgG Proteins. *J. Phys. Chem. B* **2006,** 110, (11), 5779-5789.

(4.) Dabbousi, B. O., Rodriguez-Viejo, Mikulec, F. V., Heine, J. R., Mattoussi, H., Ober, R., Jensen K. F., and Bawendi, M. G., ZnS Core-Shell Quantum Dots: Synthesis and Optical and Structural Characterization of a Size Series of Highly Luminescent Materials. *J. Phys. Chem. B* **1997,** 101, 9463-9475.

(5.) Smith, A. M.; Ruan, G.; Rhyner, M. n.; Nie, S., Engineering Luminescent Quantum Dots for *In Vivo* Molecular and Cellular Imaging. *Annals of Biomedical Engineering* **2006,** 34, (1), 3-14.

(6.) Smith, A. M.; Gao, X.; Nie, S., Quantum Dot Nanocrystals for *In Vivo* Molecular and Cellular Imaging. *Photochemistry and Photobiology* **2004,** 80, 377-385.

(7.) McBride, J., Treadway, J., Feldman, L. C., Pennycook, S. J., Rosenthal, S. J., Structural basis for near unity quantum yield core/shell nanostructures. *Nano Letters* **2006,** 6, (7), 1496-1501.

(8.) Fu, A.; Gu, W.; Larabell, C.; Alivisatos, A. P., Semiconductor nanocrystals for biological imaging. *Current Opinion in Neurobiology* **2005,** 15, 568-575.

(9.) Alivisatos, A. P., Perspectives on the physical chemistry of semiconductor nanocrystals. *J. Phys. Chem.* **1996,** 100, 13226-13239.

(10.) Schmelz, O., Mews, A., Basché, T., Herrmann, A., and Müllen, K., Supramolecular complexes from CdSe nanocrystals and organic fluorophores. *Langmuir* **2001,** 17, (2861-2865).

(11.) Peng, Z. A., and Peng, X., Formation of high-quality CdTe, CdSe, and CdS nanocrystals using CdO as precursor. *J. Am. Chem. Soc.* **2001,** 123, 183-184.

(12.) Hines, M. A., and Guyot-Sinnest, P., Synthesis and characterization of strongly luminescing ZnS-capped CdSe nanocrystals. *J. Phys. Chem.* **1996,** 100, 468-471.

(13.) Peng X., S., M. C., Kadavanich, A. V., and Alivisatos, A. P., Epitaxial growth of highly luminescent CdSe/CdS core/shell nanocrystals with photostability and electronic accessibility. *J. Am. Chem. Soc.* **1997,** 119, 7019-7029.

(14.) Michalet, X., Pinaud, F., Lacoste, T. D., Dahan, M., Bruchez, M. P., Alivisatos, A. P., and Weiss, S., Properties of fluorescent semiconductor nanocrystals and their application to biological labeling. *Single Mol.* **2001,** 2, 261-276.

(15.) Bruchez, M., Moronne, M., Gin, P., Weiss, S., and Alivisatos, A. P., Semiconductor nanocrystals as fluorescent biological labels. *Science* **1998,** 281, 2013-2016.

(16.) Chan, W. C. W., and Nie, S., Quantum dot bioconjugates for ultrasensitive nonisotopic detection. *Science* **1998,** 281, 2016-2018.

(17.) Klarreich, E., Biologists join the dots. *Nature* **2001,** 413, 450-452.

(18.) Swafford, L. A.; Weigand, L. A.; Bowers, M. J., III; McVride, J. R.; Rapaport, J. L.; Watt, T. L.; Dixit, S. K.; Feldman, L. C.; Rosenthal, S. J., Homogeneously Alloyed CdS_xSe_{1-x} Nanocrystals: Synthesis, Characterization, and Composition/Size-Dependent Band Gap. *JACS* **2006,** 128, (32), 12299-12306.

(19.) Xie, R.; Kolb, U.; Li, J.; Basche, T.; Mews, A., Syntesis and Characterization of Highly Luminescent CdSe-Cor $CdS/Zn_{0.5}Cd_{0.5}S/ZnS$ Multishell Nanocrystals. *JACS* **2005,** 127, (20), 7480-7488.

(20.) Garrett, M. D.; Dukes, A. D., III; McBride, J. R.; Smith, N. J.; Pennycook, S. J.; Rosenthal, S. J., Band Edge Recombination in CdSe, CdS, and CdS_xSe_{1-x} Alloy Nanocrystals Observed by Ultrafast Fluorescence Upconversion: The Effect of Surface Trap States. *J. Phys. Chem. C* **2008,** 112, (33), 12736-12746.

(21.) Medintz, I. L.; Uyeda, H. T.; Goldman, E. R.; Mattoussi, H., Quantum dot bioconjugates for imaging, labeling and sensing. *Nature Materials* **2005,** 4, 435-446.

(22.) Wu, X., Liu, H., Liu, J., Haley, K. N., Treadway, J. A., Larson, J. P., Ge, N., Peale, F., Bruchez, M., P., Immunofluorescent labeling of cancer marker Her2 and other cellular targets with semiconductor quantum dots. *Nat. Biotech.* **2002,** 21, 41-46.

(23.) Sukhanova, A.; Devy, J.; Venteo, L.; Kaplan, H.; Artemyev, M.; Oleinikov, V.; Klinov, D.; Pluot, M.; Cohen, J. H. M.; Nabiev, I., Biocompatible fluorescent nanocrystals for immunolabeling of membrane proteins and cells. *Analytical Biochemistry* **2004,** 324, 60-67.

(24.) Tolumasu, F.; Dvorak, J., Development and application of quantum dots for immunocytochemistry of human erythrocytes. *Journal of Microscopy* **2003,** 211, 256-261.

(25.) Larson, D. R.; Zipfel, W. R.; Williams, R. M.; Clark, S. W.; Bruchez, M. P.; Wise, F. W.; Webb, W. W., Water-Soluble Quantum Dots for Multiphoton Fluorescence Imaging *In Vivo*. *Science* **2003,** 300, 1434-1436.

(26.) Ness, J. M.; Akhtar, R. S.; Latham, C. B.; Roth, K. A., Combined Tyramide Signal Amplification and Quantum Dots for Sensitive and Photostable Immunofluorescence Detection. *The Journal of Histochemistry and Cytochemistry* **2003,** 51, (8), 981-987.

(27.) Breus, V. V.; Heyes, C. D.; Nienhaus, G. U., Quenching of CdSe-ZnS-Shell Quantum Dot Luminescence by Water-Soluble Thiolated Ligands. *J. Phys. Chem. C* **2007,** 111, 18589-18594.

(28.) http://www.invitrogen.com

(29.) Dubertret, B., Skourides, P., Norris, D. J., Noireaux, V., Brivanlou, A. H., and Libchaber, A., In vivo imaging of quantum dots encapsulated in phospholipid micelles. *Science* **2002,** 298, 1759-1762.

(30.) Bentzen, E. L.; Tomlinson, I. D.; Mason, J.; Gresch, P.; Warnement, M. R.; Wright, D.; Sanders-Bush, E.; Blakely, R.; Rosenthal, S. J., Surface Modification To Reduce Nonspecific Binding of Quantum Dots in Live Cell Assays. *Bioconjugate Chem* **2005,** 16, (6), 1488-1494.

(31.) Gerion, D., Pinaud, F., Williams, S. C., Parak, W. J., Weiss, S., Alivisatos, A. P., Synthesis and properties of biocompatible water-soluble silica-coated CdSe/ZnS semiconductor quantum dots. *J. Phys. Chem. B* **2001,** 105, (37), 8861-8871.

(32.) Gao, X. H., Cui, Y. Y., Levenson, R. M., Chung, L. W. K., Nie, S. M., In vivo cancer targeting and imaging with semiconductor quantum dots. *Nature Biotechnology* **2004,** 22, (8), 969-976.

(33.) Jovin, T. M., Quantum dots finally come of age. *Nature Biotechnology* **2003,** 21, (1), 32-33.

(34.) Chun-Yang, Z., Yi-Xuan, G., Hui, M., Cheng-Cai, A., Die-Yan, C., Trichosanthin induced calcium-dependent generation of reactive oxygen species in human choriocarcinoma cells. *Analyst* **2000,** 125, (9), 1539-1542.

(35.) Minet, O.; Dressler, C.; Beuthan, J., Heat STress Induced Redistribution of Fluorescent Quantum Dots in Breast Tumor Cells. *Journal of Fluorescence* **2004,** 14, (3), 241-247.

(36.) Tomlinson, I. D., Mason, J. N., Blakely, R. D., Rosenthal, S. J., Peptide-conjugated quantum dots - Imaging the angiotensin type 1 receptor in living cells. In *Methods Mol. Bio.*, ed.; Rosenthal, S. J., Wright, D. W., HUMANA PRESS INC: 2005; 51-60.

(37.) Lidke, D. S., Nagy, P., Heintzmann, R., Arndt-Jovin, D. J., Post, J. N., Grecco, H. E., Jares-Erijman, E.A., Jovin, T.M., Quantum dot ligands provide new insights into erbB/HER receptor-mediated signal transduction. *Nature Biotechnology* **2004,** 22, (2), 198-203.

(38.) Åkerman, M. E., Chan, W. C. W., Laakkonen, P., Bhatia, S. N., and Ruoslahti, E., Nanocrystal targeting in vivo. *Proc. Natl. Acad. Sci. U.S.A.* **2002,** 99, 12617-12621.

(39.) Gussin, H. A., Tomlinson, I. D., Little, D. M., Warnement, M. R., Qian, H., Rosenthal, S. J., Pepperberg, D. R., Binding of Muscimol-Conjugated Quantum Dots to $GABA_C$ Receptors. *J. Am. Chem. Soc.* **2006,** 128, (49), 15701-15713.

(40.) Rosenthal, S. J., Tomlinson, A., Adkins, E. M., Schroeter, S., Adams, S., Swafford, L., McBride, J., Wang, Y. Q., DeFelice, L. J., Blakely, R. D., Targeting cell surface receptors with ligand-conjugated nanocrystals. *J. Am. Chem. Soc.* **2002,** 124, (17), 4586-4594.

(41.) Tomlinson, I. D., Mason, J. N., Blakely, R. D., Rosenthal, S. J., High affinity inhibitors of the dopamine transporter (DAT): Novel biotinylated ligands for conjugation to quantum dots. *Bioorg. & Med. Chem. Lett.* **2006,** 16, (17), 4664-4667.

(42.) Ballou, B., Lagerholm, B. C., Ernst, L. A., Bruchez, M. P., and Waggoner, A. S., Noninvasive imaging of quantum dots in mice. *Bioconjugate Chem* **2004,** 15, 79-86.

(43.) Dahan, M., Levi, S., Luccardini, C., Rostaing, P., Riveau, B., Triller, A., Diffusion dynamics of glycine receptors revealed by single-quantum dot tracking. *Science* **2003,** 302, (5644), 442-445.

(44.) Goldman, E. R., Clapp, A. R., Anderson, G. P., Uyeda, H. T., Mauro, J. M., Medintz, I. L., Mattoussi, H., Multiplexed toxin analysis using four colors of quantum dot fluororeagents. *Anal. Chem.* **2004,** 76, (3), 684-688.

(45.) Mason, J. N., Farmer, H., Tomlinson, I. D., Schwartz, J. W., Savchenko, V., DeFelice, L. J., Rosenthal, S. J., Blakely, R. D., Novel fluorescence-based approaches for the study of biogenic amine transporter localization, activity, and regulation. *J. Neurosci. Meth.* **2005,** 143, (1), 3-25.

(46.) Osaki, F., Kanamori, T., Sando, S., Sera, T., Aoyama, Y., A Quantum Dot Conjugated Sugar Ball and Its Cellular Uptake. On the Size Effects of Endocytosis in the Subviral Region. *J. Am. Chem. Soc.* **2004,** 126, (21), 6520-6521.

(47.) Parak, W. J., Boudreau, R., Le Gros, M., Gerion, D., Zanchet, D., Micheel, C. M., Williams, S. C., Alivisatos, A. P., Larabell, C., Cell Motility and Metastatic Potential Studies Based on Quantum Dot Imaging of Phagokinetic Tracks. *Adv. Mater.* **2002,** 14, (12), 882-885.

(48.) Gomez, N., Winter, J. O., Shieh, F., Saunders, A. E., Korgel, B. A., Schmidt, C. E., Challenges in quantum dot-neuron active interfacing. *Talanta* **2005,** 67, 462-471.

(49.) Hanaki, K., Momo, A., Oku, T., Komoto, A., Mainosono, S., Yanaguchi, Y., Yamamoto, K., Semiconductor quantum dot/albumin complex is a long-life and highly photostable endosome marker. *Biochem. and Biophys. Res. Comm.* **2003,** 302, 496-501.

(50.) Hoshino, A., Hanaki, K., Suzuki, K., Yamamoto, K., Applications of T-lymphoma labeled with fluorescent quantum dots to cell tracing markers in mouse body. *Biochem. and Biophys. Res. Comm.* **2004,** 314, 46-53.

(51.) Voura, E. B., Haiswal, J. K., Mattoussi, H., Simon, S. M., Tracking metastatic tumor cell extravasation with quantum dot nanocrystals and fluorescnece emission-scanning microscopy. *Nature Medicine* **2004,** 10, (9), 993-998.

(52.) Estrada, C. R.; Salanga, M.; Bielenberg, D. R.; Harrell, W. B.; Zurakowski, D.; Zhu, X.; Palmer, M. R.; Freeman, M. R.; Adam, R. M., Behavioral Profiling of Human Transitional Cell Carcinoma *Ex vivo*. *Cancer Research* **2006,** 66, (6), 3078-3086.

(53.) Clarke, S. J.; Hollmann, C. A.; Zhang, Z.; Suffern, D.; Bradforth, S. E.; Dimitrijevic, N. M.; Minarik, W. G.; Nadeau, J. L., Photophysics of dopamine-modified quantum dots and effects on biological systems. *Nature Materials* **2006,** 5, 409-417.

(54.) Chu, T. C.; Shieh, F.; Lavery, L. A.; Levy, M.; Richards-Kortum, R.; Korgel, B. A.; Ellington, A. D., Labeling tumor cells with fluorescent nanocrystal-aptamer bioconjugates. *Biosensors and Bioelectronics* **2006,** 21, 1859-1866.

(55.) Giepmans, B. N. G.; Deerinck, T. J.; Smarr, B. L.; Jones, Y. Z.; Ellisman, M. H., Correlated light and electron microscopic imaging of multiple endogenous proteins using Quantum dots. *Nature Methods* **2005,** 2, (10), 743-749.

(56.) Howarth, M., Takao, K., Hayashi, Y., Ting, A. Y., Targeting quantum dots to surface proteins in living cells with biotin ligase. *PNAS* **2005,** 102, (21), 7583-7588.

(57.) Orndorff, R. L.; Warnement, M. R.; Mason, J. N.; Blakely, R. D.; Rosenthal, S. J., Quantum Dot Ex Vivo Labeling of Neuromuscular Synapses. *Nano Letters* **2008,** 8, (3), 780-785.

(58.) Goldin, A. L., Ion Channel Disorders. *Neurobiology of Disease* **2007,** 12, 135-148.

(59.) Puljak, L.; Kilic, G., Emerging roles of chloride channels in human diseases. *Biochimica et Biophysica Acta* **2006,** 1762, 404-413.

(60.) McFerrin, M. B.; Sontheimer, H., A role for ion channels in glioma cell invasion. *Neuron Glia Biology* **2006,** 2, 39-49.

(61.) Mouhat, S.; Jouirou, B.; Mosbah, A.; De Waard, M.; Sabatier, J.-M., Diversity of folds in animal toxins acting on ion channels. *Biochem. J.* **2004,** 378, 717-76.

(62.) Soroceanu, L.; Gillespie, Y.; Khazaeli, M. B.; Sontheimer, H., Use of Chlorotoxin for Targeting of Primary Brain Tumors. *Cancer Research* **1998,** 58, 4871-4879.

(63.) Wiley, R. G.; Lappi, D. A., Targeted toxins in pain. *Advanced Drug Delivery Reviews* **2003,** 55, (8), 1043-1054.

(64.) Wiley, R. G., Neural lesioning with ribosome-inactivating proteins: suicide transport and immunolesioning. *Trends in Neurosciences* **1992,** 15, (8), 285-290.

(65.) Granier, C.; Novotny, J.; Gontecilla-Camps, J.-C.; Fourquet, P.; El Ayeb, M.; Bahraoui, E., The Antigenic Structure of a Scorpion Toxin. *Molecular Immunology* **1989,** 26, (6), 503-513.

(66.) Cleland, J. C.; Griggs, R. C., Channelopathies of the Nervous System. *Neurobiology of Disease* **2007,** 31, 319-332.

(67.) Kim, S.; Lim, Y. T.; Soltesz, E. G.; De Grand, A. M.; Lee, J.; Nakayama, A.; Anthony;, P. J.; Mihaljevic, T.; Laurence, R. G.; Dor, D. M.; Cohn, L. H.; Bawendi, M. G.; Frangioni, J. V., Near-infrared fluorescent type II quantum dots for sentinel lymph node mapping. *Nature Biotechnology* **2004,** 22, (1), 93-97.

(68.) Soltesz, E. G., Kim, S., Laurence, R. G., DeGrand, A. M., Parungo, C. P., Dor, D. M., Cohn, L. H., Bawendi, M. G., Frangioni, J. V., Mihaljevic, T., Intraoperative sentinel lymph node mapping of the lung using near-infrared fluorescent quantum dots. *Annals of Thoracic Surgery* **2005,** 79, (1), 269-277.

(69.) Soltesz, E. G., MD, MPH;; Kim, S., PhD;; Kim, S.-W., PhD;; Laurence, R. G., BS;; De Grand, A. M., BS;; Parungo, C. P., MD;; Cohn, L. H., MD;; Bawendi, M. G., PhD;; Frangioni, J. V., MD, PhD, Sentinel Lymph Node Mapping of the Gastointestinal Tract by Using Invisible Light. *Annals of Surgical Oncology* **2006,** 13, (3), 386-396.

(70.) Turchin, I. V.; Balalaeva, I. V.; Vasil'ev, R. B.; Zlomanov, V. P.; Plehanov, V. I.; Orlova, A. G.; Zagaynova, E. V.; Kamensky, V. A.; Kleshnin, M. S.; Shirmanova, M. V.; Dorofeev, S. G.; Dirin, D. N., Imaging of QDs-labeled tumors in small animals by fluorescence diffuse tomography. *Laser Phys. Lett.* **2006,** 3, (4), 208-211.

(71.) Persson, A. I.; Fan, Q.; Phillips, J. J.; Weiss, W. A., Glioma. *Neurobiology of Disease* **2007,** 39, 433-444.

(72.) Sun, C.; Veiseh, O.; Gunn, J.; Fang, C.; Hansen, S.; Lee, D.; Sze, R.; Ellenbogen, R. G.; Olson, J.; Zhang, M., In Vivo MRI Detection of Gliomas by Chlorotoxin-Conjugated Superparamagnetic Nanoprobes. *Small* **2008,** 4, (3), 372-379.

(73.) Chang, C. C., Looking Back on the Discovery of α-Bungarotoxin. *J. Biomed. Sci* **1999,** 6, 368-375.

(74.) Connolly, J. G., Structure-Function Relationships in Nicotinic Acetylcholine Receptors. *Comp. Biochem. Physiol.* **1989,** 93A, (1), 221-231.

(75.) Fairchough, R. H.; Josephs, R.; Richman, D. P., Imaging Ligand Binding Sites on the *Torpedo* Acetylcholine Receptor. *Annals of the New York Academy of Sciences* **1993,** 681, 113-125.

(76.) Gotti, C.; Clementi, F., Neuronal nicotinic receptors: from structure to pathology. *Progress in Neurobiology* **2004,** 74, 363-396.

(77.) Lindstrom, J. M., Nicotinic Acetylcholine Receptors of Muscles and Nerves: Comparison of Their Structures, Functional Roles, and Vulnerability to Pathology. *Annals of the New York Academy of Sciences* **2003,** 998, 41-52.

(78.) Arias, H. R., Localization of agonist and competitive antagonist binding sites on nicotinic acetylcholine receptors. *Neurochemistry International* **2000,** 36, 595-645.

(79.) Unwin, N., Nicotinic Acetylcholine Receptor at 9 A Resolution. *J. Mol. Biol.* **1993,** 229, 1101-1124.

(80.) Unwin, N., Acetylcholine receptor channel imaged in the open state. *Nature* **1995,** 373, 37-43.

(81.) Zeng, H.; Moss, L.; Grant, M. A.; Hawrot, E., The solution structure of the complex formed between α-bungarotoxin and an 18-mer cognate peptide derived from the α_1 subunit of the nicotinic acetylcholine receptor from *Torpedo californica*. *J. Biol. Chem.* **2001,** 276, 22930-22940.

(82.) Gautam, M.; Noakes, P. G.; Mudd, J.; Michol, M.; Chu, G. C.; Sanes, J. R.; Merlie, J. P., Failure of postsynaptic specialization to develop at neuromuscular junctions of rapsyn-deficient mice. *Nature* **1995,** 377, 232-236.

(83.) Stephenson, F. A.; Harrison, R.; Lunt, G. G., The Isolation and Characterisation of the Nicotinic Acetylcholine Receptor from Human Skeletal Muscle. *European Journal of Biochemistry, FEBS* **1981,** 115, 91-97.

(84.) Delano, W. L. *The PyMOL Molecular Graphics System*, De Lano Scientific, LLC.: 1998-2009.

(85.) DeBin, J. A.; Maggio, J. E.; Strichartz, G. R., Purification and characterization of chlorotoxin, a chloride channel ligand from the venom of the scorpion. *American Journal of Physiology* **1993,** 264, (Cell Physiology 33), C361-C369.

(86.) Goudet, C.; Chi, C.-W.; Tytgat, J., An overview of toxins and genes from the venom of the Asian scorpion *Buthus martensi* Karsch. *Toxicon* **2002,** 40, 1239-1258.

(87.) Lippens, G.; Najib, J.; Wodak, S. J.; Tartar, A., NMR Sequential Assignments and Solution Structure of Chlorotoxin, a Small Scorpion Toxin That Blocks Chloride Channels. *Biochemistry* **1995,** 34, (1), 13-21.

(88.) Lippens, G.; Najib, J.; Wodak, S. J.; Tartar, A., NMR sequential assignments and solution structure of chlorotoxin, a small scorpion toxin that blocks chloride channels. *Biochemistry* **1995,** 34, 13-21.

(89.) Deshane, J.; Garner, C. C.; Sontheimer, H., Chlorotoxin Inhibits Glioma Cell Invasion via Matrix Metalloproteinase-2. *The Journal of Biological Chemistry* **2003,** 278, (6), 4135-4144.

(90.) Veiseh, M.; Gabikian, P.; Bahrami, S.-B.; Veiseh, O.; Zhang, M.; Hackman, R. C.; Ravanpay, A. C.; Stroud, M. R.; Kusuma, Y.; Hansen, S. J.; Kwok, D.; Munoz, N. M.; Sze, R. W.; Grady, W. M.; Greenberg, N. M.; Ellenbogen, R. G.; Olson, J. M., Tumor Paint: A Chlorotoxin:Cy5.5 Bioconjugate for Intraoperative Visualization of Cancer Foci. *Cancer Research* **2007,** 67, (14), 6882-6888.

(91.) Rousaire-Dubois, B.; Milandri, J. B.; Bostsel, S.; Dubois, J. M., Control of cell prolilferation by cell volume alterations in rat C6 glioma cells. *European Journal of Physiology* **2000,** 440, 881-888.

(92.) Soroceanu, L.; Manning, T. J., Jr.; Sontheimer, H., Modulation of Glioma Cell Migration and Invasion Using Cl^- and K^+ Ion Channel Blockers. *the Journal of Neuroscience* **1999,** 19, (14), 5942-5954.

(93.) Suzuki, M.; Morita, T.; Iwamoto, T., Diversity of Cl^- Channels. *Cellular and Molecular Life Sciences* **2006,** 63, 12-24.

(94.) Bidard, J.-N.; Mourre, C.; Gandlofo, G.; Schweitz, H.; Widmann, C.; Gottesmann, C.; Lazdunski, M., Analogies and differences in the mode of action and properties of binding sites (localization and mutual interactions) of two K^+ channel toxins, MCD peptide and dendrotoxin I. *Brain Research* **1989,** 495, 45-57.

(95.) Wang, F. C.; Bell, N.; Reid, P.; Smith, L. A.; McIntosh, P.; Robertson, B.; Dolly, J. O., Identification of residues in dendrotoxin K responsible for its discrimination between neuronal K^+ channels containing Kv1.1 and 1.2 α subunits. *European Journal of Biochemistry* **1999,** 263, 222-229.

(96.) Gasparini, S.; Danse, J.-M.; Lecoq, A.; Pinkasfeld, S.; Zinn-Justin, S.; Young, L. C.; Medeiros, C. C. L. d.; Rowan, W. G.; Harvey, A. L.; Menez, A., Delineation of the Functional Site of α-Dendrotoxin. *The Journal of Biological Chemistry* **1998,** 273, (39), 25393-25403.

(97.) Allen, M. L.; Koh, D.-S.; Tempel, B. L., Cyclic AMP regulates potassium channel expression in C6 glioma by destabilizing Kv1.1 mRNA. *Proceedings of the National Academy of Sciences USA* **1998,** 95, 7693-7698.

(98.) Lancelin, J. M.; Foray, M. F.; Poncin, M.; Hollecker, M.; Manon, D., Proteinase inhibitor homologues as potassium channel blockers. *Nat. Struct. Biol.* **1994,** 1, 246-250.

(99.) Orndorff, R. L.; Rosenthal, S. J., Neurotoxin Quantum Dot Conjugates Detect Endogenous Targets in Live Cancer Cells. *Accepted to Nano Letters,* **2009**.

(100.) Sine, S. M.; Engel, A. G., Recent advances in Cys-loop receptor structure and function. *Nature* **2006,** 440, (23), 448-455.

(101.) Flucher, R. F.; Daniels, M. P., Distribution of Na^+ Channels and Ankyrin in Neuromuscular Junctions Is Complementary to That of Acetylcholine Receptors and the 43 kd Protein. *Neuron* **1989,** 3, 163-175.

(102.) Ruff, R. L., Neurophysiology of the Neuromuscular Junction: Overview. *Annals of the New York Academy of Sciences* **2003,** 998, 1-10.

(103.) Clark, P. B. S.; Schwartz, R. D.; Paul, S. M.; Pert, C. B.; Pert, A., Nicotinic binding in rat brain: autoradiographic comparison of [3H]acetylcholine, [3H]nicotine and [125I] α-bungarotoxin. *Journal of Neuroscience* **1985,** 5, 1307-1315.

(104.) Bogdanov, Y.; Michels, G.; Armstrong-Gold, C.; Haydon, P. G.; Lindstrom, J.; Pangalos, M.; Moss, S. J., Synaptic GABAA receptors are directly recruited from their extrasynaptic counterparts. *The EMBO Journal* **2006,** 25, (18), 4381-4389.

(105.) Gottschalk, A.; Schafer, W. R., Visualization of integral and peripheral cell surface proteins in live *Caenorhabditis elegans*. *Journal of Neuroscience Methods* **2006,** 154, 68-79.

(106.) Ferguson, S. M.; Bazalakova, M.; Savchenko, V.; Tapia, J. C.; Wright, J.; Blakely, R. D., Lethal impairment of cholinergic neurotransmission in hemicholinium-3-sensitive choline transporter knockout mice. *PNAS* **2004,** 101, (23), 8732-8767.

(107.) Sekine-Aizawa, Y.; Huganir, R. L., Imaging of receptor trafficking by using α-bungarotoxin-binding-site-tagged-receptors. *Proc. Natl. Acad. Sci. U.S.A.* **2004,** 101, (49), 17114-17119.

(108.) Fountaine, T. J., Wincovitch, S. M., Geho, D. H., Gargield, S. H., Pittaluga, S., Multispectral imaging of clinically relevant cellular targets in tonsil and lymphoid tissue using semiconductor quantum dots. *Modern Pathology* **2006,** 19, 1181-1191.

(109.) Tholouli, E., Hoyland, J. A., Di Vizio, D., O'Connell, F., MacDermott, S. A., Twomey, D., Levenson, R., Liu Yin, J. A., Golub, T. R., Loda, M., Byers, R., Imaging of multiple mRNA targets using quantum dot based *in situ* hybridization and spectral deconvolution in clinical biopsies. *Biochem. and Biophys. Res. Comm.* **2006,** 348, 628-636.

(110.) Chan, P., Yuen, T., Ruf, F., Gonzalez-Maeso, J., Sealfon, S. C., Method for multiplex cellular detection of mRNAs using quantum dot fluorescent *in situ* hybridization. *Nuc. Acids Res.* **2005,** 33, (18), e161-e169.

(111.) Ferrara, D. E.; Weiss, D.; Carnell, P. H.; Vito, R. P.; Vega, D.; Gao, X.; Nie, S.; Taylor, W. R., Quantitative 3D fluorescence technique for the analysis of en face preparations of arterial walls using quantum dot nanocrystals and two-photon excitation laser scanning microscopy. *Am j. Physiol Regulatory Integrative Comp Physiol* **2006,** 290, 114-123.

(112.) Levene, M. J., Dombeck, D. A., Kasischke, K. A., Molloy, R. P., Webb, W. W., In Vivo Multiphoton Microscopy of Deep Brain Tissue. *J. Neurophysiol.* **2004,** 91, 1908-1912.

(113.) Misgeld, T.; Burgess, R. W.; Lewis, R. M.; Cunningham, J. M.; Lechtman, J. W.; Sanes, J. R., Roles of neurotransmitter in Synapse Formation:

Development of Neuromuscular Junctions Lacking Choline Acetyltransferase. *Neuron* **2002,** 36, 635-648.

(114.) Harel, M.; Kasher, R.; Nicolas, A.; Guss, J. M.; Balass, M.; Fridkin, M.; Smit, A. B.; Brejc, K.; Sixma, T. K.; Katchalski-Katzir, E.; Sussman, J. L.; Fuchs, S., The Binding Site of Acetylcholine Receptor as Visualized in the X-Ray Structure of a Complex between α-Bungarotoxin and a Mimotope Peptide. *Neuron* **2001,** 32, (2), 265-275.

(115.) McCann, C. M.; Bracamontes, J.; Steinbach, J. H.; Sanes, J. R., The cholinergic antagonist α-bungarotoxin also binds and blocks a subset of GABA receptors. *PNAS* **2006,** 103, (13), 5149-5154.

(116.) Benda, P.; Lightbody, J.; Sato, G.; Levine, L.; Sweet, W., Differentiated rat glial cell strain in tissue culture. *Science* **1968,** 161, (839), 370-371.

(117.) Ullrich, N.; Bordey, A.; Gillespie, G. Y.; Sontheimer, H., Expression of Voltage-Activated Chloride Currents in Acute Slices of Human Gliomas. *Neuroscience* **1998,** 83, (4), 1161-1173.

(118.) Frisch, M. J.; Trucks, G. W.; Schlegel, H. B.; Scuseria, G. E.; Robb, M. A.; Cheeseman, J. R.; Montgomery, J. A., Jr.; Vreven, T.; Kudin, K. N.; Burant, J. C.; Millam, J. M.; Iyengar, S. S.; Tomasi, J.; Barone, V.; Mennucci, B.; Cossi, M.; Scalmani, G.; Rega, N.; Petersson, G. A.; Nakatsuji, H.; Hada, M.; Ehara, M.; Toyota, K.; Fukuda, R.; Hasegawa, J.; Ishida, M.; Nakajima, T.; Honda, Y.; Kitao, O.; Nakai, H.; Klene, M.; Li, X.; Knox, J. E.; Hratchian, H. P.; Cross, J. B.; Bakken, V.; Adamo, C.; Jaramillo, J.; Gomperts, R.; Stratmann, R. E.; Yazyen, O.; Austin, A. J.; Cammi, R.; Pomelli, C.; Ochterski, J. W.; Ayala, P. Y.; Morokuma, K.; Voth, G. A.; Salvador, P.; Dannenberg, J. J.; Zakrzewski, V. G.; Dapprich, S.; Daniels, A. D.; Strain, M. C.; Farkas, O.; Malick, D. K.; Rabuck, A. D.; Raghavachari, K.; Foresman, J. B.; Ortiz, J. V.; Cui, Q.; Baboul, A. G.; Clifford, S.; Cioslowski, J.; Stefanov, B. B.; Liu, G.; Liashenko, A.; Piskorz, P.; Komaromi, I.; Martin, R. L.; Fox, D. J.; Keith, T.; Al-Laham, M. A.; Peng, C. Y.; Nanayakkara, A.; Challacombe, M.; Gill, P. M. W.; Johnson, B.; Chen, W.; Wong, M. W.; Gonzalez, C.; Pople, J. A. *Gaussian 03, Revision D.01*, Gaussian, Inc.: Wallingford, CT, 2004.

(119.) Lee, C. T., Yang, W. T., Parr, R. G., Development of the Colle-Salvetti Correlation-Energy Formula into a Functional of the Electron-Density. *Phys. Rev. B* **1988,** 37, (2), 785-789.

(120.) Becke, A. D., Density-Functional Exchange-Energy Approximation with Correct Asymptotic-Behavior. *Phys. Rev. A* **1988,** 38, (6), 3098-3100.

(121.) Gies, A. P.; Vergne, M. J.; Orndorff, R. L.; Hercules, D. M., MALDI-TOF/TOF CID Study of Polystyrene Fragmentation Reactions. *Macromolecules* **2007,** 40, (21), 7493-7505.

(122.) Gies, A. P.; Ellison, S. T.; Vergne, M. J.; Orndorff, R. L.; Hercules, D. M., MALDI-TOF/TOF CID of poly(α-methylstyrene) fragmentation reactions. *Anal. Bioanal. Chem.* **2008,** 392, 627-642.

(123.) Gies, A. P.; Vergne, M. J.; Orndorff, R. L.; Hercules, D. M., MALDI-TOF/TOF CID study of 4-alkyl-substituted polystyrene fragmentation reactions. *Anal. Bioanal. Chem.* **2008,** 392, 609-626.